12-2012

Characterization of Polyacrylonitrile Carbon Fibers

Christian Burke Iversen

Abstract

Carbon fiber composites are a widely used, advanced material with exceedingly high strength to weight properties. In this thesis, a literature overview of carbon fiber manufacturing was provided, as well as a thorough analysis of in-house electrospun polyacrylonitrile fiber stabilization and surface modification of the resulting carbon fibers. In the first section, an overview of precursor fiber fabrication is provided, followed by an analysis of stabilization using surface and bulk composition, dimensional analysis, and functional group analysis via FTIR. The second section uses the current stabilization procedure to develop carbon nanofibers. Fibers first underwent a nitric acid oxidation time series experiment analyzed by surface composition and base neutralization. Using a semi-quantitative function developed in the current research, stoichiometric ratios of a silane-coupling agent were applied to oxidized carbon fibers, and an analysis was conducted on two solution types, and three stoichometries. The functionalized surface properties were determined using XPS and EDX, and provide the foundation for future studies on the effect of the fiber-matrix interphase on shape memory composite performance.

Characterization of Polyacryonitrile Carbon Fibers

By

Christian Burke Iversen
B.S. Rose-Hulman Institute of Technology, 2010

Thesis

Submitted in partial fulfillment of the requirements for
the degree of Master of Science in Bioengineering
in the Graduate School of Syracuse University

December 2012

Acknowledgments

I must first share my gratitude for my thesis adviser, Professor Patrick T. Mather, for his help and support throughout my studies and experiences at Syracuse University. His combined effort and partnership with Dr. Ingrid Rousseau provided me the means and opportunity to continue my studies, and I am grateful to them both for their help throughout my work, as well as the National Science Foundation and General Motors for financial support. Cornell's Center for Materials Research (CCMR) was also critical to the development of my work.

I would also like to extend my gratitude to my thesis committee members, including Dr. Mathew Maye, Dr. Julie Hasenwinkel, and Dr. Jeremy Gilbert for their participation on my committee, as well as their help in and out of the lab.

My work within the Mather Research Group and the Syracuse Biomaterials Institute could not have succeeded without the help of many others: Dr. Xiaofan Luo provided the foundation for my research, and senior lab members including Ifeanyi Onyejekwe, Richard Baker, Erika Rodriguez, Amir Torbati, Dr. Kazuki Ishida, Pine Yang, Dr. Eric Finkelstein and Dr. Youxin Yuan helped set the stage for my work and provided assistance along the way. Friends and family played a vital role in my completion of this degree with their support and amusing times: Hossein was with me from the beginning (best of luck on your PhD buddy!), and we were joined by Erin, Eric, Kayla, Derek, Amber, Afshin, Sam and many others.

Table of Contents

List of Tables

List of Schemes

List of Figures

Chapter 1. Introduction

1.1. Carbon Fibers

Carbon fillers (e.g. fibers, particles, tubes) have been produced, modified, and characterized for several decades and exhibit a wide range of properties. A unique class of materials, high purity carbon can provide high thermal- and chemical-stability, surface area, and a highly ordered (i.e. graphitic) atomic structure that contributes to strength and thermal- or electrical-conductivity.

Carbon fiber properties are dependent on many aspects of production, but the process is typically broken down into three primary regions: precursor selection/fiber fabrication, thermal treatment, and post-processing. In terms of precursors, pitch, cellulose, and polyacrylonitrile materials have been studied for over 50 years. Generally speaking, pitch based fibers provide high stiffness, and electrical- and thermal-conductivity due to an easily achievable graphitic structure, and have applications in thermal dissipation and anodic materials;[1-3] cellulose fibers provide higher carbonization surface area and mesoporosity optimal for filtration, but suffer reduced yield due to high precursor oxygen content;[4-6] and polyacrylonitrile (PAN) fibers provide the highest strength and hardness and have typically been applied in structural composites, and are the primary feedstock for aerospace composites.[7, 8]

Worth emphasizing is the fact that many properties are achievable regardless of precursor, but the extent and ease of achieving the desired characteristic varies significantly. For example, activation – which can increase surface area of PAN materials to over 2000 m^2/g – can be achieved concurrently with carbonization by impregnating the precursor with certain acids or salts, or after carbonization through high temperature exposure to steam or oxygen.[4, 9, 10] While

certain characteristics can be enhanced, limitations are set by the inherent nature of the materials; electrical conductivity of PAN based fibers suffers because PAN cannot form graphite, and increased treatment temperatures will only increase the order within the turbostratic carbon.[11] Additionally, industrial fiber fabrication does not use homopolymer meltspinning, but involves solvents and comonomers, which affect thermal treatment reactions and fiber properties (e.g., strength, conductivity). Polyacrylonitrile decomposes before melting, and requires wet or dry spinning with a highly polar solvent for fiber fabrication; furthermore, a copolymer of acrylonitrile (AN) and another monomer such as acrylic acid or methyl acrylate provides better fiber properties, and aids fiber processing (e.g. catalyzes acrylonitrile polymerization, promotes drying) when compared to homopolymer fibers.[12, 13]

In the current research, we use polyacrylonitrile (PAN) as the sole precursor due to its moderate carbon yield (typically 50-55% vs 25-30% or 85% for cellulosic or pitch, respectively),[11] high strength/modulus capability, and the ability to be easily electrospun into nanofibers.[14, 15] Dealing with polyacrylonitrile fibers specifically, stabilization in air (sometimes referred to as oxidation) between 250-300 ºC is required to prevent polymer degradation at high temperatures, followed by thermal treatment in an inert atmosphere – typically nitrogen or argon – to temperature ranging from 1000-3000 ºC yield the interwoven, turbostratic carbon layers required for high strength fibers.

1.2. Carbon Fiber Composites: Interface and Interphase

Carbon fiber reinforced composites (CFRCs) are fabricated using carbon fibers and a matrix (e.g., thermoset epoxy) and are of great interest for industrial applications due to their favorable properties: extremely high strength to weight ratio (as much ½ the specific gravity of

steel, with 5-10 times the ultimate tensile strength), corrosion resistance, and thermal stability limited only by the composite matrix. Furthermore, the relatively simple laminate fabrication allows versatile composite construction and strategic reinforcement during manufacturing.

When fabricating composites, the interaction between filler and matrix is integral to achieving optimal performance.[16] In the current study, two terms are used with distinct intentions: interface and interphase. The interface of the fiber is considered more generally as the surface, while the interphase is the finite interaction distance between two different materials; in this region, both materials can affect one another based on the prevailing forces. Put another way, carbon fiber used in the current study is composed of 'bulk' carbon at the core of the fiber, in addition to a surface (interface) characterized by various features, including morphological (e.g. roughness, surface area, pore size) and chemical (e.g. acidic and basic groups, polarity, compositional changes). When carbon fiber is used in a composite, the epoxy interacts with the carbon fiber surface (and vice versa), to form a distinct interphase. Depending on the type of interaction, the interphase can range in thickness and strength. Furthermore, the level of interaction between two materials depends on both their physical and chemical characteristics: a rough surface that readily imbibes the matrix can provide a strong mechanical connection, though minimal chemical adhesion; while chemical reactivity between two flat materials can promote chemical interactions (i.e. covalent or ionic) without mechanical support.

The interphase between filler and matrix is fundamental to increasing composite properties. Composite failure and crack propagation first occurs in one of three phases of the composite: i) bulk fiber, ii) bulk matrix, or iii) the interphase. In a laminated composite, the distinction between inter- or intra-laminure failure is made, where intralaminure failure is within a ply of the laminate, and interlaminure failure occurs between plies. Depending on the

application or mode of testing – tensile, compression, shear, 3-point bend – the mode of failure will vary.

To enhance composite properties, carbon fibers are often treated before integration into composite laminates. As mention previously, activation can be used to increase surface area; this is desirable in particulate carbon materials for filtration, but also can be used to increase mechanical adhesion between the fiber and matrix. A chemical sizing agent is more often applied with carbon fibers. Sizing is applied during fiber production, and consists of either deposition from a polymer solution, electrodeposition, electropolymerization, or plasma polymerization, where the process and sizing type are chosen based on the desired effect: enhanced wetting with a specific matrix, increased durability for weaving, etc.[11] A pretreatment of fibers with an epoxy-based sizing can provide control of the interphase properties, as well as promote bonding between fiber and matrix.[16, 17]

1.3. Shape Memory Polymers (SMP) as a Matrix

Shape memory polymers (SMPs) are a class of polymers with the capacity to undergo controlled shape transformation between a permanent and temporary shape when provided the appropriate stimulus (e.g. heat, water).[8, 14, 18, 19] Fixing of a temporary shape is possible by exploiting mechanisms within the polymer system, such as molecular mobility and intermolecular interactions. In the case of a carbon fiber epoxy composite, the permanent shape is fixed through chemical crosslinking of the epoxy matrix; when heated above the glass transition, polymer chains are free to deform and upon cooling stores any deformation in the form of strain energy. Heating above the glass transition allows the epoxy to return to its more entropically favored state, resulting in shape revovery.[20, 21] This has been applied in our own lab

for electrically activated shape memory.[14] An active area of research, applications for shape memory polymers range from self-deploying neuronal electrodes,[22] to active cell substrates,[23] and self-healing materials.[24]

SMP research was predated by and continues alongside shape memory alloys (SMAs); SMPs offer enhanced tunability of properties due to the wide variety of synthesis methods and compositions available.[25] Specifically, a wide range of transition temperatures; higher yield-strain, strain-to-failure, and fixing strain; as well as lower material cost weighs in favor of polymeric systems over alloys. Of particular interest to our motivation of studying SMPs is the much higher shape fixing and recovery when compared to SMAs; polymers allow up to 100% reversible strain, while alloys are limited to ~10%. On the other hand, alloys have superior recovery force.

1.4. Carbon Fiber Fabrication and Surface Modification: Motivation of Study

The present research is part of an ongoing collaboration between Syracuse University (SU) and General Motors Company (GM) funded by the National Science Foundation (GOALI #1004807). It was hypothesized in the funding grant that, "the polymer-[filler] interface and interphase is of paramount important in controlling shape memory polymer composite properties," and in pursuit of this investigation, research has been conducted to determine the interface of pristine in-house electrospun polyacrylonitrile based carbon fibers and those modified by nitric acid and a silicon based coupling agent.

The thesis is organized as follows: Chapter 2 includes a discussion of industrial carbon fiber precursors and fabrication methods, as well as the fabrication methods used in the present study. A thorough analysis of precursor stabilization was conducted. Chapter 3 includes an

overview of carbonization procedures and surface modification techniques, including details of chemical oxidation and silane coupling used in the current study. Analysis of oxidized and silanized carbon fiber surfaces were conducted, directed towards understanding the reaction mechanisms and surface chemistry, which would affect composite performance. This section laid the foundation for future investigation into how the interface and interphase affect shape memory composite performance. Finally, Chapter 4 includes a summary of findings and a demonstration of the effect of changing the epoxy-fiber interphase using fiber pullout, along with suggested future work in the areas of fiber development, surface treatment, and methods of shape memory evaluation.

1.5. References

1. Bright, A. A.; Singer, L. S., Electronic and Structural Characteristics of Carbon-Fibers from Mesophase Pitch. *Carbon* **1979,** 17, (1), 59-69.

2. Cato, A. D.; Edie, D. D., Flow behavior of mesophase pitch. *Carbon* **2003,** 41, (7), 1411-1417.

3. Endo, M.; Kim, C.; Nishimura, K.; Fujino, T.; Miyashita, K., Recent development of carbon materials for Li ion batteries. *Carbon* **2000,** 38, (2), 183-197.

4. Laszlo, K.; Bota, A.; Nagy, L. G., Comparative adsorption study on carbons from polymer precursors. *Carbon* **2000,** 38, (14), 1965-1976.

5. Laszlo, K.; Tombacz, E.; Josepovits, K., Effect of activation on the surface chemistry of carbons from polymer precursors. *Carbon* **2001,** 39, (8), 1217-1228.

6. Alcaniz-Monge, J.; Blanco, C.; Linares-Solano, A.; Brydson, R.; Rand, B., Development of new carbon honeycomb structures from cellulose and pitch. *Carbon* **2002,** 40, (4), 541-550.

7. Flock, J.; Friedrich, K.; Yuan, Q., On the friction and wear behaviour of PAN- and pitch-carbon fiber-reinforced PEEK composites. *Wear* **1999,** 225, 304-311.

8. Lan, X.; Liu, Y. J.; Lv, H. B.; Wang, X. H.; Leng, J. S.; Du, S. Y., Fiber reinforced shape-memory polymer composite and its application in a deployable hinge. *Smart Materials & Structures* **2009,** 18, (2).

9. Im, J. S.; Park, S. J.; Kim, T. J.; Kim, Y. H.; Lee, Y. S., The study of controlling pore size on electrospun carbon nanofibers for hydrogen adsorption. *Journal of Colloid and Interface Science* **2008,** 318, (1), 42-49.

10. Lu, A. H.; Zheng, J. T., Study of microstructure of high-surface-area polyacrylonitrile activated carbon fibers. *Journal of Colloid and Interface Science* **2001,** 236, (2), 369-374.

11. Morgan, P., *Carbon Fibers and Their Composites*. 1 ed.; CRC Press: 6000 Broken Sound Parkway NW, Suite 300 Boca Raton, FL 33487, 2005.

12. Edie, D. D., The effect of processing on the structure and properties of carbon fibers. *Carbon* **1998,** 36, (4), 345-362.

13. Bajaj, P.; Paliwal, D. K.; Gupta, A. K., Acrylonitrile Acrylic Acids Copolymers .1. Synthesis and Characterization. *Journal of Applied Polymer Science* **1993,** 49, (5), 823-833.

14. Luo, X.; Mather, P. T., Conductive shape memory nanocomposites for high speed electrical actuation. *Soft Matter* **2010,** 6, (10), 2146-2149.

15. Fennessey, S. F.; Farris, R. J., Fabrication of aligned and molecularly oriented electrospun polyacrylonitrile nanofibers and the mechanical behavior of their twisted yams. *Polymer* **2004,** 45, (12), 4217-4225.

16. Hughes, J. D. H., The Carbon-Fiber Epoxy Interface - a Review. *Composites Science and Technology* **1991,** 41, (1), 13-45.

17. Peters, P. W. M.; Springer, G. S., Effects of Cure and Sizing on Fiber-Matrix Bond Strength. *Journal of Composite Materials* **1987,** 21, (2), 157-171.

18. Luo, X.; Mather, P. T., Triple-Shape Polymeric Composites (TSPCs). *Advanced Functional Materials* **2010,** 20, (16), 2649-2656.

19. Rousseau, I. A.; Xie, T., Shape memory epoxy: Composition, structure, properties and shape memory performances. *Journal of Materials Chemistry* **2010,** 20, (17), 3431-3441.

20. Liu, C.; Qin, H.; Mather, P. T., Review of progress in shape-memory polymers. *Journal of Materials Chemistry* **2007,** 17, (16), 1543-1558.

21. Behl, M.; Lendlein, A., Shape-memory polymers. *Materials Today* **2007,** 10, (4), 20-28.

22. Sharp, A. A.; Panchawagh, H. V.; Ortega, A.; Artale, R.; Richardson-Burns, S.; Finch, D. S.; Gall, K.; Mahajan, R. L.; Restrepo, D., Toward a self-deploying shape memory polymer neuronal electrode. *Journal of Neural Engineering* **2006,** 3, (4), L23-L30.

23. Davis, K. A.; Burke, K. A.; Mather, P. T.; Henderson, J. H., Dynamic cell behavior on shape memory polymer substrates. *Biomaterials* **2011,** 32, (9), 2285-2293.

24. Rodriguez, E. D.; Luo, X. F.; Mather, P. T., Linear/Network Poly(epsilon-caprolactone) Blends Exhibiting Shape Memory Assisted Self-Healing (SMASH). *Acs Applied Materials & Interfaces* **2011,** 3, (2), 152-161.

25. Hornbogen, E., Comparison of shape memory metals and polymers. *Advanced Engineering Materials* **2006,** 8, (1-2), 101-106.

Chapter 2. Polyacrylonitrile (PAN) Precursor Fiber Fabrication and Stabilization

2.1. Synopsis

In the present chapter, an overview of polyacrylonitrile comonomers and fiber fabrication is provided to expand understanding of carbon fiber development. Following the introduction to typical industrial processes, an analysis is provided for the current method of electrospinning and stabilizing homopolymer PAN fibers using compositional, dimensional, and functional group analysis to assess stabilization reactions.

2.2. Background of Carbon Fiber Precursor Fabrication

Polyacrylonitrile (PAN) fibers are the most popular industrial precursor for carbon fibers due to their high strength and reasonable carbon yield.[1] Precursor fiber fabrication, stabilization, and carbonization account for 51%, 22%, and 15% of carbon fiber cost, so substantial effort has been put forth to reduce cost of stabilization and carbonization in an effort to make them more economical.[1, 2] A short review of the various processes for fabrication and stabilization follows.

First, monomers are polyermized into a desirable copolymer, which is spun into a precursor fiber. Copolymer formulations using acrylonitrile (AN) monomer and various acids are preferred over homopolymer PAN because the copolymers catalyze stabilization and improve carbon fiber properties.[3-8] Comonomers reduce interaction between highly polar nitrile groups, increasing segment mobility and crystalline orientation, and improving fiber properties.[9] A mathematical model has been proposed to describe the processes with a single comonomer,[10] and reviews are provided by P. Bajaj and A.K. Roopanwal[11] and Peter Morgan.[1] Manufacturers can use a single or use several comonomers to catalyze and control the exothermic cyclization and

crosslinking reactions (e.g., itaconic acid [IA] and methacrylic acid [MAA]),[12] increase mechanical properties (e.g., IA), and occasionally as a plasticizer (e.g., acrylic acid [AA], MAA, or IA).[1] Comonomers can account for 5-15% of the copolymer, with a target copolymer number average molecular weight (M_w) and polydispersity index (PDI) of M_w~40-70 kg/mole and 1.5-3, respectively.[1]

Industrial PAN precursor fiber is produced by dissolving the copolymer in a solvent such as dimethylformamide (DMF), followed by wet- or dry-spinning with a spinneret. Wet-spinning entails extrusion into a coagulation bath where the fiber is exposed to a non-solvent and 'gels', whereas dry-spinning involves extrusion and quickly heating the fiber above the solvent evaporation point. Wet-spun fibers are slightly stretched in their gel state – when molecular mobility is high – providing molecular orientation and a fibrillar structure, but a similar structure is achieved in dry-spun fibers when supplied tension during stabilization.[1]

Following precursor fabrication, tows of fiber are rolled through furnaces for stabilization/oxidation, low- and high-temperature carbonization, surface treatment, sizing, and collection.[1] During stabilization, fibers are heated in air to between 200 ºC and 300 ºC and the linear PAN molecules undergo cyclization to develop a ladder structure with greatly improved thermal resistance. At the elevated temperature, free radicals are created at the end of polymer chains, nitrile groups, and impurities.[1, 3] These radicals result in cyclization of 3-6 adjacent nitrile groups, limited by steric and backbone hindrances;[13] highly polar nitrile groups cause the polyacrylonitrile chains to prefer a helical structure with the pendant group directed radially away from the center,[14] so reactions are limited along a single polymer molecule. Reactions can occur between adjacent chains via azomethine crosslinks or intermolecular nitrile cyclization to satisfy residual free radicals.

Fibers are drawn during stabilization and carbonization to promote polymer chain alignment along the fiber axis. Otherwise, when PAN fibers are heated above the glass transition (~125 ºC) during stabilization, molecular orientation decreases and the fiber will shrink due to entropic relaxation and the previously discussed nitrile reactions.[15-17] While neither crystallinity nor molecular orientation is greatly enhanced by applying tension, achieving high modulus and high tensile strength fibers requires tension to maintain axial orientation.[8, 15, 18, 19] It has been suggested that interamolecular cyclization and intermolecular crosslinks can be differentiated by analyzing stress relaxation in a constant-length sample: intramolecular cyclization will result in stress relaxation, while intermolecular crosslinking will sustain stress buildup.[14]

Throughout stabilization and concurrent to cyclization, oxygen uptake occurs and has a dramatic effect on reaction kinetics and resulting fiber properties. Oxygen is typically integrated in the form of carbonyl groups,[5, 20, 21] where it plays several roles:

1) Facilitates formation of activated centers for cyclization;[3]
2) Catalyzes dehydrogenation of the polyacrylonitrile backbone;[20]
3) Through cyclization and dehydrogenation, the PAN backbone increases in rigidity and creates a ‘skin’ that decreases oxygen diffusion to the core of the fiber;[22]
4) Coloration of the fiber.[23]

As point (3) indicates, there are problems associated with traditional carbon fiber production that involve transport mechanisms, summarized by Fitzer et al.[24] in Table 2-1. When heated too quickly, exothermic cyclization reactions paired with volatile production can introduce fiber defects.[24] Polyacrylonitrile copolymers are often used to control the exothermic reaction during stabilization.[12] Changing fiber dimension can also benefit heat and mass

transport problems by dramatically altering the scale; typical carbon fibers are on the order of 7 μm diameter, while electrospun fibers can reach 200 nm.

2.2.1. Electrospun Fiber Fabrication

Electrospinning is a widely reported method to prepare polymer fibers ranging from nanometers to micrometers in diameter.[25-27] Unlike traditional dry-spinning, electrospinning solidifies the extruded fiber at room temperature using the dynamics and scale of the spinning process. Placing a polymer solution in a charged syringe and opposite a grounded or negatively biased collector, the electrostatic force in the solution overcomes the surface tension and extrudes the solution into a Taylor cone, and further into a fiber. Fiber instability results in '*whipping'*, and is driven by the electric field between the syringe and collector, as well as Coulombic interaction between the lengths of fiber.[28] During the extrusion process, PAN fibers have been reported to reach velocities greater than 100 m/s with a draw ratio on the order of 1:300,000, and it is believed that this provides molecular alignment along the fiber axis.[29] Renker et al.[28] suggest that a large draw ratio paired with a short distance and time of extrusion results in molecular orientation along the axis because the strain rate greatly exceeds molecular relaxation times; a coiled polymer chain fixes a strain when the product of strain rate and conformational relaxation time exceeds 0.5, and in the case of electrospinning the product is on the order of 10-10^3. Contrary to these suggestions, molecular orientation in electrospun polyamide-6 and polylactide fibers as narrow as 50 nm were shown to have no more as-spun orientation than micrometer melt-spun fibers, complicating the assumption about intrinsic orientation due to electrospinning.[30] Reduced orientation could be due to residual solvent in fibers that provides molecular mobility that allows chains to slowly relax over time.

As previously mentioned, industrial fibers are slightly drawn during extrusion and stabilization to promote molecular orientation. Despite the high amount of orientation previously suggested for electrospun fibers,[29] tension is required during stabilization if orientation is to be maintained. Zussman et al.[31] stabilized and pyrolized ~200 nm electrospun homopolymer PAN fibers without constraint and used x-ray diffraction (XRD) to measure molecular orientation using Herman's Orientation Function (f_c) (Equation 2-1) and azimuthal scans (α) of the (*100*, θ = 22.5°) basal plane. Critical values of f_c include 1, 0, and -0.5 for perfect, random, or perpendicular orientation, respectively. They achieved a molecular orientation of f_c = 0.34 for their homopolymer pan fibers compared to f_c = 0.6 and 0.66 for melt- and wet-spun PAN copolymers cited in the same paper.

$$f_\alpha = \frac{3\langle \cos^2 \alpha \rangle_{av} - 1}{2} \tag{2-1}$$

Despite the potentially innate advantage of small diameter electrospun fibers – it is suggested that carbon fiber strength increases with decreasing diameter due to a volume effect of the Weibull distribution for defects[1], but this is hard to achieve in practice[31] – maintaining orientation is challenging. Specifically, the fibers used in the present study are randomly oriented, non-woven mats. In an effort to maintain planar isotropy, no tension was provided during stabilization.

2.2.2. Optimizing Stabilization

Determining the optimal stabilization conditions is essential to precursor fiber development, and several endpoints have been proposed to achieve the highest performance carbon fibers. Stabilized fibers characterized with a density of 1.375 g/cm^3,[32] water uptake of 5-

10 wt-%,[33] oxygen content of 5-15 at-%,[24, 34] and differential scanning calorimetry (DSC) based aromatization index (Equation 2-2) of 58%[23] have yielded favorable carbon fiber properties.

$$AI_{DSC} = \frac{H_v - H_o}{H_v} x100 \tag{2-2}$$

H_v = Exothermic heat of precursor PAN

H_o = Exothermic heat of stabilized PAN

Other techniques can be used to monitor the development of various elements of stabilization. Fourier transform infrared spectroscopy (FTIR) can characterize both dehydrogenation-based conjugation and oxygen uptake as well as nitrile cyclization and crosslinking of linear PAN; this provides insight into the chemical developments occurring during stabilization as well as extent of stabilization.[35] Dimensional analysis reveals the time and temperature dependence of shrinkage that results from nitrile cyclization and intermolecular reactions; 25% shrinkage has been reported as the upper limit for isotactic chains, though homopolymer PAN has been shown to vary from 13 to 35%.[36] X-ray diffraction (XRD, Equation 2-3) can also be used to analyze conversion from polyacrylonitrile ($I_{2\theta = 19^o}$) to the nitrile cyclized ladder polymer ($I_{2\theta = 25^o}$).[37]

$$AI_{XRD} = \frac{I_{25^\circ}}{I_{25^\circ} + I_{19^\circ}} x100 \tag{2-3}$$

Zhu et al.[35] compared FTIR, DSC, and XRD methods of characterizing nitrile conversion and determined FTIR was a better measure throughout stabilization due to XRD underestimation of nitriles in early stabilization and DSC overestimation of nitriles at the end of stabilization.

2.3. Material Selection and Fiber Fabrication Method

Precursor PAN fibers were fabricated using the electrospinning method described previously, and carbon fibers were developed following Scheme 2-1.[38-40] First, 1 g of polyacrylonitrile (PAN, 150 kg/mol, Scientific Polymer Products) was dissolved in 10 ml of dimethylformamide (DMF, Sigma Aldrich). A homogenous solution was achieved after roughly 2 hours of mixing at 80 ºC. This solution was electrospun using the parameters in Figure 2-1, dried at 40 ºC for 2 days, and 70-75 ºC for at least 2 hours to remove residual solvent. Dried PAN mats (Scheme 2-1[A]) were stabilized in air without constraint by heating at 2 ºC/min to 280 ºC, followed by a 3-hour isothermal hold. Stabilized fibers (Scheme 2-1[B]) were pyrolized in a nitrogen environment by heating at 2 ºC/min to 1000 ºC, followed by a 1-hour isothermal hold (Scheme 2-1[C]).

The current chapter is dedicated to stabilization of fibers, so carbonization will not be considered. All fiber mats were processed without constraint. The randomly oriented, continuous fiber mats posed difficulty when trying to find a reliable constraint method. Typically, single fibers are stabilized and pyrolized continuously under a uniaxial tension, but the randomly oriented, non-woven mat prevented the use of uniaxial constraint if planar-isotropy was to be maintained.

2.4. Characterization Methods

Temperature-series samples were taken with fibers being removed at various temperature points during stabilization in order to assess reaction progress following past procedures, stabilization included heating at 2 °C/min to 280 °C, followed by isothermal treatment for 3 hours.[40] Samples in the current study were removed at 150, 200, 250, and 280 °C, as well as after 10-, 30-, 60-, and 180-minutes of isothermal treatment at 280 °C.

2.4.1. Fourier Transform Infrared (FTIR) Spectroscopy

FTIR absorbance spectra of electrospun PAN fiber samples heated to various temperature points during stabilization were acquired using a Perkin Elmer Spectrum One. Fibers were removed from the hot oven, immediately weighed, and placed into the FTIR. Spectra were averaged over 64 scans, with 4 cm^{-1} resolution, between 4000-450 cm^{-1}. Precursor samples were prepared from a single electrospun mat fabricated using 1 ml of solution (Section 2.3) to provide samples of equal starting thickness to facilitate quantitative comparison; all spectra had >10% transmission with the exception of the 280 $ºC_{t = 180\ min}$ sample where a single peak reached 2 Abs (1% transmission). Spectra were processed as follows: 1) background correction and baseline subtraction within Spectrum One software, 2) a small baseline-constant was subtracted using OriginPro 8.6 (Origin Lab) with a zero-point at 1800 cm^{-1} to standardize a zero-baseline, followed by 3) peak fitting with Gaussian curves using OriginPro 8.6, allowing peak centers to shift and constraining FWHM < 150 cm^{-1} to reduce the Chi-squared value to convergence; peak areas were studied to allow sample-to-sample variations in FWHM and peak centers. No normalization was conducted.

2.4.2. Scanning Electron Microscope (SEM)

Scanning electron microscope (SEM) images were captured using a JEOL 5600 in order to determine fiber diameter during stabilization. Samples were dried at 40 ºC under vacuum and mounted on aluminum stumps with carbon tape. SEM images were taken at 5 kV, 19 mm working distance, spot size of 25, and were sputter coated for 30 seconds with gold (to prevent sample charging) as needed. Fiber diameters were measured using ImageJ (NIH, http://rsbweb.nih.gov/ij/) analysis software, and are the average of at least 100 fiber measurements.

2.4.3. Energy Dispersive X-ray Spectroscopy (EDX)

Bulk composition was obtained using energy dispersive x-ray spectroscopy (EDX) spectra acquired with a PRISM IG Detector (Princeton Gamma Tech) using the included eXcalibur software (v 4.03.01, Princeton Gamma Tech). The instrument had been previously upgraded to include a Si(Li) detector and ultra-thin window to enhance low-*Z* element contrast. Spectra were acquired at 5 kV, 19 mm working distance, 1000x magnification, spot size of 50, and acquisition time of 3-5 minutes depending on the sample dead-time and count-rate in order to achieve a peak count of at least 1500, or longer until count uncertainties (as calculated within eXcalibur) decreased to below 10%. A voltage of 5 kV was selected because it was an adequate overvoltage to excite the K_{α} transition for all elements of interest (C, N, O), but was rarely enough to result in signal from the sample-mount. To prevent spectral contamination from the carbon mounting tape, spectra were measured above the aluminum stump; any aluminum signal was disregarded during analysis. Background subtraction of Bremsstrahlung (continuous) x-rays was conducted within the software.

2.4.4. X-ray Photoelectron Spectroscopy (XPS)

Surface composition and chemical state analysis was conducted using x-ray photoelectron spectroscopy (XPS) in collaboration with the Cornell Center for Materials Research (SSX-100, Surface Science Instruments/FISONS, Cornell University, Ithaca, NY). XPS is a surface sensitive technique that analyzes the top-most 3-10 nm of a surface. Surface composition was measured for all samples tested at various temperature points during stabilization. Chemical state analysis allowed for determination of functional groups and was conducted for the sample treated to the full stabilization regime: 2 ºC/minute to 280 ºC, followed by 3 hours isothermal.

First, samples were fixed on a mount with carbon tape, placed in the XPS SSX 100, and vacuum was pulled to 10^{-9} Torr (Figure 2-2). Samples were then tested for effects of charging. Charging is caused by the x-ray beam exciting/ejecting photoelectrons from the sample that fail to be replenished due to poor conductivity, causing a gradual shift in binding energy over many scans as more electrons are ejected from the sample. Because they are poorly conducting, all temperature-series stabilized fiber samples experienced charging. This does not demonstrably affect composition, but greatly alters high-resolution binding state analysis. As such, the single high-resolution scan was proceeded by ~20 minutes of compositional scans to achieve a charging equilibrium, followed by the placement of a conductive grid over the sample along with a supply of a low energy electron provided by a 'flood gun'. Remaining shifts in binding energies detected during chemical state analysis were manually corrected by reference point on the spectra. Other relevant specifications are included in Table 2-2.

Compositional analysis was conducted using CasaXPS (www.casaxps.com, v. 2.3.15). Counts per second (Intensity) vary by element energy binding energy and are converted into

molar concentrations using relative sensitivity factors (RSF), where carbon, nitrogen, and oxygen values are 1, 1.8, and 2.93, respectively. Binding state analysis was conducted using OriginPro 8.6. A mixed Gaussian-Lorentzian (70:30) function (Equation 2-4) adopted from CasaXPS with the parameters specified in Table 2-3 used for peak fitting; variables x_c, w, and m, represent the peak center, width, and shape parameter, respectively.

$$GL(x,x_c,w,m) = \frac{e^{-4\ln 2(1-m)\frac{(x-x_c)^2}{w^2}}}{1+4m\frac{(x-x_c)^2}{w^2}} \tag{2-4}$$

2.4.5. Gravimetric Analysis

Weight loss of stabilized samples was recorded concurrently to FTIR acquisition, and results are the average of two replicates.

2.4.6. Dynamic Mechanical Analysis (DMA)

Controlled-force mechanical analysis was conducted using a Q800 DMA (TA Instruments) to determine shrinkage during stabilization. In controlled-force mode and under a 0.005 N preload force to simulate tension-free conditions, the temperature was ramped at 2 ºC/min from room temperature to 280 ºC, where it was held isothermally for 3 hours. Two samples of dimension

2.5. Results and Discussion

2.5.1. Chemical Group Analysis Using Fourier Transform Infrared (FTIR) Spectroscopy

FTIR provided a basis to quantify the structural evolution of polyacrylontrile (PAN) into its ladder form, including nitrile-induced cyclization and crosslinking, which create the thermally stable polymer which can be pyrolized at temperatures above 3000 °C (Scheme 2-1[C]). Other reactions include dehydrocyanation,[9] oxygen integration,[5, 20, 21] and dehydrogenation.[14, 24] The full spectra for all time-series samples is provided in Figure 2-3, paired with scanning electron microscope (SEM) and macroscopic images in Figure 2-4. Several temperature stabilization regions are analyzed in Sections 2.5.2 through 2.5.5 using the wavenumbers (cm^{-1}) of interest (Table 2-4). Furthermore, Scheme 2-2 highlights the suspected chemical development during stabilization.

2.5.2. Solvent Removal (< 200 ºC)

Decreasing intensity of DMF peaks verifies the removal of the residual solvent upon heating through its boiling point (BP = 153 ºC). Key groups include the amide peak (1670 cm^{-1}), O=C-N peak (660 cm^{-1}), and CH/CH_2 peaks (2940, 1460, 1360, 1260, and 1070 cm^{-1}). Importantly, decreasing intensity without addition of new peaks supports the conclusion that solvent removal is the only process.

2.5.3. Low Temperature Stabilization: Initial Cyclization, Crosslinking, and Oxygen Integration (200 - 250 ºC)

Cyclization initiates between 200 and 250 ºC, consistent with other reports.[9, 13, 36] Homopolymer PAN requires increased initiation temperatures and extended duration of stabilization to achieve equivalent cyclization compared to common copolymers. Between 150 ºC and 200 ºC there were no noticeable developments of reaction peaks, but upon heating to 250 ºC peaks were formed at 1190, 1495, 1595, 1660, and 1725 cm^{-1}. Peaks at 1250 and 1365 cm^{-1} increased, and peaks at 1070 and 1460 cm^{-1} decreased.

The primary peak at 1595 cm^{-1} and shoulder peaks at 1660 and 1725 cm^{-1} are often attributed to a combination band of C=N, C=C, and N-H stretching, conjugated (acridone) ketones, and aliphatic (naphthridine) ketones, respectively.[5, 21, 41, 42] The bands at 1190 and 1495 cm^{-1} are attributed to C-N and terminal vinyl groups, respectively.[42] The peak increase for 1365 cm^{-1} can be attributed to partially nitrogenated rings,[42] and CH_3 segmentation of PAN.[7] A subtle peak shift occurs from 1260 to 1250 cm^{-1}, representing CH_2 bands for original PAN and C-N/C-C groups for partially nitrogenated rings, respectively. Peaks at 1070 and 1450 cm^{-1} are considered to be CH/CH_2 peaks from linear polyacrylonitrile and DMF. Lastly, a subtle 15% decrease of the nitrile peak (2240 cm^{-1}) occurs, supporting cyclization.[42]

These changes are consistent with the initial development of nitrogen containing ring systems as a result of nitrile cyclization. Based on other analyses it is anticipated that cyclization is the dominant mechanism, and shoulder peaks that develop at 1660 and 1725 cm^{-1} for two cyclic ketones support cyclization over azometine crosslinking (1190/1610 cm^{-1}).[43] Moderate levels of oxygen integrated in the form of the ketones can be beneficial for dehydrogenation, but too much has also been shown to retard cyclization.[20] It is expected that ring formation is limited

to 1-3 adjacent rings as suggested by Olive,[9] or at most 3-6 adjacent units as suggested by Fochler et al.[13]

Initiation of cyclization between 200 ºC and 250 ºC is supported by previous analysis by Simitzis and Soulis[36] who studied nitrile cylization with NMR and FTIR and determined the isothermal time for onset of cyclization (t_{onset}) in a 95:5 mol-% AN:MAA copolymer was a two-parameter function of the form $t_{onset} = 1/(Ax+B)$, where A = -0.3876 min^{-1}, B = 0.00088 $min^{-1}K^{-1}$, and x is the absolute temperature (K) of the isothermal hold. With increasing temperature, the residence time to onset of cyclization decreases; through extrapolation they determined the theoretically minimum temperature for onset was 168 ºC, but this results in a near-infinite time scale for reaction. The theory predicts a required 35-minute residence time for cyclization at 200 ºC. At the programmed ramp of 2 ºC/minute, fibers in the present study are only above the theoretical threshold of 168 ºC for 16 minutes, so it is not anticipated that any cyclization occurs before 200 ºC, but cyclization below 250 ºC is certainly expected. The AN:MAA copolymer studied catalyzes cyclization and reduces the onset temperature, further supporting the lack of this reaction for our homopolymer PAN below 200 ºC.[8, 11, 12, 44]

2.5.4. Intermediate Temperature Stabilization: Accelerated Cyclization, Conjugation Reactions, and Oxygen Integration (250 - 280$_{t = 0\ min}$ ºC)

The most substantial chemical reactions occur during the course of heating from 250 ºC to 280 ºC. The dominant peak at 1595 cm^{-1} increases by several orders of magnitude, along with the shoulder peaks at 1660 cm^{-1} and 1725 cm^{-1}. As previously stated, these are attributed to a mixed-mode peak cyclic (C=N, C=C, and NH), and two ketones, respectively.[21] The area for the dominant peak at 1595 cm^{-1} for nitrogenated rings overtook the 1450 cm^{-1} peak for linear PAN, supporting greatly increased amounts of stabilized rings. The shoulder peak at 1660 cm^{-1} scales

with the 1595 cm^{-1} consistently, while the shoulder at 1725 cm^{-1} increases more substantially during this stage of stabilization, suggesting that the rate of formation of naphthridine ketone groups accelerates due to the increasing temperature activating more free radical centers for cyclization and oxydehydrogenation. The changing ratio of naphthridine ketones to acridone ketones could be related to higher levels of oxygen, reducing cyclization of adjacent nitriles.

Other notable changes include a peak at 810 cm^{-1} (C=C-H) attributed to aromatic ring formation in the form of various substitutions on benzene like rings, predominantly of disubstituted varieties.[45] The second largest peak at 1365 cm^{-1} and the respective shoulder at 1250 cm^{-1} are attributed to partially nitrogenated rings.[42] The peak at 1190 cm^{-1} (C=N) and paired with a (shrouded) peak at 1610 cm^{-1} can been attributed to azomethine crosslinks.[43]

Dehydrogenation processes are also important to consider. Conjugation of the backbone requires dehydrogenation, and although some researchers determined the reaction did not occur without high temperatures and residence times (>300 ºC) under vacuum,[42] it has also been found that ketones catalyze dehydrogenation and it has been suggested that the reaction can occur nearer 280 ºC.[41] Splitting of the nitrile peak between nitriles at 2240 cm^{-1} and conjugated nitriles at 2210 cm^{-1} is attributed to dehydrogenation processes along the PAN backbone.[5] Changing intensity of the alkene group (2940 cm^{-1}) also supports dehydrogenation, but broad peaks above 3000 cm^{-1} quickly overtake the group and minimizing its use. The development of a conjugated backbone produced a more rigid structure, providing stability, but also one less capable of reacting with adjacent groups. Section 2.5.6 discuses this further.

2.5.5. Prolonged High Temperature Stabilization ($280_{t = 0\ min}$ ºC − $280_{t = 180\ min}$ ºC)

During extended stabilization, peak areas for 1250, 1365 and 1595 cm^{-1} increase, though the peaks at 1365 and 1595 cm^{-1} equalized with respect to each other which could suggest an increase in chain scission resulting in increased terminal vinyl groups. The total peak area of peaks between 760 and 810 cm^{-1} associated with various di-substitued benzene rings increased dramatically through 60 minutes, and then slightly decreased through 180 minutes. Additionally, the ketone peaks increased through 60 minutes of stabilization at 280 ºC, where they remained stable for the following 2 hours. These results suggest cyclization and oxygen uptake continued throughout the three-hour stabilization, though less dramatically between 60 minutes and 3 hours isothermal.

Conjugation was detected between 250 ºC and 280 ºC by observing the split nitrile peak, and isothermally treating fibers at 280 ºC resulted in a full shift to conjugated nitriles (2210 cm^{-1}) within 30 minutes. The nitrile peak never completely disappeared due to steric hindrances[10] and the increasingly rigid backbone attributed to dehydrogenation as well as cyclic ladder formation,[22] but the time to reach a conversion plateau is consistent with literature.[5]

2.5.6. FTIR Based Conversion Indexes

Using FTIR to track cyclization and conjugation allows more precise evaluation of the stabilization reactions. Two typical indexes include an cyclization index (Equation 2-5) and conjugation index (Equation 2-6) where A indicates area rather than intensity (I), and subscripts note the various wavenumbers (cm^{-1}) of interest, specifically being the two nitrile peaks and the dominant cyclization peak. A correction constant ($f = 0.29$) was supplied to account for changing absorbance in the spectrum from high to low wavenumber.[46] Lastly, an estimate of crosslinking

was calculated by comparing the azomethine peak (1190 cm^{-1}) to the cyclic peak (1595 cm^{-1}) using Equation 2-7. In their current form, these equations take into account peak area rather than intensity or height because the fitting parameters allowed wide bounds on FWHM and floating peak centers. Peak area data used for calculations is provided in Table 2-5, and results are provided in Table 2-6.

$$CI_{Cyclization} = \frac{f \times A_{1595}}{(A_{2240} + A_{2210}) + f \times A_{1595}} \tag{2-5}$$

$$CI_{Conjugation} = \frac{A_{2210}}{A_{2240} + A_{2210}} \tag{2-6}$$

$$CI_{Crosslink} = \frac{A_{1190}}{A_{1595} + A_{1190}} \tag{2-7}$$

These results coincide with the general trends mentioned earlier, where cyclization occurred between 200 ºC and 250 ºC, and conjugation initiated between 250 ºC and 280 ºC. By both these measures, reactions progress at varying rates through 60 minutes isothermal at 280 ºC; the cyclization index increased by over 5% between 30- and 60-minutes of isothermal treatment, but increased less than 1% for two hours additional treatment. Similar values were determined using the peak at 1250 cm^{-1} (C=N) to gauge cyclization in place of the peak at 1595 cm^{-1}. The index for crosslinking was not as meaningful as the other two, as shown by the development and plateau between 250 and 280 ºC. The relatively stark transition could be indicative of true azomethine crosslinks, and the limited increase could be due to backbone stiffness as a result of conjugation, paired with cyclization, which would dramatically reduce the ability for intermolecular reactions. The standard stabilization treatment includes short duration at high temperature, consistent with the above findings.

2.5.7. Bulk and Surface Composition Using X-ray Photoelectron Spectroscopy (XPS) and Energy Dispersive X-ray Spectroscopy (EDX)

The evolving composition during stabilization is useful to determine extent of oxidation, and when paired with functional group information, composition can provide information about the level of stabilization, as well as the associated chemical reactions. Stabilization involves the removal of adsorbed moisture, residual solvent, free radical induced nitrile cyclization, and crosslinking. Cyclization and crosslinking create the thermally stable ladder polymer which can be pyrolized at temperatures above 3000 °C (Scheme 2-1[C]). In addition – and concurrent – to nitrile group reactions – such as cyclization or dehydrocyanation of linear PAN to produce HCN[9] – the integration of oxygen is important to consider during stabilization because of its effects on both cyclization and carbon yield. In varying amounts, oxygen has been reported to accelerate cyclization by introducing active centers,[3] inhibit cyclization as a result of amide formation,[13] and contribute to other processes such as oxydehydrogenation.[14, 24] When stabilizing homopolymer PAN, oxygen integration is predominantly in the form of carbonyl groups,[5, 20, 21] which are linked to catalyzed dehydrogenation.[20] As discussed earlier, oxygen content is one method of determining optimal stabilization conditions, where roughly 5-15 at-% is acceptable, but nearer 10 at-% is preferred for optimal carbonization; below 5 at-% reduces yield, while content above 15 at-% reduces tensile properties.[24, 34]

Small levels of silicon (~2-5 at-%) in the temperature-series stabilized samples were detected using XPS, though no silicon is found in any of the chemicals or polymers used for synthesis. It is believed that this contamination is due to a silicone-based oil used on aluminum foils not intended for use under high vacuum. Typically, samples were electrospun onto standard aluminum foil (Fisher Scientific), pealed from the foil (leaving a film of PAN), and then placed

back on the foil for drying and stabilization; silicone or mineral/paraffinic oils can degrade below the stabilization temperature and could contaminate surfaces other than the substrate side of the electrospun mat, though no consistent trend in temperature and silicon content was found. This could be complicated by the fact that the substrate side of the mat was not considered during XPS analysis. Aluminum foils are typically treated with mineral or parrafinic oils, which do not contain silicon, and no specifications were provided by the manufacturer to allow accommodation of their particular surface treatment. As such, silicon contamination was ignored during further analysis and relative concentrations of carbon, nitrogen, and oxygen were calculated. While not optimal, the contamination was not sufficient to affect FTIR results, and was almost completely removed with pyrolysis (~0.5 at-% silicon) and not expected to affect later surface treatments.

Compositional analysis using EDX and XPS was used to determine oxygen content, as well as information about nitrogen loss through the aforementioned dehydrocyanation. Surface composition was measured using XPS (Table 2-7), where the detection depth was estimated to be between 3-10 nm. Due to the surface-sensitive nature, XPS does not describe the fiber composition as a whole, but represents the skin that first reacts to thermal treatment. Bulk composition was measured using EDX (Table 2-8), providing much greater detection depth (~1 μm), but reduced accuracy for low atomic weight elements; the manufacturer quotes window transmissions of roughly 40%, 32%, and 43% for carbon, nitrogen, and oxygen, respectively.[47] Reduced transmission paired with the relatively low fluorescence yield for low *Z* elements (in favor of low energy Auger electrons) limits accuracy of EDX when detecting elements below $Z \approx 20$. A temperature-series oxygen composition plot (Figure 2-5) and a full composition (Figure

2-6) using the ratio of EDX-to-XPS (at-%/at-%) composition provide insight into the effect of stabilization on oxygen content, as well as the differences between EDX and XPS analysis.

The amount of oxygen in the unstabilized mat was surprising high considering pristine PAN contains none. Two other reports of prestabilized electrospun polyacrylonitrile fibers give C/N/O at-% of 78/19/3[48] and 68/29/3 at-%,[45] with oxygen attributed to adsorbed moisture and residual solvent. Various explanations for the atypically high surface oxygen content were considered, including residual solvent, adsorbed moisture, and potential reaction between moisture and PAN to hydrolize the nitrile groups: (I) residual DMF was completely removed after heating to 150 ºC as demonstrated by FTIR (Section 2.5.2). (II) XPS analysis of a fully stabilized PAN (280 ºC$_{t = 180}$ min) sample detects ~1.5 at-% oxygen attributed to chemisorption based on binding energy (Section 2.5.8), and due to the sample preparation that included closed containers and vacuum chambers, and the high vacuum achieved for XPS analysis, it is not expected that bulk oxygen is due to adsorbed moisture. (III) Nitrile hydrolysis typically requires basic or acidic solutions and high temperature, so it was unexpected, and confirmed by no presence of the functional group for the resulting carboxylic acid or carboxylate anion using FTIR analysis (Section 2.5.2). Worth considering, due to the surface sensitive nature of XPS and the different chemical structures, the measure of adsorbed moisture using the fully stabilized sample may not be representative of 150 ºC sample. Additionally, the inflated oxygen content could be due to the previously discussed oil.

Despite the large amount of pre-existing oxygen on the surface of the sample, XPS results followed the trends as observed in FTIR analysis. Between 150 and 250 ºC, the samples showed a 1 at-% increase in oxygen, which was attributed to ketone group development due to the small development in FTIR shoulder peaks associated with ketones (1660 and 1725 cm^{-1}).

The XPS measurement at 280 ºC$_{t=0\ min}$ appears to be an outlier, and made it difficult to track oxygen uptake using this measurement. Extrapolation between 250 and 280$_{t\ =\ 10\ min}$ ºC suggested an oxygen composition of ~13.5 at-% at 280$_{t\ =\ 0\ min}$ ºC, which indicated a 2 at-% increase in oxygen between 250 and 280$_{t\ =\ 0\ min}$ ºC. This is low compared to the 10-fold increase in FTIR based ketone peak area, but once again, XPS is limited to surface analysis while FTIR samples the entire sample volume. With isothermal treatment at 280 ºC, the surface oxygen content increases roughly 4 at-% over one hour isothermal and an additional 2 at-% over the following 2 hours. Using EDX, oxygen increased rapidly to 6 at-% through 30 minutes, where it slowly increased 1 at-% through the following 2.5 hours; oxygen content increased nearly 3 times over the course of the 3-hour isothermal hold, and ketone development determined by FTIR increased 4-times. This supports the notion that XPS analysis fails to account for sub-surface compositional changes associated with prolonged stabilization, and suggests that despite the narrow fiber diameter, composition develops continually throughout the three hours of stabilization.

Nitrogen analysis using XPS and EDX supported the evolution of nitrogen by oxydenitrogenation and HCN, or NH_3 production through chain scission.[1, 20] Following a similar stabilization procedure as in the current study, evolution of HCN and CO_2 were studied by Fitzer et al.[24] Maximum evolution rate of HCN occurred upon reaching 280 ºC, and trailed off through an hour of isothermal hold; CO_2 similarly peaked at 280 ºC, and decreased throughout the three-hour isothermal hold.

Using atomic ratios of EDX/XPS elemental analysis, carbon was consistently ‘oversampled’, and nitrogen and oxygen ‘undersampled’ using EDX compared to surface surface composition using XPS. With the exception of the outlier at 280$_{t\ =\ 0\ min}$ ºC, nitrogen was steady

until 60- and 180-minutes, where a decreasing surface concentration indicated removal of nitrogen through HCN and NH_3. Oxygen reached a plateau at 60- and 180-minutes, suggesting oxygen integration occurred equally at the surface and bulk with prolonged stabilization.

2.5.8. High Resolution Binding State Analysis Using XPS

Element binding state analysis was performed on polyacrylonitrile fibers stabilized by heating in air from room temperature at 2 ºC/min to 280 ºC, followed by a 3-hour isothermal hold (Table 2-9 and Figure 2-7). As mentioned, most oxygen is integrated onto the stabilized ladder structure in the form of C=O, and the analyzed fibers contained 26 at-% in the form of carbonyl (530.5 and 531.3 eV), and 42 at-% that can be attributed to carbonyls and more complex amides, esters, and anhydrides (532.5 eV). These latter groups are not expected to promote basal plane formation as readily as the more simple functionalities and, specifically, amides have been shown to retard cyclization;[13] over-oxidation could lead to poor yield and poor quality fibers. Nitrogen is divided between pyridine (398.5 eV) and a mix of pyrrole/lactam/imide/amide groups (400 eV). Carbon is predominantly found in –C=C– (284.8 eV) and carbonyl (288 eV) groups, accounting for nearly 72 at-%. The peak at 286.4 eV can be associated with C-OH, C-O-C, or C-N groups, so it is unclear whether this is cyclic nitrogen or oxygen groups; it is expected that this peak was representative of both ladder structures and some development of oxygenated groups.

The large proportion of C=O groups is not considered advantageous for carbonization, but a high resolution analysis was not conducted on the temperature series during stabilization due to expense, so no quantification can be made using XPS concerning the changing functional sites. Based on FTIR and compositional analysis, reduced stabilization time would reduce the

bulk oxygen content and likely reduce the proportion of C=O groups. Based on FTIR evidence, 30 minutes would substantially reduce the amount of ketones, though stabilizing through 1 hour improved cyclization and conjugation values.

2.5.9. Fiber Shrinkage: Chemical Reactions and Corresponding Dimensional Analysis

Chemical shrinkage is the result of cyclization and intermolecular crosslinking of adjacent chains. In addition to comonomers decreasing the activation energy of cyclization and crosslinking, they enhance molecular mobility and allow favorable nitrile alignment when subjected to tension during stabilization.[9] This, in turn, results in a higher amount of stress-free shrinkage during stabilization. Importantly, it is desirable to minimize shrinkage during stabilization to achieve high strength fibers,[49] and thus it appears that stress-free shrinkage capacity may provide insight into tension-stabilized strength; similarly, G. Olivé and S. Olivé[9] believed fibers with the highest constant-length shrinkage force would produce the best fibers.

Chemical reactions examined using FTIR are also associated with macroscopic changes of the polyacrylonitrile fiber, including weight loss (Figure 2-8), fiber diameter (Figure 2-9), and mat dimension (Figure 2-10). Fiber diameter and mat shrinkage are inherently linked and related to both physical and chemical processes, while weight loss is resultant of chemical reactions throughout stabilization. Through 150 ºC, no substantial chemical or physical processes occur with the exception of solvent removal. Figures 2-8/2-9 show 3.5% weight loss and fiber diameter contraction attributed to solvent-swelled fibers, where DMF was removed above its boiling point (153 ºC). Figure 2-10 shows the slight increase in strain through 150 ºC that is attributed to the

initiation of entropic molecular relaxation of amorphous chains above the glass transition (T_g = 150 ºC).

There is no reported reaction mechanism for PAN heated through 200 ºC, but molecular strain relaxation continued and was paired with a subtle increase in fiber diameter. Entropic relaxation was the predominant force through 215 ºC, which was reported as the T_m transition for a copolymer PAN fiber.[14] Fiber diameter continued to increase through 250 ºC, though above the glass transition the fiber mat started to contract. It appears as though the pre-cyclization relaxation causes the fiber diameter to increase a small margin, while the entire fiber mat follows shows higher sensitivity to initiation of cyclization between 200 and 220 ºC, which is consistent with other reports.[11] During the course of relaxation processes and initiation of cyclization, no measureable weight loss is detected.

Above 250 ºC and through 280 ºC, the rate of shrinkage/cyclization accelerated as measured by both strain and fiber diameter. Mat strain reaches -10%, and fiber diameters contract. This increase in nitrile reactions also results in 4% mass loss. Immediately upon reaching 280 ºC and initiating the isothermal hold, the rate of shrinkage started to decrease and reached a plateau at roughly 1-hour isothermal. Despite large-scale contraction slowing above reaching 280 ºC, both weight loss and fiber diameter decrease notably during the first 30 minutes, and mass loss continues steadily throughout stabilization. Both strain and fiber diameter reached a relatively steady-state value after 1 hour isothermal at 280 ºC, and prolonged treatment only appears to result in weight loss.

The plateau of bulk shrinkage occurs between 23-27%, which is consistent with reports of 25% shrinkage for stress-free isotactic chains.[36] Similarly, the fiber diameter decreased by 27%, suggesting shrinkage occurs both radially and axially along the fiber system; uniaxial

constraint would prevent axial shrinkage, perhaps in favor of radial fiber shrinkage to promote orientation along the fiber axis.

2.6. Summary of Findings and Conclusions

Thermal stabilization of homopolymer polyacrylonitrile (PAN) based electrospun fibers was studied using a variety of techniques in order to link the critically important chemical processes – cyclization and crosslinking – with both surface and bulk composition, as well as macro- and microscopic changes. Understanding the stabilization process is integral to creating high performance carbon fibers, and the current study was performed in an effort to optimize stabilization in hopes to improve bulk fiber properties, fiber yield, as well as the electrical properties important to current applications. Though not the primary focus of the thesis, this work was done in conjunction in order to provide future students some foundation in carbon fiber fabrication processes. The following is a summary of results from the temperature-series analyses.

1) Below 200 ºC, no chemical reactions occurred. FTIR analysis revealed solvent was not removed from the 500 nm electrospun fiber despite drying under vacuum at 70 ºC, and heating to 150 ºC was required to remove all solvent. Solvent removal was observed by gravimetric weight loss when heating through DMF's boiling point (153 ºC). The extended duration between electrospinning and stabilization could result in molecular relaxation and decreased orientation, which is an undesirable result. Solvent removal resulted in fiber diameter shrinkage, followed by small increases attributed to molecular relaxation above the glass transition. This was paired with a

small increase in mat strain, supporting molecular relaxation processes. Composition was not dramatically affected.

2) Between 200 and 250 ºC, FTIR analysis showed the initiation of cyclization, though small levels of crosslinking, conjugation, and oxygen integration also occurred. Oxygen uptake was supported by ketone development (FTIR) and XPS surface composition analysis, which highlighted a small increase in oxygen. Based on DMA results, cyclization is expected to occur around 215 ºC, the rough melting temperature for PAN crystallites and the peak strain. Higher temperatures resulted in shrinkage attributed to cyclization and crosslinking. Neither sample weight or fiber diameter was dramatically affected through 250 ºC.
3) The majority of reactions occurred between 250 and 280 ºC. Sample weight decreased several percent, paired with nearly 30 nm contraction in fiber diameter and over 10% sample shrinkage measured by DMA. Cyclization and conjugation reactions accelerated in this region, as demonstrated by FTIR analysis, and oxygen integration increased dramatically as measured on the surface (XPS) and in bulk (EDX). Crosslinking reached a maximum, attributed to increased rigidity of the PAN structure due to cyclization and conjugation.
4) Under isothermal conditions at 280 ºC, sample mass gradually decreased, paired with fiber diameter contraction and mat shrinkage. These processes occurred more rapidly within the first hour of isothermal hold, followed by relatively minimal changes for the following 2 hours. FTIR analysis showed similarly accelerated reaction through 280 ºC, followed by 60-minutes of sustained reaction, and 2 hours of minimal development. Compositional analysis exhibited similar trends. Continued

stabilization resulted in increased oxygen content and decreased nitrogen content, consistent with oxydenitrogenation, though over-oxidation hampers carbon fiber performance.

Given the results of the current study, it is suggested that fibers undergo a modified stabilization procedure consisting of 2 ºC/min to 280 ºC, followed by one-hour isothermal. Within one-hour at 280 ºC, the majority of favorable reactions occur, while extended stabilization only served to increase oxygen content and reduce stabilized fiber mat yield.

Furthermore, due to the more complete understanding of the fabrication process, other comprehensive suggestions can be made: 1) copolymer formulations could promote higher integrity fibers, 2) temperature and humidity controlled electrospinning environments could promote fiber drying and decrease molecular relaxation between spinning and stabilization, 3) and uniaxial fiber mats stabilized under tension could increase stabilized-orientation of polymer chains, improving fiber properties.

2.7. References

1. Morgan, P., *Carbon Fibers and Their Composites*. 1 ed.; CRC Press: 6000 Broken Sound Parkway NW, Suite 300
Boca Raton, FL 33487, 2005.

2. Leon y Leon, C. A.; O'Brien, R. A.; Dasarathy, H.; J.J., M.; Schimpf, W. C., In *Midwest Advanced Materials and Processes Conference*, The Society for the Advancement of Material and Process Engineering (SAMPE): Dearborn, MI, 2000.

3. Fitzer, E.; Muller, D. J., Influence of Oxygen on Chemical-Reactions During Stabilization of Pan as Carbon-Fiber Precursor. *Carbon* **1975,** 13, (1), 63-69.

4. Yu, M.; Wang, C.; Bai, Y.; Wang, Y.; Xu, Y., Influence of precursor properties on the thermal stabilization of polyacrylonitrile fibers. *Polymer Bulletin* **2006,** 57, (5), 757-763.

5. Dalton, S.; Heatley, F.; Budd, P. M., Thermal stabilization of polyacrylonitrile fibres. *Polymer* **1999,** 40, (20), 5531-5543.

6. Zhang, W. X.; Liu, J.; Wu, G., Evolution of structure and properties of PAN precursors during their conversion to carbon fibers. *Carbon* **2003,** 41, (14), 2805-2812.

7. Ouyang, Q.; Cheng, L.; Wang, H.; Li, K., Mechanism and kinetics of the stabilization reactions of itaconic acid-modified polyacrylonitrile. *Polymer Degradation and Stability* **2008,** 93, (8), 1415-1421.

8. Abhiraman, A. S. *Precursor Structure-Fiber Property Relationships in Polyacrylonitrile-Based Carbon Fibers*; Georgia Institute of Technology: 1990.

9. Olive, G. H.; Olive, S., The Chemistry of Carbon Fiber Formation from Polyacrylonitrile. In *Industrial Developments*, Springer: 1983; Vol. 51, pp 1-60.

10. Grove, D. A.; Abhiraman, A. S., A Mathematical-Model of Solid-State Thermooxidative Stabilization of Acrylic Fibers. *Carbon* **1992,** 30, (3), 451-457.

11. Bajaj, P.; Roopanwal, A. K., Thermal stabilization of acrylic precursors for the production of carbon fibers: An overview. *Journal of Macromolecular Science-Reviews in Macromolecular Chemistry and Physics* **1997,** C37, (1), 97-147.

12. Bajaj, P.; Sreekumar, T. V.; Sen, K., Thermal behaviour of acrylonitrile copolymers having methacrylic and itaconic acid comonomers. *Polymer* **2001,** 42, (4), 1707-1718.

13. Fochler, H. S.; Mooney, J. R.; Ball, L. E.; Boyer, R. D.; Grasselli, J. G., Infrared and Nmr Spectroscopic Studies of the Thermal-Degradation of Polyacrylonitrile. *Spectrochimica Acta Part a-Molecular and Biomolecular Spectroscopy* **1985,** 41, (1-2), 271-278.

14. Gupta, A.; Harrison, I. R., New aspects in the oxidative stabilization of pan-based carbon fibers. *Carbon* **1996,** 34, (11), 1427-1445.

15. Wu, G. P.; Lu, C. X.; Ling, L. C.; Hao, A. M.; He, F., Influence of tension on the oxidative stabilization process of polyacrylonitrile fibers. *Journal of Applied Polymer Science* **2005,** 96, (4), 1029-1034.

16. Sawai, D.; Yamane, A.; Kameda, T.; Kanamoto, T.; Ito, M.; Yamazaki, H.; Hisatani, K., Uniaxial drawing of isotactic poly(acrylonitrile): Development of oriented structure and tensile properties. *Macromolecules* **1999,** 32, (17), 5622-5630.

17. Wang, P. H., Aspects on prestretching of PAN precursor: Shrinkage and thermal behavior. *Journal of Applied Polymer Science* **1998,** 67, (7), 1185-1190.

18. Chen, J. C.; Harrison, I. R., Modification of polyacrylonitrile (PAN) carbon fiber precursor via post-spinning plasticization and stretching in dimethyl formamide (DMF). *Carbon* **2002,** 40, (1), 25-45.

19. Kumar, S.; Chae, H. G.; Minus, M.; Rasheed, A. *Stabilization and Carbonization of Gel Spun Polyacrylonitrile/Single Wall Carbon Nanotube Composite Fibers*; Georgia Institute of Technology: 2006.

20. Grassie, N.; McGuchan, R., Pyrolysis of Polyacrylonitrile and Related Polymers .3. Thermal Analysis of Preheated Polymers. *European Polymer Journal* **1971,** 7, (10), 1357-&.

21. Shimada, I.; Takahagi, T.; Fukuhara, M.; Morita, K.; Ishitani, A., Ft-Ir Study of the Stabilization Reaction of Polyacrylonitrile in the Production of Carbon-Fibers. *Journal of Polymer Science Part a-Polymer Chemistry* **1986,** 24, (8), 1989-1995.

22. Yu, M. J.; Wang, C. G.; Bai, Y. J.; Xu, Y.; Zhu, B., Effect of oxygen uptake and aromatization on the skin-core morphology during the oxidative stabilization of polyacrylonitrile fibers. *Journal of Applied Polymer Science* **2008,** 107, (3), 1939-1945.

23. Tsai, J.-S., The Relationship Between Oxidized Degree and Carbonization Temperature for Carbon Fibers. *SAMPE Journal* **1993,** 29, (5), 15-19.

24. Fitzer, E.; Frohs, W.; Heine, M., Optimization of Stabilization and Carbonization Treatment of Pan Fibers and Structural Characterization of the Resulting Carbon-Fibers. *Carbon* **1986,** 24, (4), 387-395.

25. Frenot, A.; Chronakis, I. S., Polymer nanofibers assembled by electrospinning. *Current Opinion in Colloid & Interface Science* **2003,** 8, (1), 64-75.

26. Huang, Z. M.; Zhang, Y. Z.; Kotaki, M.; Ramakrishna, S., A review on polymer nanofibers by electrospinning and their applications in nanocomposites. *Composites Science and Technology* **2003,** 63, (15), 2223-2253.

27. Jayaraman, K.; Kotaki, M.; Zhang, Y. Z.; Mo, X. M.; Ramakrishna, S., Recent advances in polymer nanofibers. *Journal of Nanoscience and Nanotechnology* **2004,** 4, (1-2), 52-65.

28. Reneker, D. H.; Yarin, A. L.; Fong, H.; Koombhongse, S., Bending instability of electrically charged liquid jets of polymer solutions in electrospinning. *Journal of Applied Physics* **2000,** 87, (9), 4531-4547.

29. Fennessey, S. F.; Farris, R. J., Fabrication of aligned and molecularly oriented electrospun polyacrylonitrile nanofibers and the mechanical behavior of their twisted yams. *Polymer* **2004,** 45, (12), 4217-4225.

30. Dersch, R.; Liu, T. Q.; Schaper, A. K.; Greiner, A.; Wendorff, J. H., Electrospun nanofibers: Internal structure and intrinsic orientation. *Journal of Polymer Science Part a-Polymer Chemistry* **2003,** 41, (4), 545-553.

31. Zussman, E.; Chen, X.; Ding, W.; Calabri, L.; Dikin, D. A.; Quintana, J. P.; Ruoff, R. S., Mechanical and structural characterization of electrospun PAN-derived carbon nanofibers. *Carbon* **2005,** 43, (10), 2175-2185.

32. Takaku, A.; Hashimoto, T.; Miyoshi, T., Tensile Properties of Carbon-Fibers from Acrylic Fibers Stabilized under Isothermal Conditions. *Journal of Applied Polymer Science* **1985,** 30, (4), 1565-1571.

33. Kinoshita, Y. High Tensile Strength, High Young's Modulus Carbon Fiber Having Excellent Internal Structure Homogeneity, and Process for Producing the Same. 1976.

34. Saito, K.; Ogawa, H. Process for producing carbon fibers. 1976.

35. Zhu, Y.; Wilding, M. A.; Mukhopadhyay, S. K., Estimation, using infrared spectroscopy, of the cyclization of poly(acrylonitrile) during the stabilization stage of carbon fibre production. *Journal of Materials Science* **1996,** 31, (14), 3831-3837.

36. Simitzis, J.; Soulis, S., Correlation of chemical shrinkage of polyacrylonitrile fibres with kinetics of cyclization. *Polymer International* **2008,** 57, (1), 99-105.

37. Deurbergue, A.; Oberlin, A., Stabilization and Carbonization of Pan-Based Carbon-Fibers as Related to Mechanical-Properties. *Carbon* **1991,** 29, (4-5), 621-628.

38. Zhou, Z. P.; Lai, C. L.; Zhang, L. F.; Qian, Y.; Hou, H. Q.; Reneker, D. H.; Fong, H., Development of carbon nanofibers from aligned electrospun polyacrylonitrile nanofiber bundles and characterization of their microstructural, electrical, and mechanical properties. *Polymer* **2009,** 50, (13), 2999-3006.

39. Zhou, Z. P.; Liu, K. M.; Lai, C. L.; Zhang, L. F.; Li, J. H.; Hou, H. Q.; Reneker, D. H.; Fong, H., Graphitic carbon nanofibers developed from bundles of aligned electrospun polyacrylonitrile nanofibers containing phosphoric acid. *Polymer* **2010,** 51, (11), 2360-2367.

40. Luo, X.; Mather, P. T., Conductive shape memory nanocomposites for high speed electrical actuation. *Soft Matter* **2010,** 6, (10), 2146-2149.

41. Xue, T. J.; McKinney, M. A.; Wilkie, C. A., The thermal degradation of polyacrylonitrile. *Polymer Degradation and Stability* **1997,** 58, (1-2), 193-202.

42. Leroy, S.; Boiziau, C.; Perreau, J.; Reynaud, C.; Zalczer, G.; Lecayon, G.; Legressus, C., Molecular-Structure of an Electropolymerized Polyacrylonitrile Film and Its Pyrolyzed Derivatives. *Journal of Molecular Structure* **1985,** 128, (4), 269-281.

43. Issam, A. M.; Ismail, J., Improvement of thermal stability of new heteroaromatic poly(azomethine urethane)s. *Journal of Applied Polymer Science* **2006,** 100, (2), 1198-1204.

44. Wu, X.-p.; Zhang, X.-l.; Lu, C.-x.; Ling, L.-c., Thermo-Chemical Reactions and Structural Evolution of Acrylamide-Modified Polyacrylonitrile. *Chinese Journal of Polymer Science* **2010,** 28, (3), 367-376.

45. Wu, M. Y.; Wang, Q. Y.; Li, K. N.; Wu, Y. Q.; Liu, H. Q., Optimization of stabilization conditions for electrospun polyacrylonitrile nanofibers. *Polymer Degradation and Stability* **2012,** 97, (8), 1511-1519.

46. Collins, G. L.; Thomas, N. W.; Williams, G. E., Kinetic Relationships between Heat-Generation and Nitrile Consumption in the Reaction of Poly(Acrylonitrile) in Air at 265-Degrees-C. *Carbon* **1988,** 26, (5), 671-679.

47. Instruments, P. G.-T., PGT Germanium and Silicon X-Ray Detectors. In.

48. Zander, N. E.; Strawhecker, K. E.; Orlicki, J. A.; Rawlett, A. M.; Beebe, T. P., Coaxial Electrospun Poly(methyl methacrylate)-Polyacrylonitrile Nanofibers: Atomic Force Microscopy and Compositional Characterization. *Journal of Physical Chemistry B* **2011,** 115, (43), 12441-12447.

49. Gupta, A.; Harrison, I. R., New aspects in the oxidative stabilization of PAN-based carbon fibers .2. *Carbon* **1997,** 35, (6), 809-818.

50. Xie, Y. M.; Sherwood, P. M. A., X-Ray Photoelectron Spectroscopic Studies of Carbon-Fiber Surfaces .11. Differences in the Surface-Chemistry and Bulk Structure of Different Carbon-Fibers Based on Poly(Acrylonitrile) and Pitch and Comparison with Various Graphite Samples. *Chemistry of Materials* **1990,** 2, (3), 293-299.

51. He, J. M.; Huang, Y. D., Effect of silane-coupling agents on interfacial properties of CF/PI composites. *Journal of Applied Polymer Science* **2007,** 106, (4), 2231-2237.

52. Palencia, C.; Rubio, F.; Merino, C.; Rubio, J.; Oteo, J. L., Study of the Silanization Process in CNFs: Time, Temperature, Silane Type and Concentration Influence. *Journal of Nano Research* **2008,** 4, 33-43.

53. Palencia, C.; Rubio, J.; Rubio, F.; Fierro, J. L. G.; Oteo, J. L., Silane Coupling Agent Structures on Carbon Nanofibers. *Journal of Nanoscience and Nanotechnology* **2011,** 11, (5), 4142-4152.

54. Lakshminarayanan, P. V.; Toghiani, H.; Pittman, C. U., Nitric acid oxidation of vapor grown carbon nanofibers. *Carbon* **2004,** 42, (12-13), 2433-2442.

55. Yue, Z. R.; Jiang, W.; Wang, L.; Gardner, S. D.; Pittman, C. U., Surface characterization of electrochemically oxidized carbon fibers. *Carbon* **1999,** 37, (11), 1785-1796.

56. Pamula, E.; Rouxhet, P. G., Bulk and surface chemical functionalities of type IIIPAN-based carbon fibres. *Carbon* **2003,** 41, (10), 1905-1915.

57. Takahagi, T.; Shimada, I.; Fukuhara, M.; Morita, K.; Ishitani, A., Xps Studies on the Chemical-Structure of the Stabilized Polyacrylonitrile Fiber in the Carbon-Fiber Production Process. *Journal of Polymer Science Part a-Polymer Chemistry* **1986,** 24, (11), 3101-3107.

Table 2-1. Inherent issues to precursor fiber stabilization and carbonization, adopted from Fitzer et al.[24] Small diameter fibers can reduce issues such as oxygen diffusion into the fiber core, providing faster and more uniform stabilization.

Stabilization	Mass Transport	• Diffusion of O_2 into fiber for dehydrogenation • Volatiles produced (HCN, NH_3, H_2O)
	Heat Transport	• Overheating of fiber due to exothermic cyclization
	Shrinkage	• Should be inhibited
Carbonization	Mass Transport	• Volatiles (HCN, H_2O, CO, CO_2, CH_4, N_2)
	Heat Transport	• Facilitated by thermal conductivity of fiber
	Shrinkage	• Mainly cross-sectionally

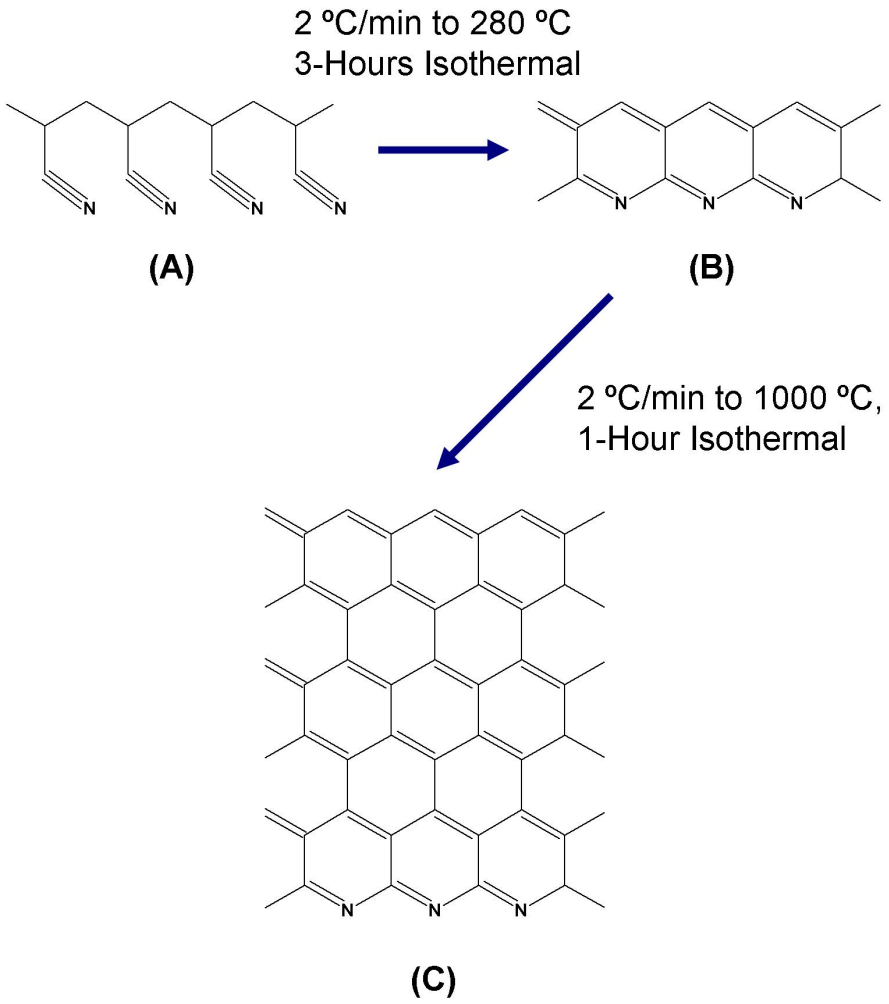

Scheme 2-1. Idealized chemical structural development of PAN with heat treatment. (A) Electrospun homopolymer PAN was (B) stabilized in air heated at 2 ºC/min to 280 ºC with 3-hours isothermal, and (C) further pyrolized in a nitrogen environment by heating at 2 ºC/min to 1000 ºC followed by 1-hour isothermal.

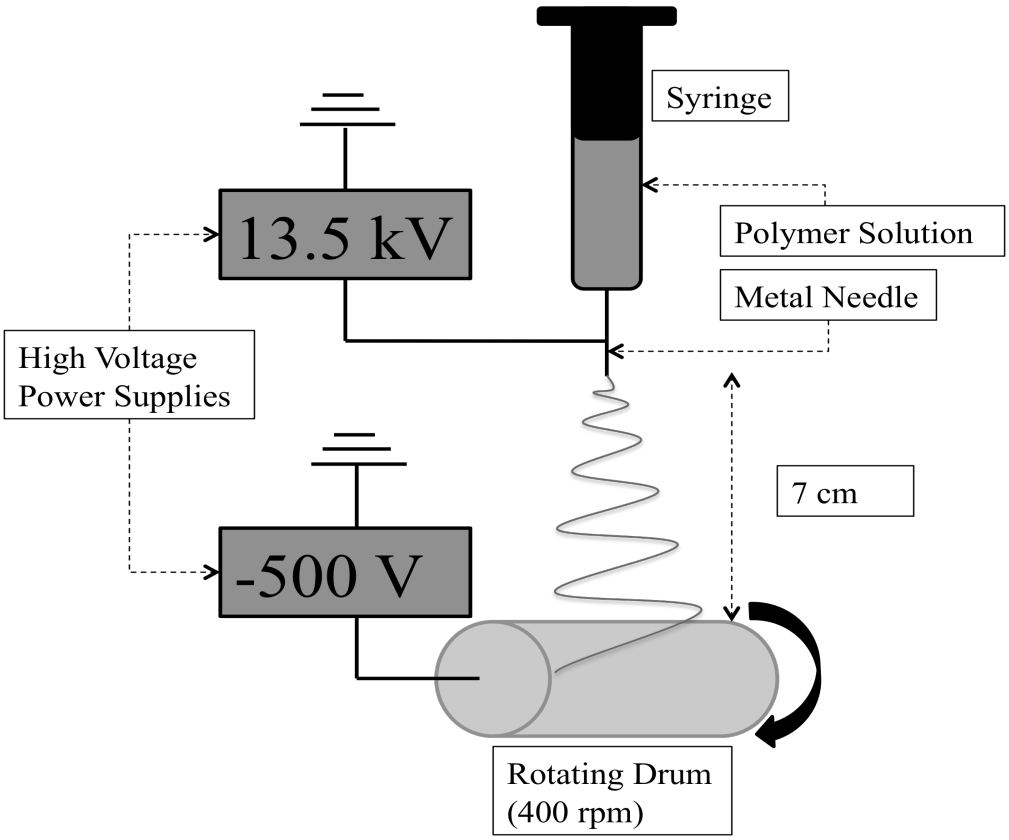

Figure 2-1. Electrospinning setup used for fabrication of polyacrylonitrile (PAN) precursor fiber. A syringe containing a solution of 1 g PAN dissolved in 10 ml DMF was connected to a syringe pump flowing at 1 ml/h. A 20 G needle with the beveled tip removed was charged at 13.5 kV and placed 7 cm in distance from a colleting drum charged with a reverse bias of -500 V. The collector was a 4 cm diameter, 15.4 cm long drum rotating at 400 rpm and translating 8 cm to create a mat roughly 15.4 x 25.1 cm. The syringe needle was on axis with the drum, and each mat was electrospun for 6 hours (6 ml).

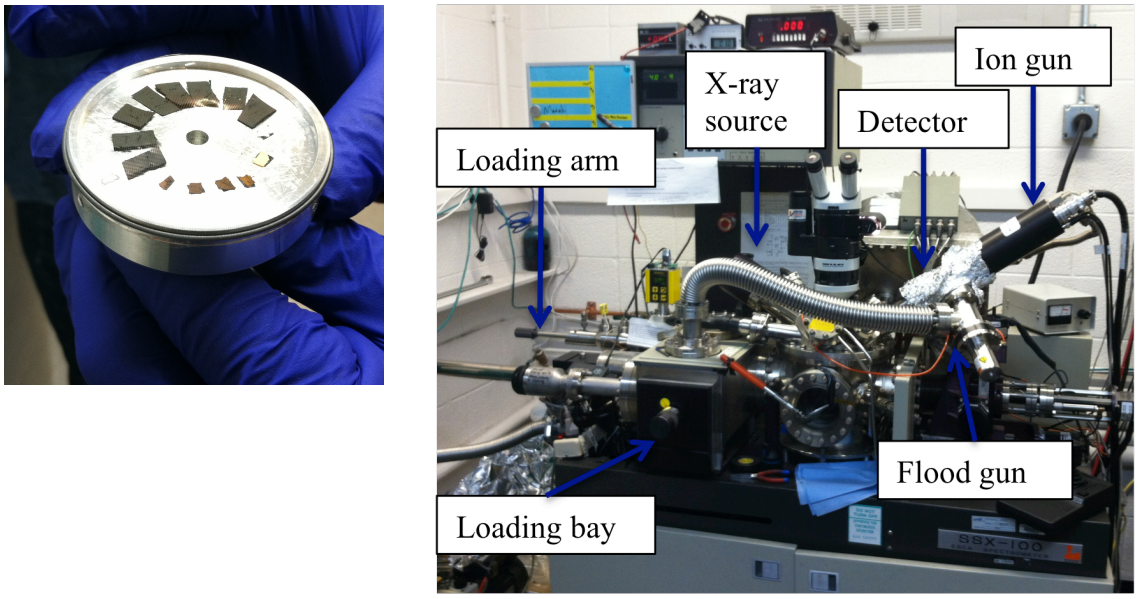

Figure 2-2. X-ray photoelectron spectroscopy setup, including (left) a sample mount of carbon fibers and series-stabilized fibers, and (right) layout of SSX-100 (Cornell University, Ithaca, NY).

Table 2-2. Equipment parameters used during XPS acquisition. Survey scans are used for higher counts and more precise composition measurements, while element site scans provide resolution necessary to determine chemical binding states.

XPS Equipment Constants:			
Source, Al (K_α) (eV)		1486.6	
Spot Size (um) / Power (W)		800 / 200	
Dwell Time (s)		0.25	
Source / Detector Angle (°)		75 / 55	
	Variables:	**Survey Scans**	**Site Scans**
Pass Energy Filter (eV)		150	50
Resolution (eV)		4	2
eV/step		1	0.065
Width (eV)		-	22
Scans (#)	**Survey (Composition)**	5	-
	Carbon (1s, 285 eV)	-	8
	Nitrogen (1s, 400 eV)	-	20
	Oxygen (1s, 533 eV)	-	12

Table 2-3. Fitting parameters and group designations used for analysis of XPS spectra using OriginPro 8.6. Shirley-spline backgrounds were subtracted, and the FWHM of each peak was limited to parenthetical values. Fitting iterations were performed until convergence to a Chi-squared tolerance of 10^{-9} or less. Functional group binding energies were selected based on previous XPS analysis of carbons and silanized materials.[45, 50-57]

Peak Fitting Constants:			
Background	**Shirley-Spline**		
Gaussian:Lorentzian Ratio	**70:30 (*m* = 0.3)**		
Variables:			
Element (FWHM Bounds, eV)	**Peak**	**Center (eV)**	**Group Assignment**
Carbon 1s	I	284.8	-C=C- (sp^2/sp^3), C-H
(1.6 – 2)	II	286.5	C-OH, C-O-C, C-N (Phenol, alcohol, ether)
	III	288.8	C=O, C=N (Carbonyl, quinone, carboxyl, ester)
	IV	289.2	COOH, COOR (Carboxyl, Carbonate)
	V	291	C-C Shakeup/Satellite
Nitrogen 1s	I	398.5	Pyridine, Ar-N-Ar
(1.8 – 2.2)	II	400	-NH, -O-C=N (Pyrrole, pyridine, lactam, imide, amide, amine)
	III	401	N-quaternary
	IV	403	Pyridine-N-Oxide
	V	405	NOx, N-O-C
Oxygen 1s	I	530.5	O=C (Carbonyl, carbonate)
(1.5 – 1.9)	II	531.3	O=C (Quinone, carbonyl, carboxyl)
	III	532.5	C=O-H, C=O-C (Amide, ester, hydroxyl, anhydride)
	IV	533	C-O-C (Carboxyl, phenol, ester, anhydride)
	V	534.5	Chemisorbed oxygen
Silicon 2p	I	102.3	Si-O_2 (Si-C), Si-N
(1.5 – 1.9)	II	103.5	Si-O_2 (Silica)

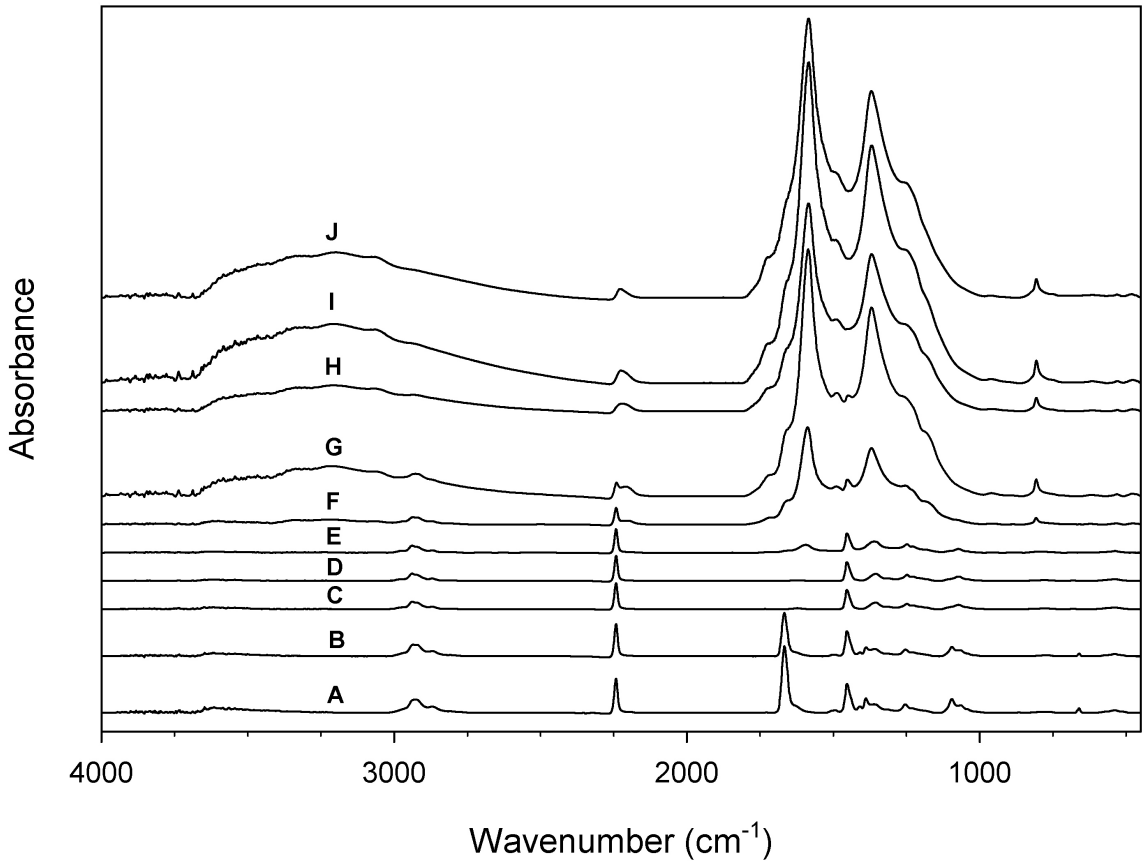

Figure 2-3. Transmission FTIR spectra of 1 ml of electrospun fiber mat from a polyacrylonitrile the standard solution (1 g PAN/10 ml DMF). (A) As-spun PAN, (B) dried at 70 ºC, and samples heated at 2 ºC/min to: (C) 150 ºC, (D) 200 ºC, (E) 250 ºC, and (F) $280_{t = 0\ min}$ ºC. Further samples were held isothermally: (G) $280_{t = 10\ min}$ ºC, (H) $280_{t = 30\ min}$ ºC, (I) $280_{t = 60\ min}$ ºC, and (J) $280_{t = 180\ min}$ ºC.

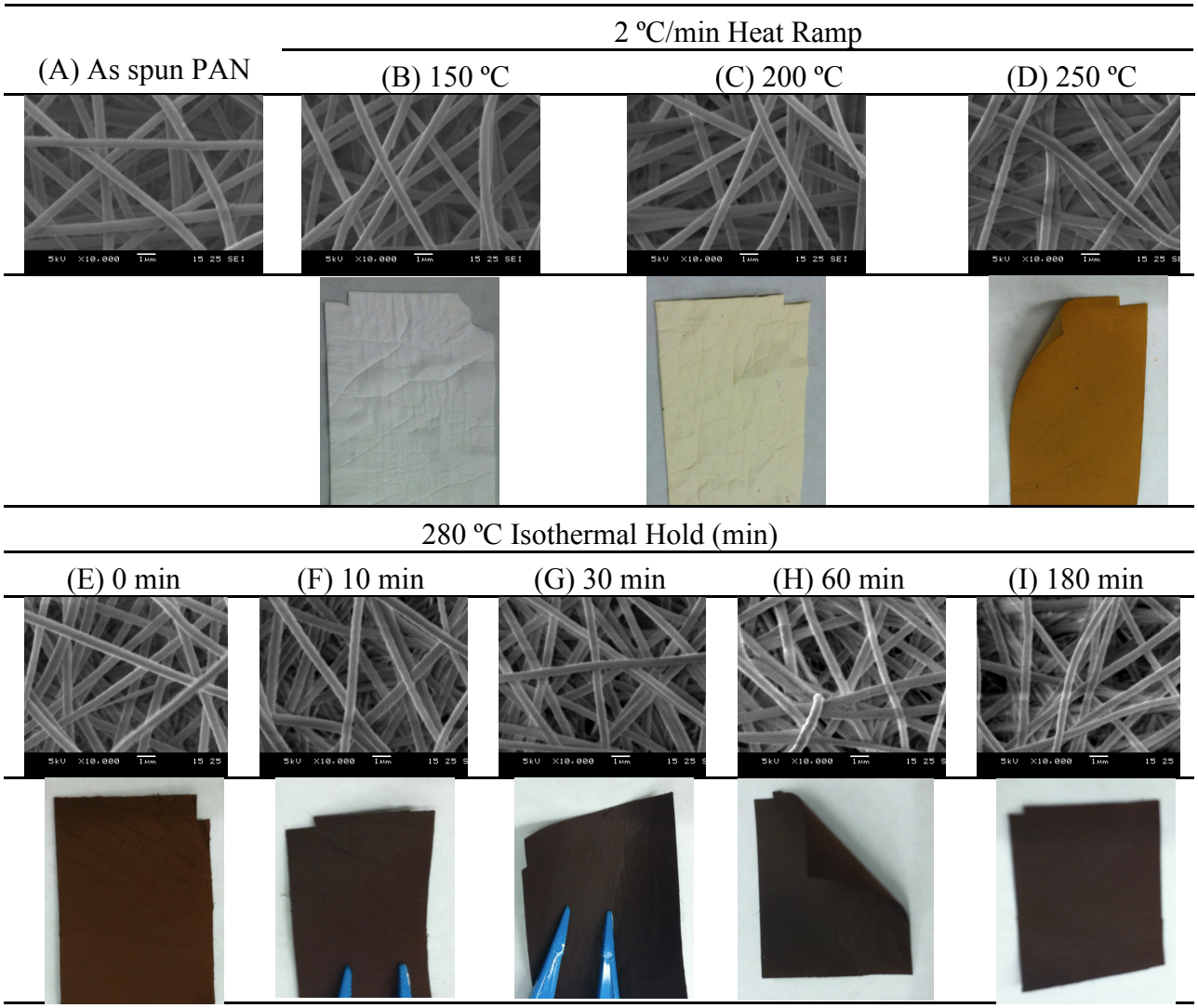

Figure 2-4. Polyacrylonitrile stabilized tension free under in air at 2 °C/min to 280 °C, followed by a 3 hour isothermal hold. Scanning electron microscope (SEM) images and standard photos are provided for: (A) as spun PAN, and samples heated at 2 ºC/min to: (B) 150 ºC, (C) 200 ºC, (D) 250 ºC, and (E) $280_{t = 0\ min}$ ºC. Further samples were held isothermally: (F) $280_{t = 10\ min}$ ºC, (G) $280_{t = 30\ min}$ ºC, (H) $280_{t = 60\ min}$ ºC, and (I) $280_{t = 180\ min}$ ºC. Curling of later samples is due to the shrinkage processes that sometimes occurred unevenly between the two sides of the fiber mat.

Table 2-4. Notable groups present in polyacrylonitrile (PAN) stabilization.[13, 21, 41, 42, 44] *Bands at 1580 and 1620 cm^{-1} are distinct for C=N, C=C, CH and aromatic respectively, but these collapse into one peak at 1595 cm^{-1} as aromatic content increases.[13]

Peak Fitting Constants:			
Background	Constant		
Gaussian:Lorentzian Ratio	70:30		
FWHM (cm^{-1})	< 150		
Peak Assignments:			
Wavenumber (cm^{-1})	**Group**	**Form**	**Associated Reaction**
3340	NH_2	Amide	
3225	NH	Acridone, Amide	
3200	NH, C=O, COOH	Amine, Carboxylic	
2940	CH/CH_2	Alkene, DMF	
2240	C≡N	Nitrile/PAN	
2210-2220	C≡N	Conjugated Nitrile	Dehydogenation
1725	C=O	Aliphatic (Naphthridine) Ketone Aliphatic Keto	Nitrile Cyclization, Oxygen Integration
1660	C=O	Conjugated (Acridone) Ketone	Dehydrogenation, Nitrile cyclization, Oxygen Integration
1595*	C=C, C=N, CH	Aromatic	Nitrile cyclization
1495	CH	Terminal Vinyl	Segmentation of PAN
1460	CH/CH_2	DMF/PAN	
1365	C=N, CH/CH_2, CH_3	Terminal Vinyl, Partially Nitrogenated Rings	Cyclization, Segmentation of PAN
1360	CH/CH_2	DMF/PAN	
1260	CH/CH_2	DMF/PAN	
1250	C-N, C-C	Partially Nitrogenated Rings	Cyclization
1190	C=N	Azomethine	Crosslinking
1070	CH/CH_2	DMF/PAN	
770-810	C=C-H	Aromatic Ring, Disubstituted Benzene	Cyclization

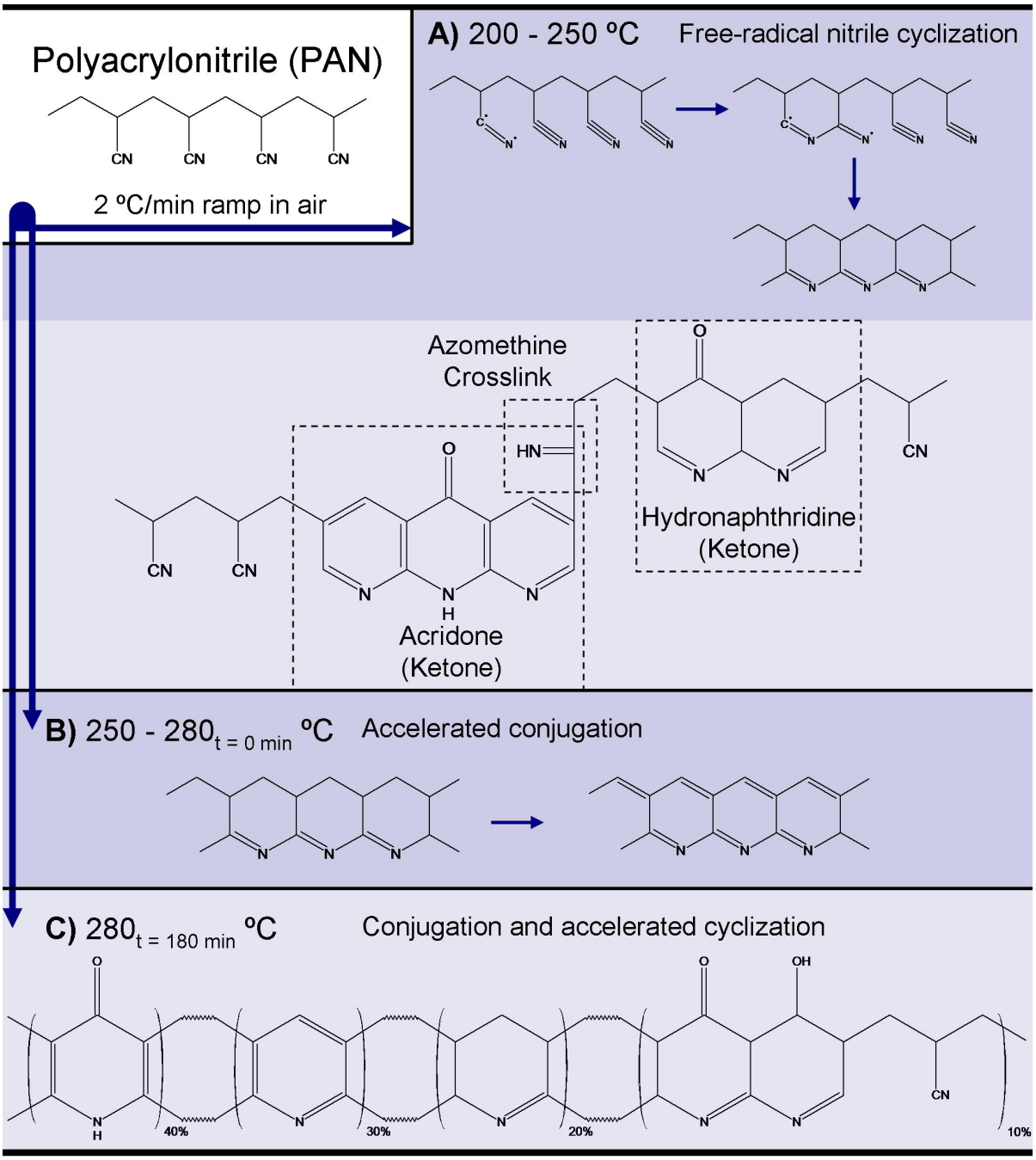

Scheme 2-2. Development of linear polyacrylonitrile (PAN) into a stable ladder and crosslinked structure. Temperature regimes highlight primary reactions, though the final structure has a mix of these components, and reactions are occurring simultaneously. A) Lower temperature reactions primarily include free radical cyclization, oxygen integration in the form of ketones, and suspected azomethine crosslinking. B) Intermediate temperature accelerates

dehydrogenation. C) Long term stabilization in results in high levels of cyclization, conjugation, and oxygen integration. A commonly cited stabilized form is also presented.[57]

Table 2-5. Select FTIR peak areas as fit using OriginPro 8.6, Gaussian line shape, and FWHM < 150 cm^{-1}. Peaks associated with DMF and linear PAN were not included.

				280 °C Isothermal Hold (time)				
Wavenumber (cm^{-1})	**150 °C**	**200 °C**	**250 °C**	**0 min**	**10 min**	**30 min**	**60 min**	**180 min**
760-810	-	-	0.97	2.4	2.0	3.5	3.1	0.97
1070	-	1.2	0.97	-	-	-	-	-
1190	-	-	0.27	8.4	23.8	22.9	27.7	37.3
1250	-	2.0	3.6	20.4	57.2	45.4	59.4	66.7
1365	-	1.6	4.4	34.2	87.2	81.0	106.8	126.2
1460	-	2.0	1.9	1.5	1.8	0.94	-	-
1495	-	-	1.4	26.9	73.2	55.9	78.6	82.6
1595	-	-	2.2	26.9	73.1	71.3	101.9	116.3
1660	-	-	0.48	5.7	15.7	13.9	22.2	21.6
1725	-	-	0.11	1.8	6.8	8.4	14.3	14.3
2210	-	-	-	1.4	3.3	2.4	3.3	1.9
2240	2.0	1.9	1.6	1.2	0.98	0.21	0.14	0.09

Table 2-6. Conversion indexed based on FTIR peak areas were used to determine reaction progress during stabilization, focusing on the predominant cyclization and crosslinking reactions. At longer stabilization times, these indexes change less dramatically due to the reaction nearing completion and less capability due to the rigid backbone resulting from conjugation and cyclization.

Conversion Index (%)			**280 °C Isothermal Hold (time)**				
	200 °C	**250 °C**	**0 min**	**10 min**	**30 min**	**60 min**	**180 min**
$CI_{Cyclization}$	-	25.2	28.0	75.0	83.3	88.8	89.6
$CI_{Conjugation}$	-	-	54.6	77.0	91.9	96.0	95.4
$CI_{Crosslink}$	-	10.9	23.9	24.5	24.3	21.4	24.3

Table 2-7. Surface composition and atomic ratios determined using XPS. Samples were heated in air at 2 ºC/min from room temperature to 280 ºC, followed by 3 hours isothermal.

			280 °C Isothermal Hold (time)			
Element (at-%)	**150 °C**	**250°C**	**0 min**	**10 min**	**60 min**	**180 min**
C	75.3	73.2	71.4	70.5	69.1	67.4
N	14.8	15.9	9.90	14.6	13.5	13.1
O	9.85	10.9	18.7	15.0	17.4	19.5
Element Ratios						
N/C	0.197	0.217	0.139	0.207	0.195	0.194
O/C	0.131	0.149	0.262	0.213	0.252	0.288

Table 2-8. Bulk composition and atomic ratios determined using EDX. Samples were heated in air at 2 ºC/min from room temperature to 280 ºC, followed by 3 hours isothermal.

					280 °C Isothermal Hold (time)				
Element (at-%)	**Dried**	**150 °C**	**200°C**	**250°C**	**0 min**	**10 min**	**30 min**	**60 min**	**180 min**
C	95.7	94.9	94.8	95.3	92.1	91.3	89.0	88.4	88.1
N	4.3	5.1	5.2	4.7	5.5	5.0	5.1	5.3	5.0
O	-	-	-	-	2.5	3.7	6.0	6.2	6.9
Element Ratios									
N/C	0.045	0.054	0.055	0.049	0.060	0.055	0.057	0.060	0.057
O/C	-	-	-	-	0.027	0.041	0.067	0.070	0.078

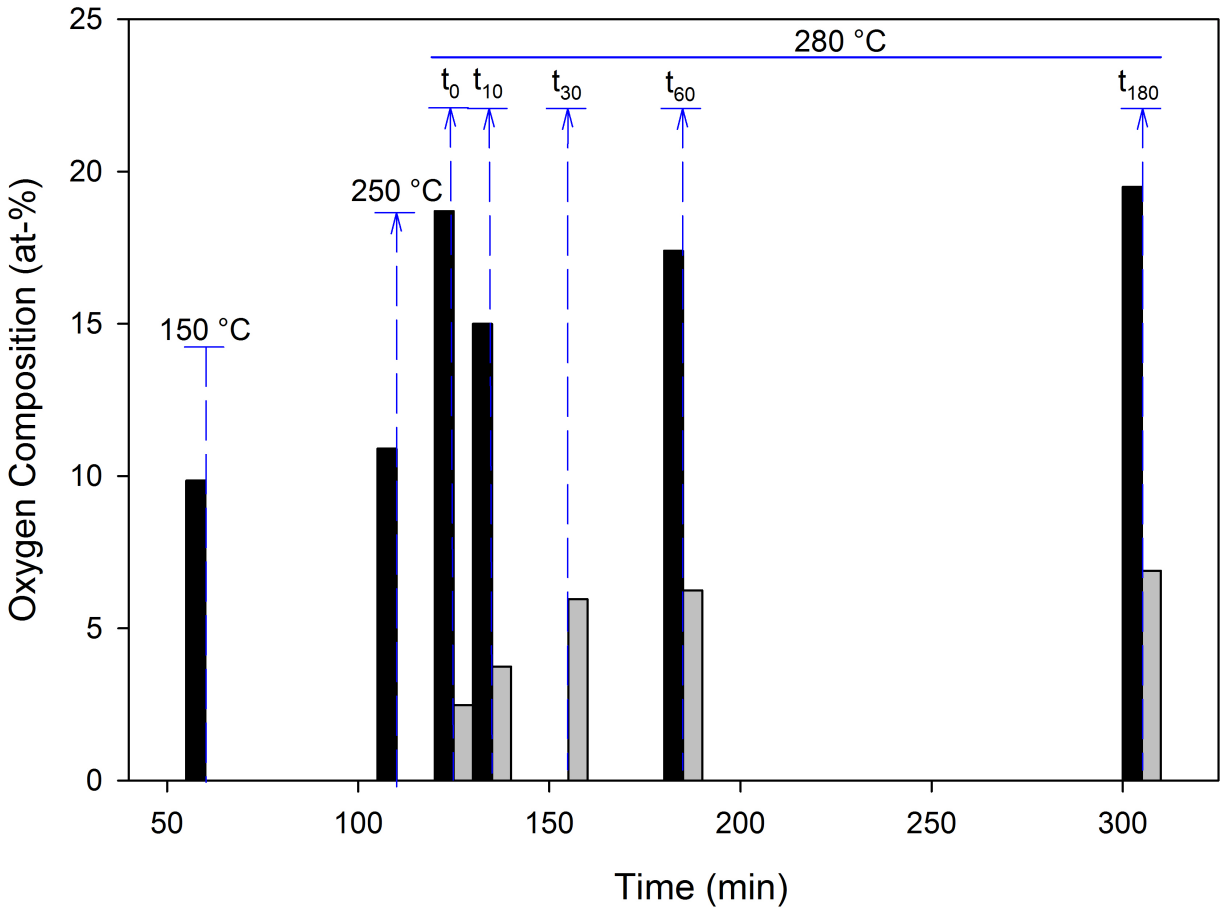

Figure 2-5. Comparison of oxygen content via XPS (black) and EDX (grey). XPS is a surface sensitive technique and only detects composition on the most superficial 10 nm, while EDX detects composition from the entire sample with reduced accuracy due to limited signal for low *Z*-elements. The $280_{t = 0\ min}$ °C time point (XPS) is considered an outlier due to results inconsistent with trends and EDX results.

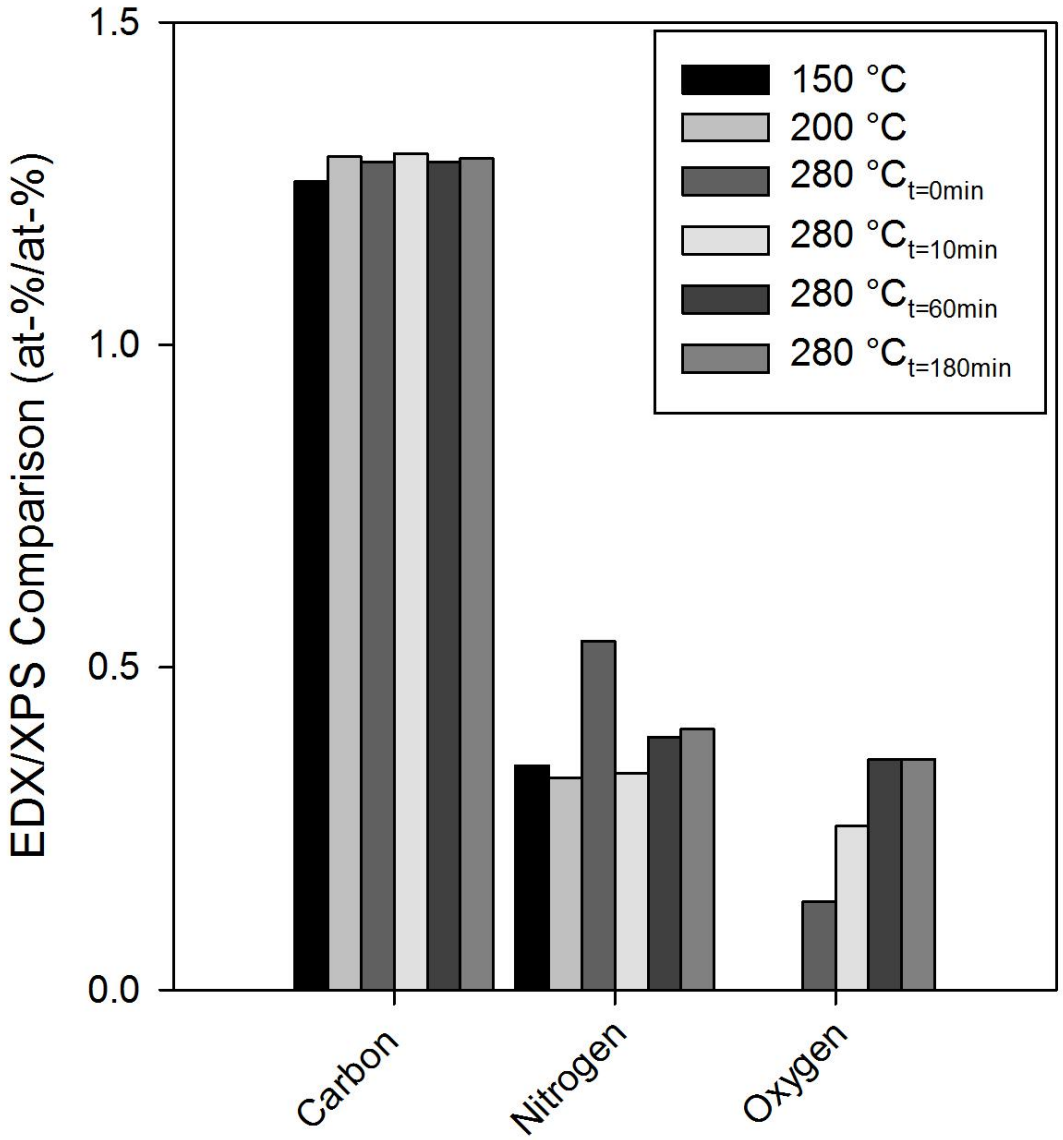

Figure 2-6. Atomic ratios of composition determined using EDX and XPS are used to understand the difference between bulk and surface compositions. XPS is superior to EDX in precision and accuracy for low-*Z* elements, but is limited to surface composition. The $280_{t = 0\ min}$ °C time point is considered an outlier, and trends are extrapolated from other samples.

Table 2-9. Peak fitting for a polyacrylonitrile mat stabilized for 3 hours at 280 ºC, where total carbon, nitrogen, and oxygen content were 67.4 at-%, 13.1 at-%, and 19.5 at-%, respectively determined by survey scans.

Element (Surface Composition at-%)	Peak	BE (eV)	Element Percentage (%)	Normalized Percentage (%)
Carbon (67.4 at-%)	I	284.6	56.8	38.3
	II	286.4	25.9	17.5
	III	287.8	14.9	10.0
	IV	289.4	2.3	1.6
	V	291	0.16	0.11
Nitrogen (13.1 at-%)	I	389.5	53.2	7.0
	II	399.6	46.8	6.1
Oxygen (19.5 at-%)	I	530.3	5.2	1.0
	II	531.1	20.8	4.1
	III	532	42.2	8.2
	IV	533.4	24.3	4.7
	V	535.2	7.5	1.5

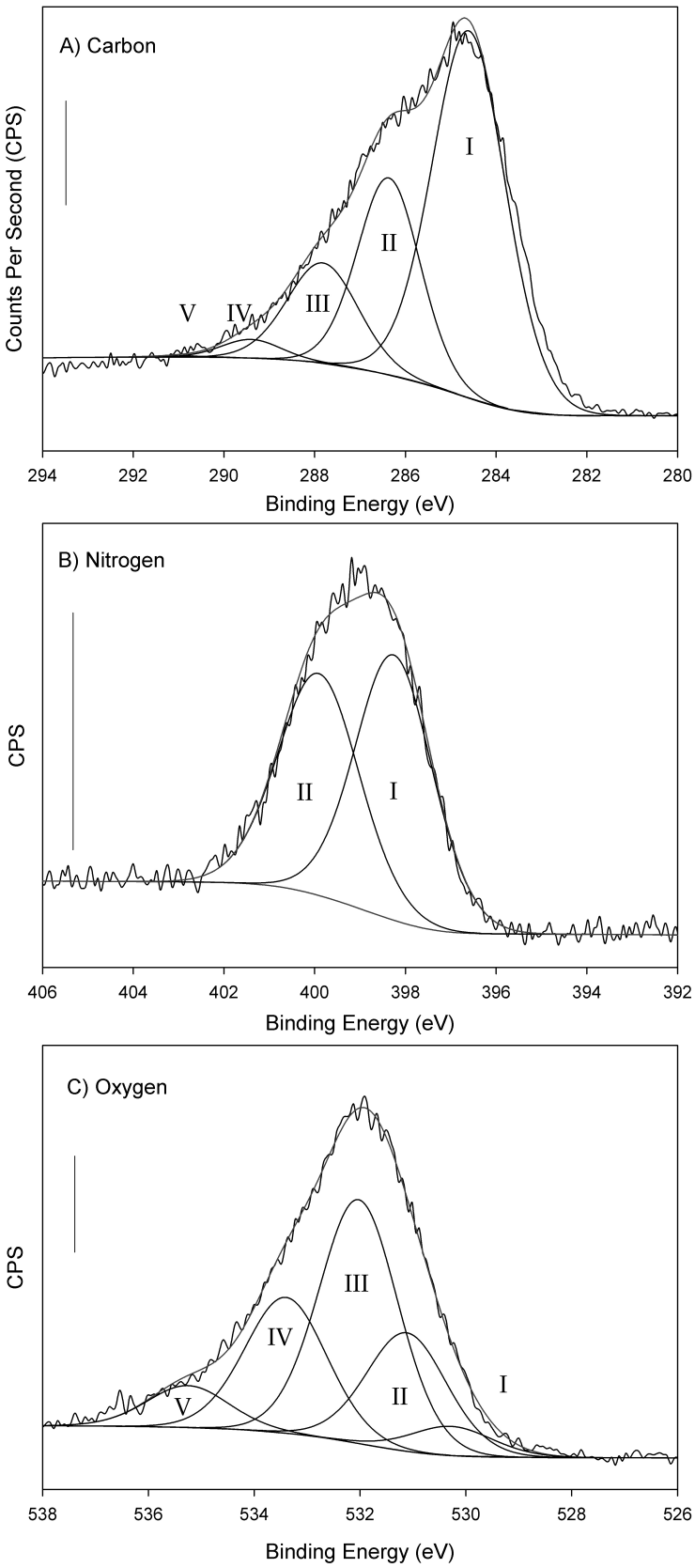

Figure 2-7. XPS analysis of polyacrylonitrile (PAN) fibers heated in air at 2 ºC/min to 280 ºC, and held isothermally for 3 hours. Scale bars measure 200 counts per second. Shirley backgrounds were subtracted. Carbon (A), nitrogen (B), and oxygen (C) peaks are fit with Gaussian(70)-Lorentzian(30) product functions, where peak centers floated around +/- 0.3 eV from designated centers, and FWHM were fixed at 1.6-2, 1.8-2.2, and 1.5-1.9 for carbon, nitrogen, and oxygen, respectively. Roman numerals designate peaks provided in Table 2-3.

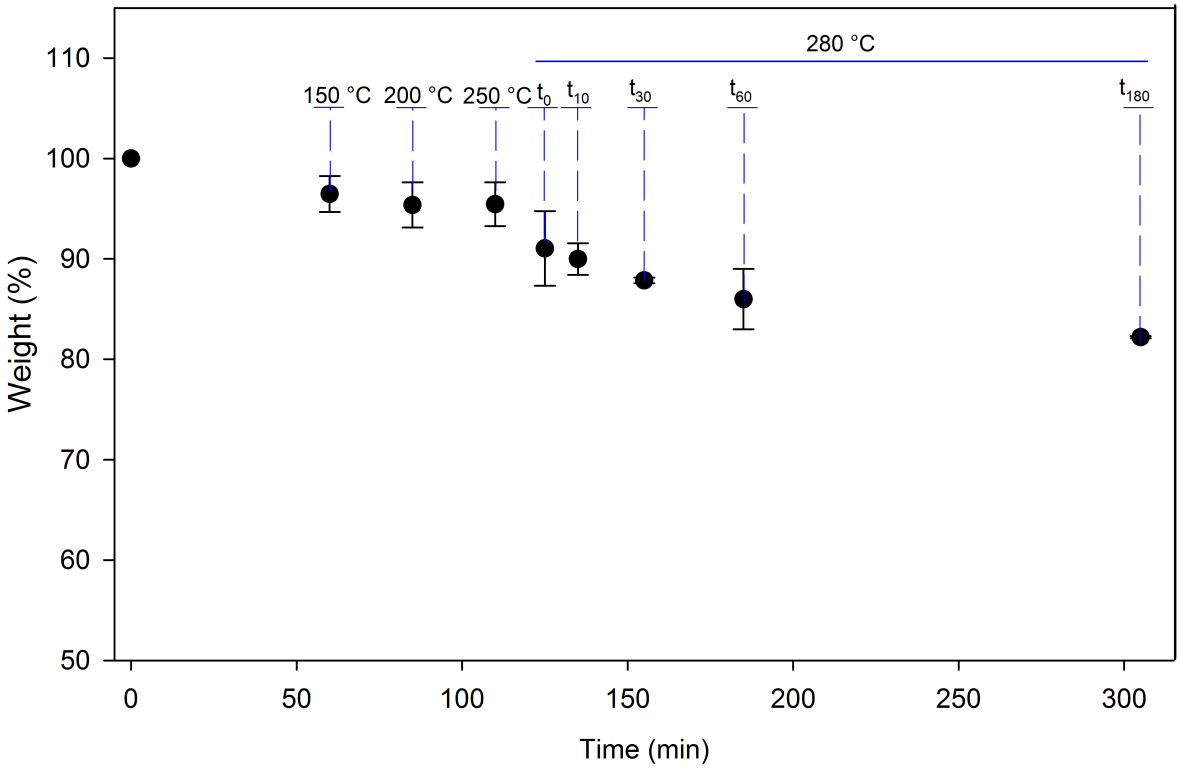

Figure 2-8. Effect of temperature on weight during stabilization in air with a temperature ramp of 2 °C/min to 280 °C, followed by 3 hours isothermal. Data points are averages of $n = 2$, and plotted with standard error. Initial weight loss was due to solvent removal, followed by: 4% between 250 °C and $280_{t = 0 \text{ minutes}}$ °C, and 1%, 2%, 2%, and 3.8% following isothermal holds for 10, 30, 60, and 180 minutes. Weight loss is variously attributed to polymer degradation, chain scission, dehydrogenation, and denitrogenation.

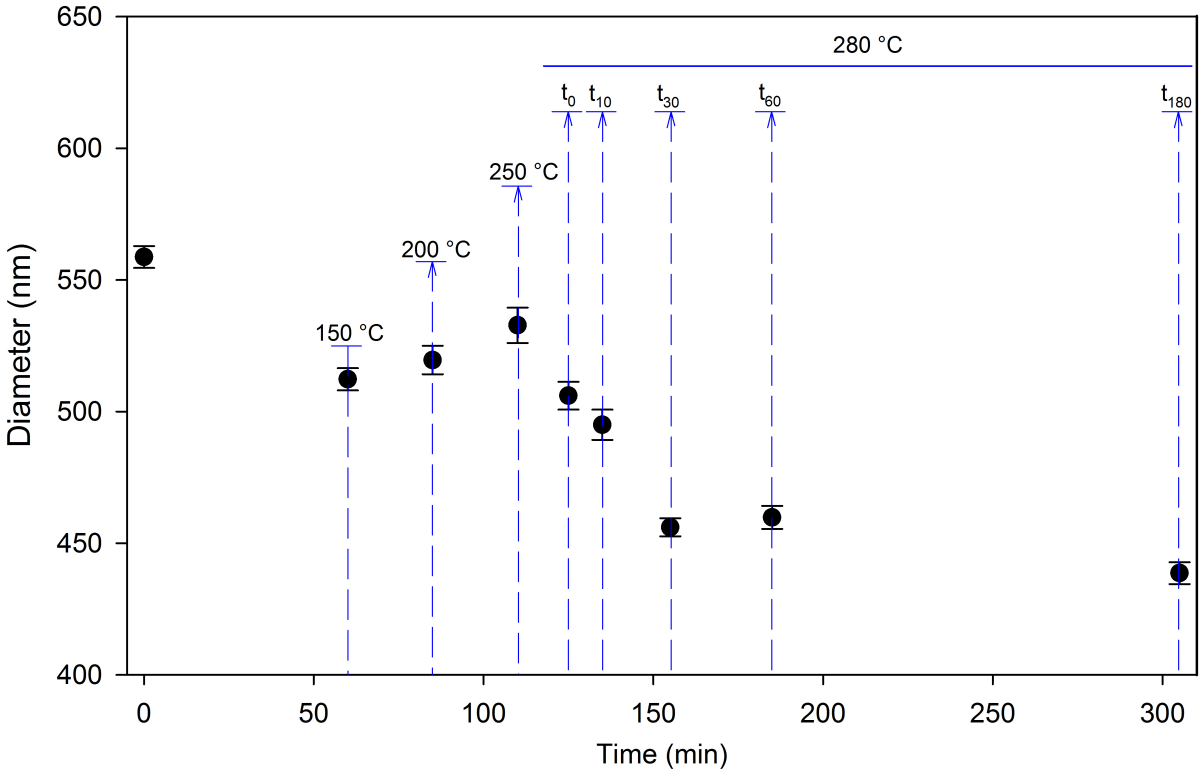

Figure 2-9. Effect of temperature on fiber diameter during stabilization in air with a temperature ramp of 2 °C/min. Data points are averages of $n > 100$ measurements and plotted with standard error. Initial fiber diameter contraction was due to solvent removal, followed by a slight expansion above the glass transition (~125 °C), followed by steep contraction through 30 minutes isothermal at 280 °C. Expansion was associated with molecular relaxation processes, while contraction was driven by cyclization and crosslinking reactions.

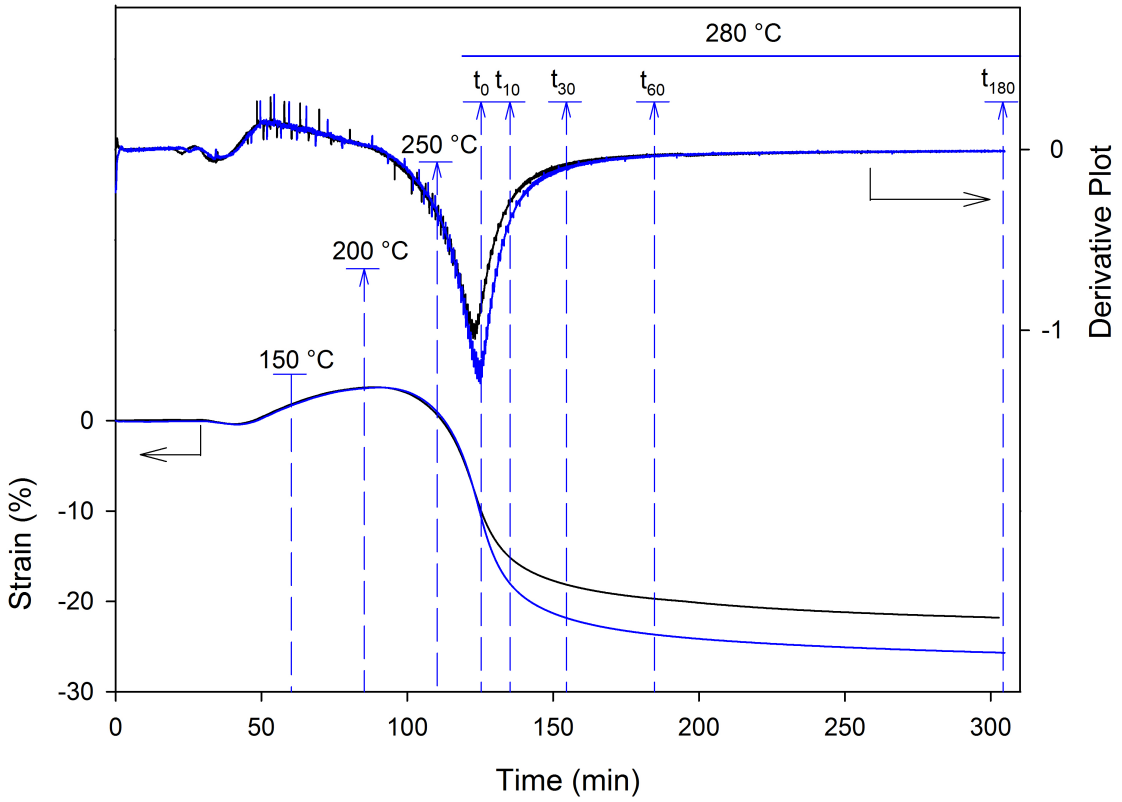

Figure 2-10. Stress-free shrinkage strain (%) of two PAN mats stabilized in the DMA under air with a temperature ramp of 2 °C/min with *length* x *width* x *thickness* of ~17 x 5.5 x 0.4 mm. A time derivative plot demonstrates the temperature ramp dependence for rate of shrinkage, where the rate of shrinkage (associated with cyclization and crosslinking) immediately decreases upon isothermal heating.

Chapter 3. Polyacrylonitrile (PAN) Carbon Fiber Fabrication and Modification

3.1. Synopsis

Chapter 2 presented an overview of polyacrylonitrile (PAN) comonomers and fiber fabrication, followed by an introduction to typical industrial manufacturing processes. The aim of the chapter was to expand understanding of carbon fiber fabrication methods. Following the overview, fabrication and stabilization of electrospun homopolymer PAN fibers was conducted using compositional, dimensional, and functional group analysis to assess stabilization processes. The current chapter provides an overview of the effect of carbonization and common surface modification procedures, including activation, oxidation, and sizing. A thorough discussion of chemical oxidation and silicon (silane) coupling is provided, followed by an analysis of both oxidation and silanization processes focusing primarily on bulk and surface composition, and surface functional group analysis. A semi-quantitative formula for silanization stoichiometry was developed based on surface acid groups in order to tailor treatment solutions.

3.2. Background of Polyacrylonitrile (PAN) Based Carbon Fiber Fabrication and Modification

Carbonization, or pyrolization, is the process of condensing sections of 1-6 carbon rings formed during stabilization into large heterocyclic, fused-ring systems (Scheme 2-1[B] to [C]). Reaching a peak temperature between 1000 ºC to 3000 ºC, the carbon rings undergo dehydrogenation and denitrogenation processes – accelerated at roughly 400 ºC and 600 ºC, respectively[1, 2] – resulting in the removal of structural defects and non-carbon elements. Stabilized fibers used in the current study contained roughly 67 at-% carbon (Table 2-7), while

fibers carbonized to 1000 ºC were nearly 92 at-% carbon. Typically, carbonization is performed in-line with stabilization, under-tension, and within an inert environment.

Unlike the dramatic effect of different stabilization procedures – initial and final temperature, heating ramp, isothermal duration, atmosphere, and tension – carbonization relies more simply on the maximum temperature. The temperature dependence of the carbon microstructure – and the resultant fiber properties – allow fibers to be tailored towards the application, divided into three types as follows: Type I fibers are treated above 2000 ºC resulting in high modulus and low strength, Type II fibers are treated between 1300-1800 ºC and have low modulus and high strength, while Type III fibers are treated below 1300 ºC and do not achieve peak modulus or strength.[3] High modulus fibers rely on basal planes that are highly oriented along the fiber axis (*c*-axis), while high strength fibers make use of small defects (remaining due to lower treatment temperature) to inhibit plane slippage resulting from relatively weak van der Waals forces that are responsible for inter-plane interaction. (Figure 3-1)

Increasing temperature treatment has several atomic level effects that are most often quantified using x-ray diffraction: increased size of heterocyclic sheets perpendicular and parallel to the fiber axis ($L_{a\perp}$, $L_{a||}$), increased stacking thickness of basal planes (crystal thickness, L_c), and decreased inter-plane spacing (d_{002}) using Equations 3-1, 3-2, 3-3, and 3-4, respectively.[4] The Scherrer constant (K) varies by the reflection and crystalline structure, but is reported to be 0.89 for the (*00l*, $\theta = 12.5°$) peak and 2.0 for the (*hk0*, $\theta = 22.5°$) peak when using FWHM (radians) measurement of β.[4] Absence of a strong (*00l*) peak indicates a predominantly turbostratic structure, more typical in fibers treated below 1300 ºC.[5-7] As the treatment temperature increases, the inter-plane spacing decreases towards that of graphite ($d_{002} = 0.335$ nm), and the order is increased along the *c*-axis (Figure 3-2).[8]

$$L_{a\perp} = \frac{K\lambda}{\beta_{100,equitorial}\cos(\theta)} \quad (3\text{-}1) \qquad L_{a\parallel} = \frac{K\lambda}{\beta_{100,meridional}\cos(\theta)} \quad (3\text{-}2) \qquad L_c = \frac{K\lambda}{\beta_{002}\cos(\theta)} \quad (3\text{-}3) \qquad d_{002} = \frac{\lambda}{2\sin\theta} \quad (3\text{-}4)$$

Specifics of the carbonization process of polyacrylonitrile are still debated because of the complex, non-graphitic structure that develops.[9] (Figure 3-3) It has been suggested that the development of 5- and 7-member rings at low carbonization temperature (1000 ºC) condense into hexagonal ring systems at increased temperatures (1500 – 3000 ºC).[10] This supports previous reports of decreasing density with intermediate temperature treatment, followed by rapid increases in density at higher temperature.[9-11] Diffraction and TEM studies have yet to provide conclusive evidence for these mixed-ring systems, contributing to ongoing debates.[10] Radicals on the carbon lattice formed during pyrolitic cleavage as a result of the removal of oxygen and nitrogen impurities are said to be stabilized during the formation of the higher stability ring-systems or triple-bonded carbons under inert conditions, but can also be satisfied using chemisorbed oxygen when exposed to air.[12]

Despite controversy regarding development of the chemical structure, the effects of high-temperature treatment are clear and have been summarized elsewhere.[13-16] Some relevant and demonstrative results are included in Table 3-1. Increased stacking of basal plans (L_c) and decreased inter-plane spacing (d_{002}) as a result of high-temperature treatment has been shown by Zhou et al.[5] to improve electrical conductivity, tensile strength and tensile modulus. Liu et al.[11] showed a similar increase in basal plane stacking with increasing temperature, and demonstrates the transition from high tensile strength to high modulus fibers with increasing treatment temperature.[16, 17]

3.2.1. Carbon Fiber Surface Modification Methods to Improve the Interphase

The increased order achieved by high-temperature treatment is also associated with chemical resistivity through the development of an increasingly inert surface. The low surface energy of increasingly pristine carbon material is unfavorable to wetting during composite fabrication, contributing to minimal interaction between fiber and matrix and the poor resulting interphase. Failure to achieve a chemically active fiber interface results in suboptimal shear strength, electrical- and thermal-conductivity, and tensile strength off-axis from fiber orientation.[18, 19] Surface modifications to improve fiber-matrix interaction take many forms, but three often-used in academia and industry include activation, oxidation, and sizing.

Activation is the processes of increasing surface area of a material, allowing physical interaction between matrix and fiber via porosity. Lászlo et al.[20] and Im et al.[21] demonstrated activation of carbonized PAN in unique ways, where Lászlo post-treated fibers with hot steam while Im used dissolved silica in electrosprayed and carbonized PAN, followed by silica leaching with hydrofluoric acid. Activation greatly increased surface area (i.e., 6.7 to 544 m^2/g and 11.4 to 340 m^2/g for Lászlo and Im, respectively) and can enhance the surface chemistry,[22] depending on the activation method; this can promote either physical or chemical interaction with a composite matrix.

Oxidation acts to chemically modify surfaces while only minimally affecting physical surface features. Driven by oxygen integration, these techniques increase surface polarity to improve wetting and promote covalent bond formation between the carbon surface and matrix. Popular techniques include plasma oxidation,[18] ozone treatment,[19] electrochemical oxidation,[23] and high temperature chemical oxidation.[24-26] The various oxidation techniques increase oxygen functionalities, and as a result increase properties like the critical stress intensity factor and

energy release rate for fractured composites,[19] and increase tensile strength (with decreasing electrical conductivity due to basal plane disordering).[24]

Industrial carbon fiber fabrication often includes a sizing process used to protect fibers during handling and also improve composite properties. Typically the process occurs soon after oxidation and includes immersing or spraying fibers with a 5% solution of resin sizing agent (such as an epoxy) in water or an organic solvent, and then quickly heating.[17] The coating improves adhesion to matrix materials as well as handling properties.

3.2.2. Chemical Oxidation of Carbon Fibers

Pristine carbon fibers in the current study were treated using high temperature nitric acid (HNO_3, 70%) following Yuen,[24] Toebes,[25] and Lakshminarayanan[26] in order to enhance the fiber-matrix interphase. Oxidation reactions are thought to occur at the saturated, incompletely bonded edges and defect sites on basal planes,[27, 28] and some common groups are shown in Scheme 3-1.[29] On single walled carbon nanotubes (SWCNTs) it has been suggested that chemisorption of NO_3 occurs before energetically favorable conditions occur to remove nitrogen in favor of carbon-oxygen functionalities; furthermore, the researchers believe oxidation occurs in clusters due to the changing energetics.[30]

The chemical stability and inaccessibility of the mid-plane minimizes oxidation from occurring outside the fringe regions of basal planes, though it has been shown that solvents can increase L_c and decrease L_a as oxygen levels increase;[31] as a corollary, more graphitically-structured carbons are more resistant to chemical oxidation due to the reduction of defect sites, incompletely bonded edges, and tighter packing of basal planes. This effect could account for the reduced conductivity for fibers studied by Yuen et al.;[24] the oxidation produces fibers less

ordered, and thus with a reduced electrical conductivity, comparable to a less graphitic (lower carbonization temperature) fiber. Surface area of the pristine carbon also contributes to the oxidizing capacity, where low surface area (large diameter or unactivated) carbon fibers are oxidized less readily and have less oxidizing capacity when compared to an equivalent weight of high surface area (small diameter or activated) carbons.[27]

3.2.3. Coupling Agents Applied to Composite Fillers

Similar to sizing, coupling agents can be used to improve fiber-matrix adhesion. Both carbon and silicon based agents can be used, with primary differences including: a) silicon does not form stable double bonds, providing four independent functional groups; b) silicon is more electropositive than carbon; and c) group reactivity varies when bonded to silicon versus carbon, where methoxy will form stable methyl ether in carbon based compounds, but is highly reactive towards hydrolysis and alcohol formation when bonded to silicon.[32]

Silicon based (silane) coupling agents originally gained interest for their ability to improve strength retention over time in fiberglass composites during the 1940's.[32] Since then a wide variety of chemistries have been developed to accommodate diverse applications ranging from fiber and particle fillers – mineral,[33-35] glass[36, 37], carbon,[18, 38] or metal[39] – used in composites, to decrease agglomerations,[40] or in surface treatments used to promote cell adhesion.[41, 42] The key to silane coupling lies in the bifunctionality that provides reactivity between dissimilar constituents. Silanes typically come in the form $R\text{-}Si\text{-}R'_3$, where *R'* is a hydrolysable group, and *R* is the functional group. Several primary reactions must occur when treating materials with a silane coupling agent:[32]

1) Hydrolysis of the *R'* (i.e., *R'* = OCH_3) group in the presence of H_2O:

Ex. $R - Si(OCH_3)_3 + 3H_2O \longrightarrow R - Si(OH)_3 + 3CH_3OH$

2) Condensation of silane molecules after hydrolysis:

Ex. $_{(HO)_2}^{R} > Si - OH + HO - Si <_{(OH)_2}^{R} \longrightarrow _{(HO)_2}^{R} > Si - O - Si <_{(OH)_2}^{R} + H_2O$

3) Hydrogen bonding occurring between hydrolyzed groups and a substrate

4) Bond formation with a substrate, such as carbon nanofibers (CNFs):

Ex. $CNF - OH + HO - Si <_{(OH)_2}^{R} \xrightarrow{T} CNF - O - Si <_{(OH)_2}^{R} + H_2O$

While the functional group (*R*) is tailored to the application – e.g., *R* can be an amine (NH_2) or epoxide for use in amine cured epoxy composites – the hydrolyzable group (*R'*) selection is critical to favorable bonding with a given filler. Furthermore, differences in application procedure can affect silane choice: slow hydrolization may be desired for some applications, while others require accelerated hydrolysis for treatment within minutes. The kinetics of the hydrolysis and condensation reactions are controlled both by solution composition and silane chemistry. Generally speaking, acidic and basic solutions favor hydrolysis and condensations, respectively; additionally, the rate of hydrolysis increases with decreasing alkoxy group size (i.e., $CH_3O > C_2H_5O$), though each consecutive hydrolysis on the same silane molecule proceeds at different rates.[43] Further complicating the matter, it has been shown that amine functionalization accelerates hydrolysis, proving the unique interactions that can occur between hydrolysable groups and the functional group.[44]

Despite the complex kinetics, silanes have been intensely studied and applied to a variety of applications. Specific to the present study, several groups have studied 3-(2-amino-ethylamino)propyl-trimethoxysilane, and its coupling to carbon fibers. A short review follows, with supporting information by Beari et al.,[45] and a summary of the application of silanes in composites can be found in a review written by Shokoohi et al.[42]

Paquet et al.[41] recently undertook a study of the hydrolysis and condensation kinetics of 3-(2-amino-ethylamino)propyl-trimethoxysilane in D_2O and an 80:20 (w/w) solution of ethanol-d6 and D_2O using ^{29}Si NMR. To study the effects of pH, they used the as-mixed solution pH of 10.5 as well as a solution acidified to 4.5 using glacial acetic acid; they determined that the basic 80:20 solution that was hydrolyzed before the first 10-minute time point was reached, while the acidified 80:20 solution took longer and was fully hydrolyzed within 20 minutes. Of particular interest are the much different kinetics of condensation between the two solutions: the basic 80:20 solution showed complete conversion from hydrolyzed silanols to single-*R'* group condensation within 10 minutes, and further condensation using two- and three-*R'* groups within 1 hour. Conversely, the acidic 80:20 solution showed a mixture of hydrolyzed silanols and single-group condensation through 30 minutes, and showed minimal second-group condensation through 1 hour. This reinforces previous studies showing acidic and basic solutions stabilizing either hydrolysis or condensation, respectively.[43, 46] Pure D_2O showed much less discrete transitions between hydrolyzed and single-, double-, and triple-group condensation compared to the aqueous solution, though similar trends based on the effect of acidity were observed. Worth noting is the very high silane content in solution (10% w/w) compared to 0.1-0.25 vol-% in the present study.

Palencia et al.[38, 47] studied the effects of time, temperature, silane type, and concentration on silanization of activated carbon nanofibers in pure H_2O; in the study, the coupling agents varied by alkoxy group (methoxy and ethoxy), length of functional group linker ($(CH_2)_3$ and $(CH_2)_3NH(CH)_2$) and functional group type (NH_2 and epoxide). Supporting previous research, they showed fast adsorption to the carbon surface, with 2 wt-% silane adsorption within 5 minutes, followed by a slow increase to 2.8 wt-% over 40 minutes. Additionally, they showed

that functional group chemistry dramatically affected adsorption when changing the silane concentration. Using 1 minute silanization times, they changed silane concentration between 0-5% with respect to solution (0-100% with respect to fiber mass) and used TGA to measure the adsorbed silane. Epoxide functionalized silane showed adsorption increasing to 16 wt-% (with respect to fiber mass), while two amine functionalized silanes showed ~4 wt-% adsorption, and the diamine silane only adsorbed 1.6% wt-%; they ascribed the reduced amount to the longer chain length of the diamine functionality. They also studied surface area and found it to decrease with increasing silanization, attributed to filling of pores. Palencia et al.[38, 47] used activated carbon fibers with high surface area and unknown functionality, while the fibers used in the current study possess relatively low surface area and are chemically oxidized to increase functionality.

3.3. Material Selection, Fiber Fabrication, and Surface Modification Methods

Polyacrylonitrile (PAN) based precursor fibers were electrospun and stabilized as previously described (Chapter 2.3). In keeping with the established method,[5, 7, 48] the source fibers included a tension-free stabilization in air under a ramp of 2 ºC/min to 280 ºC, followed by a 3-hour isothermal hold.

Stabilized mats were pyrolized under a ~50 ml/min nitrogen purge in a tube furnace (Carbolite, UK) by ramping at 2 ºC/min from room temperature to 1000 ºC, followed by a 1-hour isothermal hold. (Scheme 2-1[B] to 2-1[C]) Pyrolized carbon mats were stored under vacuum or in a dessicator until use to minimize water adsorption.

Pristine carbon nanofibers were modified using two processes: chemical oxidation and silanization. A sample of 3-(2-amino-ethylamino)propyl-trimethoxysilane silane (Z-6020, Dow Corning) was supplied by the company.

3.3.1. Chemical Oxidation of Pristine Carbon Fibers

Chemical oxidation was performed using nitric acid (70%, Sigma Aldrich) under a hood. For time-series oxidation, first an oil bath was heated to 90 ºC. Separately, roughly 50 ml of nitric acid per 150 mg of carbon fiber was added to a glass jar and tightly sealed with electrical tape. The glass jar was then secured in the oil bath and heated for the specified time periods. At the end of oxidation, fibers were lifted from the nitric acid using tweezers and allowed to cool in the vented hood. The oxidized fibers were washed in copious amounts of ethanol, and dried under vacuum at 40 ºC. Sample weight typically increased ~10 % with oxidation.

Samples intended for silanization were first oxidized for 60 minutes at 80 ºC following the procedure above to enhance chemical reactivity and available coupling functionalities, and then treated using one of two silanization schemes as follows.

3.3.2. Silanization of Oxidized Carbon Fibers

Silanization was performed with Z-6020 using two distinct methods based on theoretical reaction mechanisms (Scheme 3-2). The methods were unique in their solution preparation and proposed reaction mechanisms, but samples were washed and cured following the equivalent methods. Equation 3-9 (Section 3.5.2) was used to determine the volume of silane based on desired stoichiometry and amount of fiber; it was determined that fibers possessed on the order of 800 μmol/g of silanizable functionalities, and using this, stoichiometric ratios of silane to

available functionality were formulated (i.e., 10:1 indicated 10 moles of silane to 1 mole of available carbon fiber functional groups). Solution volume was determined based on the amount of silane required for treatment, where 10:1 and 5:1 stoichiometry solutions contained 0.25 vol-% in solvent, and 1:1 stoichiometry solutions contained 0.1 vol-% silane. The lower volume-percentage was required for the lower stoichiometry treatments to allow full immersion of fibers in solution. Furthermore, solutions are typically acidified to a pH of 4-5, but the measured pHs of the solutions were roughly 4.5 as prepared so no acidification was needed.

Method A. Solution hydrolysis (Scheme 3-2A) included preparation of a 95:5 vol-% solution of ethanol solution (Fisher Scientific) and deionized water followed by drop-wise addition of 3-(2-amino-ethylamino)propyl-trimethoxysilane (Silane Z-6020, Dow Corning), and five minutes of gentle agitation to disperse and hydrolyze silane molecules. The available H_2O in solution exceeded that required for complete hydrolysis of the methoxy groups by many orders of magnitude. A five minutes hydrolysis duration was chosen following the manufacturers guidelines;[32] while some silanes require extended periods, methoxy groups hydrolyze relatively quickly, and are accelerated by the amine functionality as discussed previously (Chapter 3.2.3). Following the hydrolysis residence time, oxidized carbon nanofibers were added to the solution, which was agitated for an additional five minutes. Hydrolyzed silane molecules could react with the hydroxyl functionalities on the carbon fibers as well as the other hydrolyzed silane molecules. In this way, solution hydrolysis was theorized to promote high levels of silanization due to enhanced hydrolysis promoting reactivity, but the reacted silane was expected to have higher proportions of silane-silane bonds (indicative of agglomerations and multilayer formation) when compared to Method B.

Method B. Hydrolysis through adsorbed H_2O (Scheme 3-2B) relied on moisture uptake by oxidized carbon fibers to locally hydrolyze the coupling agent. For consistency, silane was added in a drop-wise fashion to ethanol and agitated for five minutes. This was performed to promote silane dispersion in the solution, but hydrolysis should not occur; the ethanol solution had <1% H_2O, but dilution greatly reduced the availability for hydrolysis, and the number of water molecules was many orders of magnitude short of the 95:5 vol-% solution. Oxidized carbon fibers were added to the solution and gently agitated for five minutes. By relying on locally adsorbed water to hydrolize silane molecules, it was anticipated that silanes would be unable to react with each other, preventing agglomerations or multilayers. As such, it was expected that using adsorbed H_2O would provide lower levels of silanization on the carbon fiber surface.

After five minutes for silanization, fibers were removed from their solutions and allowed to slightly condense under the hood. Condensation prior to washing was used to increase silane adhesion through hydrogen bonding; understanding the process as dynamic, silane molecules in solution may not possess the needed activation energy to react with the oxidized functionalities present on the carbon surface. Condensation allowed reorientation of molecules to promote hydrogen bonding and physisorption with the oxidized carbon fiber surface before washing.

After 3-5 minutes, the fibers were washed twice in roughly 100 ml of ethanol, and then dried and cured at 110 ºC for 10-15 minutes until dry. Samples were stored overnight at 40 ºC under vacuum, and kept in a desiccator until use.

3.4. Characterization

3.4.1. Scanning Electron Microscope

Scanning electron microscope (SEM) images were captured using a JEOL 5600 in order to observe fiber properties such as diameter and surface features. Samples were dried at 40 ºC under vacuum and mounted on aluminum stumps with carbon tape. SEM images were taken at 5 kV, 19 mm working distance, spot size of 25, and were sputter coated for 30 seconds with gold (to prevent sample charging) as needed. Fiber diameters were measured using ImageJ (NIH, http://rsbweb.nih.gov/ij/) analysis software, and are the average of at least 100 fiber measurements.

3.4.2. Energy Dispersive X-ray Spectroscopy (EDX)

Bulk composition was obtained using energy dispersive x-ray spectroscopy (EDX) spectra acquired with a PRISM IG Detector (Princeton Gamma Tech) using the included eXcalibur software (v 4.03.01, Princeton Gamma Tech). The instrument had been previously upgraded to include a Si(Li) detector and ultra-thin window to enhance low-*Z* element contrast. Spectra were acquired at 5 kV, 19 mm working distance, 1000x magnification, spot size of 50, and acquisition time of 3-5 minutes depending on the sample dead time and count rate in order to achieve a peak count of at least 1500, or until count uncertainties (as calculated within eXcalibur) decreased to below 10%. A voltage of 5 kV was selected because it was an adequate overvoltage to excite the K_α transition for all elements of interest (C, N, O, Si), but was rarely enough to result in signal from the sample-mount. To prevent spectral contamination from the carbon mounting tape, spectra were measured above the aluminum stump; any aluminum signal

was disregarded during analysis. Background subtraction of Bremsstrahlung (continuous) x-rays was conducted within the software.

3.4.3. X-ray Photoelectron Spectroscopy (XPS)

Composition and chemical state analysis of the fiber surface was conducted by x-ray photoelectron spectroscopy (XPS), which analyzes a depth of roughly 3-10 nm. A time-series experiment for oxidation of carbon fibers in nitric acid was performed at General Motors (GM Tech Center, Warren, MI), while all further samples were tested at the Cornell Center for Materials Research (SSX-100, Surface Science Instruments/FISONS, Cornell University, Ithaca, NY).

First, samples were placed on a mount with carbon tape, placed in the XPS SSX 100, and vacuum was pulled to 10^{-9} Torr (Figure 2-2). Samples were then tested for effects of charging; charging causes a shift in binding energy, but no carbon samples were affected. High count, low resolution scans from 0-1200 eV with a 150 eV pass energy filter were used to determine composition; low count, high resolution scans with 22 eV widths around element binding energy centers were taken using a 50 eV filter for chemical state characterization. Other relevant specifications are included in Table 3-2.

Analysis was performed using CasaXPS (www.casaxps.com, v. 2.3.15) for all composition measurements, and was also used for binding state analysis of the time-series oxidized samples tested at General Motors. Counts per second (Intensity) vary by element binding energy and are converted into molar concentrations using relative sensitivity factors (RSF) based on elements, where carbon, nitrogen, oxygen, and silicon values are 1, 1.8, and 2.93, 0.813 respectively. High resolution scans of oxidized and silanized samples tested at

Cornell Center of Materials Research (CCMR) were processed within OriginPro 8.6. A mixed Gaussian-Lorentzian (70:30) function (Equation 3-5) adopted from CasaXPS was used for binding state analysis with the parameters specified in Table 3-3; variables x_c, w, and m, represent the peak center, width, and shape parameter, respectively.

$$GL(x,x_c,w,m) = \frac{e^{-4\ln 2(1-m)\frac{(x-x_c)^2}{w^2}}}{1+4m\frac{(x-x_c)^2}{w^2}} \tag{3-5}$$

3.4.4. Boehm Titration

A titration procedure proposed by Hanns-Peter Boehm has been adopted as a standard method for determining acidic functionalities on carbon materials.[28] Base-neutralization following the Boehm procedure was used to determine the number of Brønsted acidic functionalities (μmol/g), including phenols, lactones, and carboxylic acids.[28] More recently, work by Andreas[49, 50] was conducted to standardize the Boehm titration, including characterization of the effects of CO_2 removal, endpoint determination, methods of agitation, filtration, and normality of titrant. In following their recommendations and considering the available resources and materials, NaOH neutralization and back-titration was conducted on pristine carbon nanofibers, 60-minute nitric acid (70%, 80 ºC) oxidized carbon nanofibers, and two silanized samples (1:1 and 1:4 stoichiometric silanization ratios in a 95:5 vol-% EtOH:H_2O solution) for the current study.

First, ~0.05 N solutions of NaOH (>97%, Sigma Aldrich), HCl (>99%, Sigma Aldrich), and potassium hydrogen phthalate (KHP, >99.95%, Sigma Aldrich) were made with 18 MΩ (Millipore) ultrapure water. Bases were dried under vacuum at 70 ºC before weighing to remove absorbed moisture, and Millipore water was boiled to remove dissolved CO_2 that has been shown

to inflate the measured acid groups.[49] The acids and base were added to freshly boiled (and cooled) 18 MΩ water and mixed for 2 hours while bubbled with dry N_2 to remove residual CO_2.

Standardizations were performed in triplicate, with 10 ml of acid being titrated with NaOH via pipette. NaOH was standardized with KHP (Equation 3-6), and HCl was standardized using NaOH (Equation 3-7), where m_{KHP}, M_{KHP} (204.22 g/mol), V_{NaOH} are the mass of KHP (g), molar mass of KHP (g/mol), and titrant volume of NaOH (ml). Separately, thermogravimetric analysis (TGA) was performed on dried NaOH and showed roughly 5 wt-% water adsorption; this was taken into account when making the original solution. Due to the use of aliquots for titration, the mass ($m_{KHP,solution}$) and volume ($V_{Millipore,solution}$) of original solutions were scaled by the aliquot volume ($V_{Aliquot}$) to determine the amount of standardizing agent in solution.

Neutralization of fibers was performed as follows: roughly 150 mg of vacuum dried fiber was immersed in 20 ml of 0.05 N NaOH in HDPE vials and gently agitated at room temperature for 24 hours. The solutions were filtered and divided into two 10 ml aliquots, acidified with 20 ml of with 0.05 N HCl, and back-titrated with NaOH. NaOH solutions were bubbled with dry N_2 before use.

The number of carbon surface functional groups (n_{CSF}) was determined using Equation 3-8,[49] where n_{HCl} and n_{NaOH} are both unity because they are a monoprotic acid/base combination, and $V_{NaOH,neutralization}$, $V_{NaOH,aliquot}$, V_{HCl}, and $V_{NaOH,titration}$ are the volumes used for neutralization (~20 ml), aliquot (~10 ml), acidification (~20 ml), and titration (~10 ml), respectively.

$$[NaOH] = \frac{m_{KHP}}{M_{KHP} x V_{NaOH}} = \frac{(m_{KHP,solution} / V_{Millipore,solution}) x V_{Aliquot}}{M_{KHP} x V_{NaOH}} \quad (3\text{-}6)$$

$$[HCl] = \frac{[NaOH] x V_{NaOH}}{V_{HCl}} \quad (3\text{-}7)$$

$$n_{CSF} = \frac{n_{HCl}}{n_{NaOH}} [NaOH] V_{NaOH,neutralization} - ([HCl] V_{HCl} - [NaOH] V_{NaOH,titration}) \frac{V_{NaOH,neutralization}}{V_{NaOH,aliquot}} \quad (3\text{-}8)$$

3.4.5. Nitrogen Adsorption

Surface area measurements were conducted using an Autosorb-1 (Quantachrome Instruments) in collaboration with Dr. You-xin Yuan of SUNY-ESF (Syracuse, NY). Roughly 50 mg of pristine, 60-minute nitric acid (70%, 90ºC) oxidized carbon nanofiber, and 1:1 stoichiometric silanized (95:5 vol-% EtOH:H_2O solution) carbon nanofiber samples were delivered, cut length wise and added to the pre-weighed measurement cell. To maintain fibers in as-pristine condition as possible, samples were not ground, resulting in small masses being used; tested samples weighed 20-35 mg. Samples were outgassed under reduced pressure at 150 °C for 3-6 hours until stable, then the vessel was moved to a liquid nitrogen dewar to maintain a cell temperature at 77.35 K. Nitrogen gas was supplied in discrete amounts and adsorbs to the surface as the relative pressure was slowly increased to unity, whereupon the vessel was degassed and desorption of nitrogen was measured. The Brunauer-Emmett-Teller (BET) method of analysis uses linearity between relative pressures $0.05 < P/P_o < 0.35$ to determine surface area, while other methods are included and use adsorption and desorption kinetics to determine parameters such as pore distribution and geometry. The research scientist conducted these analyses within

the included software. Typical nomenclature breaks pore sizes into micropores (< 2 nm), mesopores (2 - 50 nm), and macropores (> 50 nm).

3.4.6. Thermogravimetric Analysis (TGA)

TGA was also considered as a means to determine silane content,[40, 42, 51, 52] but chemical oxidation resulted in groups that undergo desorption upon heating, including CO_2, CO, H_2O, and H_2.[53, 54] Gas-evolution is linked to type of functionality and can extend over several hundred degrees; Otake et al.[53] presented overlapping evolution profiles for H_2O, CO_2, and CO, that start as low as 125 °C and peak at 225 °C, followed by a much stronger, secondary CO peak above 600 °C. These results are similar to those of Zhou[54] with a dissimilar precursor after low temperature, extended treatment time in nitric acid. These regions overlap the degradation region for silanes that occurs between 200 °C and 800 °C.[40, 52] Use of temperature-programmed desorption (TPD) of pyridine has been used to study silanization of silica,[51] though no studies were found for TPD of silanized carbons.

3.5. Results and Discussion

3.5.1. Time Series Oxidation: Composition & High Resolution Analysis

Using XPS in collaboration with General Motors Company (GM Tech Center, Warren, MI), surface composition and binding states were determined for carbon nanofibers (CNF) subjected to nitric acid (70%) at 90 °C ranging from 10 to 90 minutes. The majority of surface oxidation as measured by oxygen percentage occurred within the first 10 minutes (Table 3-4/Figure 3-4), which is consistent with reports for nitric acid oxidized vapor grown carbon

nanofibers,[26] electrochemically oxidized type II PAN fibers,[55] and nitric acid oxidized type III PAN fibers.[56] Speaking generally, it is believed that the introduction of oxygen occurs at defect sites and saturated edges of basal planes,[27] followed by the gradual increase of interlayer spacing resulting in disordering of the carbon planes and exposing more oxidative sites.[31] The initial increase in nitrogen is consistent with the suggested mechanism of chemisorption of NO_3 onto carbon surfaces, followed by removal of nitrogen through the production of NO and NO_2.[30] Beyond 10-minutes and with exception of the 40-minute time point, the compositional effects of continued nitric acid oxidation were clear: carbon and nitrogen content decreased in favor of oxygen, where the rate of composition change slowed with continued oxidation. Small changes to surface composition are highlighted using atomic ratios N/C and O/C (Figure 3-5). Using simple composition, a plateau appeared to be approached between 60 and 90 minutes of oxidation, though atomic ratios showed continued compositional evolution.

Composition detected by XPS can reach a plateau due to the detection depth limitation innate to the instrument, where only 3-10 nm, or roughly 10 basal planes are sampled.[23, 57, 58] Gardner et al.[59] examined the effect of prolonged oxidation using angle-resolved XPS on type II PAN carbon fibers treated with nitric acid (70%) at 115 °C. By angling the x-ray source at 90° to the surface (i.e., perpendicularly), the sampling volume was greatly increased compared to shallow angles; using 10°, 50°, and 90° they estimated detection depths ranging from 3 to 10 nm. In doing so, they found that the oxygen content of the surface 3 nm increased ~10 at-% in 20 minutes, while the depth of 10 nm remained 5 at-% lower. The surface (3 nm) and sub-surface (10 nm) reached equal levels of oxidation (28 at-%) by 40 minutes, though both continued to oxidize through 60 minutes where the atomic ratios stayed constant until testing ended at 90 minutes (33 at-%).

A compositional plateau does not necessarily indicate oxidation has stopped, but Gardner's[59] work suggests plateau's could indicate a common composition through the sampling depth. Continued oxidation into the core of the fiber that goes undetected to surface-analysis techniques such as XPS is consistent with results that show increasing acidic functionalities using the Boehm titration during extended oxidation.[23, 57] The current study used reduced oxidation temperature and fibers possessed higher expected oxidizing capacity (due to reduced pyrolization temperature), which resulted in continued compositional evolution. No plateau was achieved.

Oxidation not only changed surface composition, but also modified the type of available functionalities; these changes were detected using high-resolution XPS and fitting Gaussian-Lorentzian curves at binding energies for known compounds (Figure 3-6).[56, 59-61] Two ways of functional-group analysis are by element-percent, or bulk-percent; that is to say, how does the area of the graphitic and amorphous carbon peak (284.8 eV) change as a percent of the carbon peak, or how does the peak change as a percent of surface-composition. Examining the evolution of different functionalities favors use of element-percent examination, while the composition weighted percent provides information more relevant to understanding how the material will react with a coupling agent. Both of these analyses follow. Throughout the analysis, peak areas were used as opposed to peak intensities to allow for variations in the FWHM between samples. Once again, the 40-minute time-point acts as an outlier to the trends followed by the other samples, and degradation of the 90-minute sample prevented high-resolution analysis; trends of the other samples were emphasized in the following discussion.

Considering the element-weighted composition (Table 3-5), the primary carbon peak (I) shifted towards oxygen functionalities, including C-OH/C-O-C/C-N (II) and a doubling and

tripling of the C=O (III) peak between 10- and 60-minutes, respectively. These accompanied a decrease in the carboxyl/carbonate peak (IV) and a slight decrease in the shakeup peak (V). Observing the oxygen peak, shifts occured from O=C groups (carbonyl/carbonate, I) to the O=C group (carbonyl/quinone/carboxyl, II) coupled with a drop in the C-O-C (carboxyl/phenol/ester/anhydride, IV). These changes coincide roughly with the corresponding carbon analysis due to the combined area increase of these groups compared to the increase in carbon-oxygen complexes. Additionally, a small peak developed for adsorbed moisture (V) due to increased hydrophilicity of the oxidized surface. Lastly, nitrogen showed an initial increase in the pyridine (I) group followed by a continual decrease through 60-minutes of oxidation. This was paired with the reduction of the quaternary nitrogen group (III) and removal of pyridine-N-oxides (IV) – likely formed to stabilize radicals formed during pyrolization – as well as development of both amide/pyridone/pyrrole groups (II) and oxidized nitrogen in the form of NO_2 (V).

As mentioned earlier, the largest increase in oxygen occurred within the first 10 minutes of oxidation, attributed to the functionalization of superficial defects and the edges of basal planes. The complexity of functional groups evolved throughout the process, developing polar and protonated functionalities that are expected to interact more favorably with an epoxy matrix.

Analyzing the functional groups with respect to the surface composition highlights the dramatic shift from a pristine (>90 at-%) carbon surface to a highly oxygenated (>20 at-%) surface that developed during oxidation (Table 3-6). Despite subtle changes in element-weighted functional groups, every oxygen functional group increased with respect to the pristine carbon sample when taking into account the changing surface composition.

Considering nitrogen, the first 10-minutes showed a unique change, where the presence of pyridine and Ar-N-Ar groups (I) initially increased, but then dropped off to nearly half the original amount. The initial increase could be attributed to the removal of pyrolysis degradation products that contaminate the surface, while the following decrease is the result of both decreasing bulk nitrogen content and a shift to more complex nitrogen groups. The initial increase of the peak at 400 eV indicated a shift to simple pyrrole (-NH) and more complex lactam/amide/imade groups, followed by a decrease that resulted from decreasing bulk composition. Kanai et al.[30] suggest HNO_3 can physisorb, chemisorb, or modify the surface through oxidation processes such as ether formation; furthermore, activation energies associated with each process changes with the number of acid molecules and the state of surface groups. It is suspected that rapid chemisorption and oxygen reactions at the surface result in the initial increase in these nitrogen complexes, but continued treatment reduced the bulk percentage due to primarily oxygenation reactions and denitrogenation of the chemisorbed compound. Boudou et al.[61] consider a degradation of condensed pyridine groups (III) to correlate with oxidation, resulting in increased of exposure of pyridone/pyridine groups (I & II), which can be further functionalized; this is in agreement with current results. The presence of pyridine-N-oxides (IV) on the pristine carbon surface are surprising, but could be the result of unsatisfied radicals formed during pyrolization;[12] these decrease after reaction with HNO_3, and should be considered a separate process from the development of nitro ($–NO_2$) compounds (V). The development of $–NO_2$ compounds can result from NO chemisorption adjacent to oxygen sites, or NO_2 dissolved in the solution reacting with the surface.[62] The nitric acid solution turned a deep red during fiber oxidation, indicating the production of NO_2 dissolved in solution.

Oxygen was relatively evenly divided among the functional groups on the pristine carbon surface. With oxidation, the dominant uptake mechanism was initially through O=C (II) associated with quinone, carboxyl, and carbonyl groups, and O=C (III) associated with amides, anhydrides, hydroxyl, and esters; these groups continued to increase with oxidation, though the rate decreased. The increase of C-O-C (IV) groups continued steadily through oxidation, and is attributed to carboxyl, phenol, ester, and anhydride development. The continual development carboxylic groups (IV) is consistent with the literature,[63] and current analysis of carbon (associated with both III and IV).

Surface polarity is expected to increase continually due to: 1) oxygen functionalities continually increasing through 90 minutes, and 2) nitrogen functionalities become increasingly protonated. The 60-minute oxidation time-point was selected for further study in order to produce the most functionalized surface capable of producing more pronounced effects during silanization and composite fabrication, though the oxidation temperature was decreased to 80 °C in an effort to enhance fiber integrity. Because no developmental plateau was reached, but a more simple relationship was determined to include the increased evolution of surface oxygen groups and increased complexity of these groups, changing to a lower temperature was not considered an issue. The guiding grant emphasized filler interface and composite interphase, and a producing a highly functional surface was considered important to highlighting the effect of the interphase on other properties.

3.5.2. Boehm Titration (NaOH Neutralization) to Determine Oxidized Functionality and Silanization Solution Stoichiometry

Determination of acidic funtionalities using the Boehm titration is typically conducted with bases of various neutralizing potential, where $NaHCO_3$ (pK_a = 6.37), Na_2CO_3 (pK_a = 10.25), and NaOH (pK_a = 15.74) are used to neutralize carboxyl, lactone, and phenolic groups, respectively.[28, 49, 64] The dissociation constants for surface acid groups lie on a spectrum, affected by neighboring groups and basal plane arrangements, but remain distinct enough to serve as identifiers for surface functional groups.[28] When in an adequately basic solution, acidic surface groups dissociate and are stabilized by solution ions. For example, a weakly basic 0.05 N $NaHCO_3$ solution is only strong enough to neutralize surface carboxyl groups, which form a carboxylate stabilized in a double layer by sodium ions in solution ($COO^-\ ^+Na$).[28] Due to the difficulty obtaining appropriate amounts of carbon fiber, only NaOH solutions were used in the current study.

Pristine carbon fibers were oxidized for 60-minutes with nitric acid (70%, 15 N) at 80 °C to increase the available functional groups for chemical coupling. NaOH and HCl solutions (0.05 N) were used following the Boehm titration (Section 3.4.4) to determine the number of functional groups on both pristine and oxidized fibers. (Table 3-7) Oxidation resulted in a three-fold increase in acidic functionalities compared to pristine fibers subjected to NaOH neutralization. The total number of neutralized functionalities scaled similarly to bulk oxygen content measured via XPS, where there is a 2.6 times increase after oxidation (Section 3.5.4). XPS was expected to underestimate the increase in acidic groups when using simple compositional comparisons because the initial oxygen content includes basic groups that form as the result of oxygen adsorption onto the pristine fibers after high-temperature carbonization,[65]

and acidic groups measured by acid neutralization often increase at a faster rate than XPS measurements due to depth limitations.[23, 57]

Contescu et al.[64] similarly determined functional groups on cellulose based activated carbons oxidized with nitric acid (5 N and 15 N) at 60 ºC for 1- and 2-hours, respectively. Their values for total acidic functional groups were much higher than those in the current study, attributed to increased surface area and micropore volume increasing accessible defect sites;[31] furthermore, activated carbons can have some innate oxygen surface chemistry due to processing, from which more acidic groups develop during oxidation.[66] Contescu did not show data for pristine carbon materials, but their oxidized carbons showed roughly 90% of bulk acid functionalities containing alcohols, considered as the primary reactant for silane coupling. Likewise, Papirer et al.[67] used nitric acid oxidized carbon black with intermediate surface area and found a shift from lactone/carbonyl functionalization to greater than 65% of carboxyl and phenol functionalization, and showed a similar increase in total functionality from ~300 μmol/g to 1300 μmol/g. Using refluxing HNO_3 (70%) for 1.5 hours, Pamula and Rouxhet[56] increased low functionality pristine carbon (9.9 μmol/g) to high functionality oxidized fibers (936 μmol/g); their lower original functionality compared to the current study could be the result of higher pyrolization temperature (1250 ºC), as well as lower starting surface area. Results of vapor grown carbon nanofibers (VGCNF) also reach ~1200 μmol/g after 12 hours of room temperature nitric acid treatment.[54]

Supported by similar bulk acid-group measurements, observing similar shifts towards desired functionalities during oxidation using high-resolution XPS, and using the estimation that anywhere from 65% to 90% of bulk acid groups contain alcohols reactive with the silane chosen for this study, solutions were tailored to various stoichiometric ratios of silane to available sites

on the oxidized carbon fiber. While only an estimate, this method provided a semi-quantitative foundation for silanization.

The volume of silane for a given mass of fibers was determined using Equation 3-9, where constants M_{oCNF} and m_{Silane} are 800 μmol/g and 222.365 g/mol, respectively. A correction factor ($\varepsilon_f = 0.8$) and density conversion ($\rho_{Silane} = 1.03$ g/ml) were required to account for the ~80% solution of 3-(2-amino-ethylamino)propyl-trimethoxysilane provided by the manufacturer. Knowing the mass of fibers (m_{oCNF}) undergoing treatment, the volume of silane was tailored using the stoichiometry parameter (S), where $S = 2$ indicates a 2:1 stoichiometry (i.e., two silane molecule per estimated available carbon fiber binding site).

$$V_{Silane} = S \times \frac{m_{oCNF} \times M_{oCNF} \times m_{Silane}}{\rho_{Silane} \times \varepsilon_f} \tag{3-9}$$

In following this method, samples were silanized in stoichiometric ratios of 1:4 and 1:1 silane-to-functional site using solutions of 95:5 vol-% of ethanol:H_2O, followed by NaOH neutralization. While experimental uncertainty prevented concrete conclusions from these results – only one test was conducted for silanized samples – the results provided a qualitative basis for analysis, and align with expectations concerning the mechanisms and amount of reactions. Most importantly, the decrease of acidic groups detected after silanization was consistent with the proposed reaction between silanols and surface alcohols; differences between treatment stoichiometries were too small to offer conclusive evidence based on bulk-acidity alone. Hydrolyzed silanes have three silanols, and when chemisorbed to the carbon surface only one is expected to react, while others undergo condensation with adjacent silanes or form hydrogen

bonds. In this way, a more silane-functionalized surface could result in higher bulk-acid groups measurements compared to a less functionalized sample.

3.5.3. Surface Area

Surface area was analyzed in an attempt to assess the development of surface features with oxidation and silanization. An important consideration for oxidation is the shift to microporosity, which could occlude larger silane molecules from access to functionalities measured by titration and XPS analysis, or reduce the amount of imbibed epoxy.

One of each a pristine, oxidized, and 1:1 (95:5 EtOH:H_2O silanization solution) sample were tested, and the current results are meant to guide future work (Table 3-8). First, the fibers had relatively low surface area when compared to an activated carbon (> 100 m^2/g),[64] but were higher than the unactivated, micrometer fibers (< 5 m^2/g);[56] secondly, oxidation increased the surface area, consistent with other reports for nitric acid[26, 57] and KNO_3 electo-oxidation.[23] The increase in surface area is attributed to development of pores, pits and crevices along basal planes.[23, 57] Decreasing pore-diameter and -width while simultaneously increasing surface area and micropore volume suggests predominant formation of micropores over development of macropores: i.e., formation of pits and pores. It is worth mentioning Rouxhet,[56] who used a common oxidation method involving refluxing nitric acid developed a micropore volume of 0.03 cm^3/g – where micropore volume scales with surface area[68] – which stood in contrast to the small increase in surface area and micropore volume under mild oxidation conditions in this study. The highly developed pores in Rouxhet's paper collapsed with further treatment, which was responsible for the low surface area reported in Table 3-7. Similarly, some small pores may collapse in the currently studied carbons, which could explain the increased mode for pore size.

Pore structures can collapse in vacuum and open with solvation, so underestimation of small pores by nitrogen adsorption is common.[57]

From pristine to oxidized carbon fibers, surface density of acidic oxygen groups increased from 41 to 97 groups/nm^2, and decreased to 33 groups/nm^2 for the 1:1 silanization. These densities are significantly higher than other reports for oxidized carbons, which range from 1 to 5 groups/nm^2;[64, 67] type III fibers have been reported with densities starting at 30 groups/nm^2 for pristine fibers and increasing to > 1500 groups/nm^2, though the oxidized surface area was noted as misleading due to collapsed pores. The unexpectedly high density of acidic groups in the current study suggests BET N_2 analysis underreports surface area. Despite underreporting surface area, and based on similar analysis[52, 57] it is anticipated that average pore diameter of oxidized samples in the current study are more than adequate considering the projected area of similar silanes was on the order of 0.5 nm^2,[52] but harsher oxidation conditions would not benefit silanization in terms of surface morphology.

Considering the silanized sample, increased surface area was unexpected based on literature. Silanization has been shown to reduce surface area on moderate surface area carbons (> 50 m^2/g), which was attributed to coating of the micropores.[47, 52] The rate of the decreasing specific surface area versus the adsorbed silane was shown to vary by type of silanization agent, where a diamino organosilane resulted in the largest decrease with the least silane adsorption due to its increased molecular length.[38] Despite 1:1 stoichiometry intending to silanize all available sites, XPS results suggest that the large amount of dilution limited silane uptake (Section 3.5.5); this could result in reduced amounts of silane reacting with the surface compared to literature reports, and increased opportunity for silane molecules to be in a chain extended form or in a

loop with the surface, increasing surface area.[57] Alternatively, silane could prevent pores from collapsing when dried, accounting for the substantial decrease in pore mode.

3.5.4. Silanization: Surface Composition and Binding State Analysis Using XPS

Analysis of surface composition and functionality was conducted using XPS as a method to determine the amount of silanization (using silicon as an indicator), as well estimate the orientation of silane molecules on the carbon fiber surface. At first glance, XPS results followed expectation, where the higher stoichiometric ratios of silane resulted in higher levels of silicon (silane) on the carbon surface. Furthermore, the two methods exhibited a contrast in their maximum and minimum silicon values that coincided with the design of each method. (Table 3-9/Figure 3-7 and Figure 3-8) Worth noting, silicon content makes no indication of the type of silane presence on the sample – whether the molecules are condensed with one-another and adsorbed to the surface in agglomerations, or present in monolayers on the surface – but simply the surface-composition.

The EtOH solution was designed to take advantage of adsorbed surface moisture to hydrolyze silane, and was expected to produce a near-monolayer coverage provided enough silane and adsorbed moisture; the relatively equivalent levels of silane measured by XPS for the 10:1 and 5:1 EtOH stoichiometry solutions could indicate that, upon hydrolyzing with the available moisture and reacting with the available functional groups, excess silane remained in solution. The 1:1 EtOH sample showed a decrease in silicon content, attributed to inadequate levels of silane in solution.

Alternatively, the 95:5 vol-% solutions of EtOH:H_2O was designed to allow silane to hydrolyze before contacting the carbon fiber surface, and this was anticipated to result in higher

levels of silanization in the form of multilayers and agglomerations. Unsurprisingly, silicon content scaled more directly with the stoichiometric ratio of silane in solution, indicating that, unlike in the EtOH solution, surface hydrolization and functionalization did not limit silanization. This allowed more complete coverage of the fibers. The lower value of silicon for the 1:1 stoichiometry of the 95:5 solution compared to the EtOH solution could be attributed to hydrolyzed silanes reacting in solution and failing to react with the carbon surface.

The results appear less definitive when considering all elements, where the two solutions appear to react differently with the oxidized surface. On a compositional level, silane lies in stark contrast to the oxidized carbon surface. Excluding hydrogen, unhydrolized silane (Z-6020) contains 48, 14, 24, and 14 at-% carbon, nitrogen, oxygen, and silicon, respectively, while hydrolized silane contains 37, 17, 29, and 17 at-% carbon, nitrogen, oxygen, and silicon, respectively. These are less carbon dominant than the oxidized carbon surface that was 76, 8.7, and 14.5 at-% carbon, nitrogen, and oxygen, respectively. The 95:5 solution exhibited compositional changes that coincided with a '*highly*' silanized surface when treated with the 10:1 stoichiometry solution, and changed steadily towards the oxidized fiber composition (in terms of carbon, nitrogen, oxygen, and silicon) with decreasing solution stoichiometry. This further supports a rather simple relationship linking higher levels of silane in solution to higher levels of silane on the carbon surface. Conversely, the EtOH solution did not show a simple trend following solution stoichiometry; carbon content remained relatively stable regardless of silane solution stoichiometry, and neither oxygen nor nitrogen trended towards the oxidized fiber values.

An additional consideration is the composition variation between the two ends of the silane molecule – the three hydrolysable *R'* units, and the functional *R* unit – where one end is

nitrogen dominant and the other is silicon and oxygen dominant. Molecular orientation of silane with respect to the surface can affect compositional measurements with XPS. Metwalli et al.[37] used treated glass and angle-resolved XPS to determine the protonation of nitrogen at various depths, finding protonated nitrogens (400 eV) were nearer the surface than nonprotonated nitrogens (398.5 eV). Palencia[47] used FTIR, TGA, and XPS to investigate silanization of carbon nanofibers developed using the floating catalyst method,[69] which produced low oxygen content fibers that also contain some contamination from the catalyst. With these fibers and an equivalent silane as used in the current study, they suggest the silanes were oriented horizontally to the surface, stabilized by hydrogen bonds and protonated amines.

Using a technique similar to Metwalli et al.[37] – but where samples were changed and angle stayed constant – a comparison of the protonated amine peak at 401 eV with respect to the peak at 400 eV was conducted using both element weighted (Table 3-10) and composition weighted (Table 3-11) functional group analysis; the peak designations differ because Metwalli used a smaller number of peaks. All fibers treated with the EtOH solution showed higher ratios of 401 eV/400 eV compared to the 95:5 solution of EtOH:H_2O (Table 3-10). This indicates the EtOH solutions produced higher levels of protonated nitrogen.[37] The identification of the peak at 406 eV is typically associated with nitro complexes,[61, 62] which has been suggested to be the result of chemisorption of NO between quinone groups, or chemisorption of NO_2 adjacent to quinone groups,[62] and the silanized carbon fiber samples show an increase in these nitro complexes with silanization. This is as of yet unexplained, but lies as another difference between the EtOH and 95:5 silanization solutions: the EtOH solutions showed higher formation of these oxidized nitrogen groups compared to the 95:5 solutions.

Based on the above information and reaction mechanisms proposed in literature, it is suggested that the dominant coupling reaction differs between the two solutions in the current study as follows:

1) Silane in EtOH solutions failed to hydrolyze by adsorbed moisture, and instead relied on hydrogen bonding and possibly amine reactions with surface groups as suggested by Yuen et al.[24] and Pittman et al.[57] to bond to the surface. When provided inadequate levels of H_2O to hydrolyze, silane molecules can be physisorbed to the surface via amine protonation in solution,[37] and then cure to the carbon fiber surface through an amine reaction with surface carboxylic acids, carbonyls, etc. The unhydrolyzed methoxy groups protect the silicon core from reacting. This is believed to be the case because the amount of silane on the fiber surface is independent of stoichiometry, consistently higher carbon peak at 286.5 eV (in part quantifying C-N groups for the proposed coupling reaction), more stable carbon content attributed to unhydrolyzed methoxy group, a prevalence of protonated nitrogens, and decreased nitrogen peak at 400 eV (in part quantifying –NH groups) with respect to the mixed 95:5 vol-% EtOH:H_2O solution.
2) Silane molecules in the mixed 95:5 vol-% of EtOH:H_2O undergo hydrolysis in solution, are physisorbed to the carbon surface during mixing, and then chemisorbed to the carbon fiber via the free silyl alcohol groups during cure. This was considered the more favorable reaction, allowing amine reaction during the epoxy cure for composite fabrication. The increased peak intensity at 400 eV could suggest a higher number of amines compared to the EtOH solution silanes (where amines were used in reaction with the fiber surface). Unlike the EtOH solution, the 95:5 vol-%

EtOH:H_2O solutions showed surface composition that varied predictably based on solution stoichiometry, and was thus considered the better candidate for use in further experimentation.

3.5.5. Silanization: XPS Surface Analysis Versus EDX Bulk Analysis

Compositional analysis of surface-modified samples was conducted using both XPS and EDX in an effort to compare their capabilities as well as to analyze the efficiency of various stoichiometric ratios of silane-to-CNF functionality during surface treatment; EDX is a cheaper method and accessible within the current facilities, while XPS is much more costly, time consuming, and requires outside facilities. Silicon was used as an indicator of silanization efficiency, where higher atomic-percentages of silicon represented samples with higher levels of silanization. As shown in Figure 3-9, there was a high level of disparity between the two methods.

Comparing XPS to EDX measurements, EDX detected much lower values of silicon that do not directly follow the trends observed during XPS analysis. The lower silicon atomic-percent could be explained by the fact that XPS only analyzes the top-most 3-10 nm (roughly 10 basal plane layers[58]), while EDX detected composition from the surface and bulk of many fibers; considering the carbon fibers are roughly 200 nm in diameter, the bulk sample measured by EDX is un-oxidized, un-silanized amorphous basal planes.

Two basic simulations performed using "monte CArlo SImulation of electroN trajectory in sOlids" (CASINO v 2.8/3.1, http://www.gel.usherbrooke.ca/casino/index.html) demonstrate the different interactions and sampling volumes used by each technique. Using the default software parameters and a 200 nm diameter carbon fiber, simulations were conducted for a 5 keV, 10 nm EDX beam (Figure 3-10[A]) and a 284 eV, large diameter XPS beam (Figure 3-

10[B]). EDX uses a focused beam of electrons to excite characteristic x-rays from various elements, while XPS uses the reverse process and uses a large diameter x-ray beam to excite characteristic binding energy photoelectrons. High-energy electrons used during EDX easily reach the core of narrow fibers (A) and excited x-rays are unattenuated in the material before detection; conversely, the low energy photoelectrons excited during XPS analysis (B) are highly attenuated and have a short path-length due to scattering and re-absorption by the material. As the simulations show, EDX samples the entire fiber volume and does so with a large number of fibers; alternatively, XPS only analyzes the surface and thus the relatively higher atomic percentage of silicon detected using XPS is reasonable.

With an understanding of why EDX values of silicon decreased compared to XPS, and in an effort to explain the disparity between trends using each analysis method, sample preparation was considered as the most likely cause. In order to completely immerse carbon fibers samples in solution during surface treatment, the 10:1 and 5:1 stoichiometries used 0.25 vol-% silane, while the 1:1 stoichiometry required 0.1 vol-% silane to fully immerse the fibers. The differences in dilution did not appear to affect the surface-chemistry of silanized carbon fibers (XPS), but bulk composition (EDX) of both EtOH and the mixed 95:5 vol-% EtOH:H_2O solutions showed higher levels of silane for the 5:1 stoichiometry compared to either the 10:1 or 1:1 stoichiometries. It is suggested this was due higher levels of silanization within the depth of the fibrous mats, reliant on the appropriate ratio of silane-to-solution and fiber mass.

Ratios of fiber mass (mg):silane (µl):solution (ml) were: 1.2:2.5:1, 2.3:2.5:1, and 4.6:1:1 for 10:1, 5:1, and 1:1 stoichiometry solutions, respectively. The higher stoichiometric solutions contained less fiber mass per volume of solution. Of particular interest, the 5:1 stoichiometry solution contained twice the mass of fibers for an equivalent volume of silane and solution

compared to the 10:1 stoichiometry solution, while the 1:1 stoichiometry contains twice the fiber mass of the 5:1 stoichiometry solution. From these various situations, as well as the results from surface composition (XPS) and bulk composition (EDX), three situations are expected to be occurring:

1) The 1:1 stoichiometric silane solution was 'silane-limited', where the amount of silane was too low to effectively coat the fibers either on the surface or into the depth of the fiber mat. This would coincide with both XPS and EDX results, where the surface (XPS) results showed less silane than the higher stoichiometries, and bulk (EDX) showed moderate to low levels of silanization due to uptake of many of the available silane molecules.
2) The 5:1 stoichiometric solution provided a more appropriate amount of fiber balanced with available silane to allow both surface silanization (XPS), as well as silanization into the bulk of the fiber mat (EDX).
3) The 10:1 stoichiometric solution was 'dilution-limited', where the fiber mass was too low compared to the volume of solution; while this had the highest amount of silane-per-gram of fiber in solution, the diffusion processes to get silane to the carbon surface was not strong enough to effectively coat the bulk. Silane could be readily reacted with the surface (XPS), but failed to diffuse to the center of the mat (EDX).

3.6. Summary of Findings and Conclusions

Critical to the interests of the funding grant, the current study focused on a thorough analysis the surface of in-house fabricated, electrospun carbon fibers using a variety of techniques. This analysis provided a foundation for understanding the carbon fiber surface that

was suggested to be an important factor for shape memory effects in composites. Investigating the effect of the fiber surface on shape memory properties requires understanding of the surface of both the pristine and modified fibers. The following was determined for the in-house electrospun polyacrylonitrile (PAN) based type III carbon fibers.

1) A time-series oxidation in nitric acid showed that treatment at 90 °C did not saturate the available defect sites of the outer 3-10 nm (~10 basal planes). The first 10 minutes served to oxidize the most superficial sites and resulted in a large increase in oxygen content, as well as increased nitrogen in oxidized forms. Oxygen content continually increased through 90 minutes, while both carbon and nitrogen decrease beyond the 10-minute time point. The 60 minute oxidized sample was chosen for continued investigation due to the high levels of oxygen functionalities. In an effort to promote fiber integrity, treatment temperature was reduced to 80 °C, but general trends in functionality are expected to be similar. Using high-resolution analysis of samples oxidized for 60-minutes at 80 °C, surface oxygen increased to 14.5 at-%, roughly equivalent to the 40-minute time-point when oxidized at 90 °C. The oxygen and nitrogen groups were determined to be in protonated and oxidized forms, which increased surface polarity and favorability for wetting by the epoxy resin.
2) A sodium hydroxide neutralization and titration was performed in a method similar to the Boehm titration, and results were compared with literature to estimate that the 60-minute (80°C) nitric acid oxidized carbon fibers in the current study contained roughly 800 μmol/g of alcohol-based functional groups; these were the functionalities considered most likely to react with the hydrolyzed methody groups on the currently studied silane.

Using this, a formula was developed to tailor solutions to provide various stoichiometric ratios of silane-to-CNF functionality.

3) Nitrogen adsorption was used to determine a surface area, and results suggest that surface area increased from 4.53 m^2/g to 6 m^2/g with oxidation, with increased macropore volume and decreased average pore diameter and average width, with simultaneously increased mode for pore width. Oxidation increased the density of functional groups increased from 41 to 97 groups/nm^2, which is higher than those reported for higher temperature treated carbons, but lower than other type III carbons that suffered from micropore collapse, suggesting the current surface area measurements underestimate the available pore volume. The increasing mode width could support micropores that developing and collapse.
4) Surface analysis using XPS suggests the two solutions react uniquely with the carbon surface. The 95:5 solutions of EtOH:H_2O provided surface composition consistent with stoichiometric ratios of silane, where higher stoichiometries with respect to carbon functional group resulted in higher silicon, nitrogen, and oxygen compared to oxidized samples; decreasing stoichiometry resulted in simple trends towards the oxidized carbon fiber composition. It is expected that the reaction mechanism use the hydrolyzed methoxy groups to react with the surface. Alternatively, the composition for the EtOH silanization solution did not follow any notable trend based on solution stoichiometry. It was thus considered that these silanes might result in bonding through amine coupling, or physisorption.
5) Using bulk composition analysis (EDX) compared to surface composition (XPS), three cases of silanization are considered: silane limited, balanced, and dilution limited. These

resulted in higher levels of silane integration into fibers based on the relative ratio of silane to fiber mass, considering the dilution volume of the solution. It is suggested that future work be conducted using the 5:1 stoichiometry, 95:5 vol-% EtOH:H_2O solution. If higher stoichiometries are desired, it is suggested that a ratio of fiber mass (mg):silane (μl) of ~1:1 be used, keeping the solution enough to only cover the fibers in order to reduce dilution effects.

3.7. References

1. Leroy, S.; Boiziau, C.; Perreau, J.; Reynaud, C.; Zalczer, G.; Lecayon, G.; Legressus, C., Molecular-Structure of an Electropolymerized Polyacrylonitrile Film and Its Pyrolyzed Derivatives. *Journal of Molecular Structure* **1985,** 128, (4), 269-281.

2. Wang, Y.; Santiago-Aviles, J. J.; Furlan, R.; Ramos, I., Pyrolysis temperature and time dependence of electrical conductivity evolution for electrostatically generated carbon nanofibers. *Ieee Transactions on Nanotechnology* **2003,** 2, (1), 39-43.

3. McKee, D. W., Carbon and Graphite Science. *Annual Reviews of Materials Science* **1973,** 3, 195-231.

4. Johnson, D. J., Recent Advances in Studies of Carbon-Fiber Structure. *Philosophical Transactions of the Royal Society of London Series a-Mathematical Physical and Engineering Sciences* **1980,** 294, (1411), 443-&.

5. Zhou, Z. P.; Lai, C. L.; Zhang, L. F.; Qian, Y.; Hou, H. Q.; Reneker, D. H.; Fong, H., Development of carbon nanofibers from aligned electrospun polyacrylonitrile nanofiber bundles

and characterization of their microstructural, electrical, and mechanical properties. *Polymer* **2009,** 50, (13), 2999-3006.

6. Zussman, E.; Chen, X.; Ding, W.; Calabri, L.; Dikin, D. A.; Quintana, J. P.; Ruoff, R. S., Mechanical and structural characterization of electrospun PAN-derived carbon nanofibers. *Carbon* **2005,** 43, (10), 2175-2185.

7. Zhou, Z. P.; Liu, K. M.; Lai, C. L.; Zhang, L. F.; Li, J. H.; Hou, H. Q.; Reneker, D. H.; Fong, H., Graphitic carbon nanofibers developed from bundles of aligned electrospun polyacrylonitrile nanofibers containing phosphoric acid. *Polymer* **2010,** 51, (11), 2360-2367.

8. Takaku, A.; Shioya, M., X-Ray Measurements and the Structure of Polyacrylonitrile- and Pitch-Based Carbon-Fibers. *Journal of Materials Science* **1990,** 25, (11), 4873-4879.

9. Harris, P. J. F., New perspectives on the structure of graphitic carbons. *Critical Reviews in Solid State and Materials Sciences* **2005,** 30, (4), 235-253.

10. Kumar, A.; Lobo, R. F.; Wagner, N. J., Porous amorphous carbon models from periodic Gaussian chains of amorphous polymers. *Carbon* **2005,** 43, (15), 3099-3111.

11. Liu, F. J.; Wang, H. J.; Xue, L. B.; Fan, L. D.; Zhu, Z. P., Effect of microstructure on the mechanical properties of PAN-based carbon fibers during high-temperature graphitization. *Journal of Materials Science* **2008,** 43, (12), 4316-4322.

12. Radovic, L. R.; Bockrath, B., On the chemical nature of graphene edges: Origin of stability and potential for magnetism in carbon materials. *Journal of the American Chemical Society* **2005,** 127, (16), 5917-5927.

13. Deurbergue, A.; Oberlin, A., Stabilization and Carbonization of Pan-Based Carbon-Fibers as Related to Mechanical-Properties. *Carbon* **1991,** 29, (4-5), 621-628.

14. Ferguson, J.; Mahapatro, B., Pyrolysis Studies on Polyacrylonitrile Fibers - Influence of Conditions and Molecular-Weight on Tensile Property Changes During Initial-Stages of Pyrolysis. *Fibre Science & Technology* **1978,** 11, (1), 55-66.

15. Fitzer, E.; Frohs, W.; Heine, M., Optimization of Stabilization and Carbonization Treatment of Pan Fibers and Structural Characterization of the Resulting Carbon-Fibers. *Carbon* **1986,** 24, (4), 387-395.

16. Rahaman, M. S. A.; Ismail, A. F.; Mustafa, A., A review of heat treatment on polyacrylonitrile fiber. *Polymer Degradation and Stability* **2007,** 92, (8), 1421-1432.

17. Morgan, P., *Carbon Fibers and Their Composites*. 1 ed.; CRC Press: 6000 Broken Sound Parkway NW, Suite 300
Boca Raton, FL 33487, 2005.

18. He, J. M.; Huang, Y. D., Effect of silane-coupling agents on interfacial properties of CF/PI composites. *Journal of Applied Polymer Science* **2007,** 106, (4), 2231-2237.

19. Park, S. J.; Kim, B. J., Roles of acidic functional groups of carbon fiber surfaces in enhancing interfacial adhesion behavior. *Materials Science and Engineering a-Structural Materials Properties Microstructure and Processing* **2005,** 408, (1-2), 269-273.

20. Laszlo, K.; Tombacz, E.; Josepovits, K., Effect of activation on the surface chemistry of carbons from polymer precursors. *Carbon* **2001,** 39, (8), 1217-1228.

21. Im, J. S.; Park, S. J.; Lee, Y. S., Preparation and characteristics of electrospun activated carbon materials having meso- and macropores. *Journal of Colloid and Interface Science* **2007,** 314, (1), 32-37.

22. Ryu, Z. Y.; Rong, H. Q.; Zheng, J. T.; Wang, M. Z.; Zhang, B. J., Microstructure and chemical analysis of PAN-based activated carbon fibers prepared by different activation methods. *Carbon* **2002,** 40, (7), 1144-1147.

23. Pittman, C. U.; Jiang, W.; Yue, Z. R.; Leon, C., Surface area and pore size distribution of microporous carbon fibers prepared by electrochemical oxidation. *Carbon* **1999,** 37, (1), 85-96.

24. Yuen, S. M.; Ma, C. C. M.; Chiang, C. L.; Teng, C. C., Morphology and properties of aminosilane grafted MWCNT/polyimide nanocomposites. *Journal of Nanomaterials* **2008**.

25. Toebes, M. L.; van Heeswijk, E. M. P.; Bitter, J. H.; van Dillen, A. J.; de Jong, K. P., The influence of oxidation on the texture and the number of oxygen-containing surface groups of carbon nanofibers. *Carbon* **2004,** 42, (2), 307-315.

26. Lakshminarayanan, P. V.; Toghiani, H.; Pittman, C. U., Nitric acid oxidation of vapor grown carbon nanofibers. *Carbon* **2004,** 42, (12-13), 2433-2442.

27. Hughes, J. D. H., The Carbon-Fiber Epoxy Interface - a Review. *Composites Science and Technology* **1991,** 41, (1), 13-45.

28. Boehm, H. P., Some Aspects of the Surface-Chemistry of Carbon-Blacks and Other Carbons. *Carbon* **1994,** 32, (5), 759-769.

29. Figueiredo, J. L.; Pereira, M. F. R.; Freitas, M. M. A.; Orfao, J. J. M., Modification of the surface chemistry of activated carbons. *Carbon* **1999,** 37, (9), 1379-1389.

30. Kanai, Y.; Khalap, V. R.; Collins, P. G.; Grossman, J. C., Atomistic Oxidation Mechanism of a Carbon Nanotube in Nitric Acid. *Physical Review Letters* **2010,** 104, (6).

31. Leon, C.; Solar, J. M.; Calemma, V.; Radovic, L. R., Evidence for the Protonation of Basal-Plane Sites on Carbon. *Carbon* **1992,** 30, (5), 797-811.

32. Corning, D., A guide to silane solutions. In 2005; pp 1-30.

33. Herder, P.; Vagberg, L.; Stenius, P., Esca and Contact-Angle Studies of the Adsorption of Aminosilanes on Mica. *Colloids and Surfaces* **1988,** 34, (2), 117-132.

34. Mourougou-Candoni, N.; Thibaudau, F., Formation of Aminosilane Film on Mica. *Journal of Physical Chemistry B* **2009,** 113, (39), 13026-13034.

35. Wang, M. J.; Liechti, K. M.; Wang, Q.; White, J. M., Self-assembled silane monolayers: Fabrication with nanoscale uniformity. *Langmuir* **2005,** 21, (5), 1848-1857.

36. Li, H.; Zhang, J.; Zhou, X. Z.; Lu, G.; Yin, Z. Y.; Li, G. P.; Wu, T.; Boey, F.; Venkatraman, S. S.; Zhang, H., Aminosilane Micropatterns on Hydroxyl-Terminated Substrates: Fabrication and Applications. *Langmuir* **2010,** 26, (8), 5603-5609.

37. Metwalli, E.; Haines, D.; Becker, O.; Conzone, S.; Pantano, C. G., Surface characterizations of mono-, di-, and tri-aminosilane treated glass substrates. *Journal of Colloid and Interface Science* **2006,** 298, (2), 825-831.

38. Palencia, C.; Rubio, J.; Rubio, F.; Fierro, J. L. G.; Oteo, J. L., Silane Coupling Agent Structures on Carbon Nanofibers. *Journal of Nanoscience and Nanotechnology* **2011,** 11, (5), 4142-4152.

39. Chehimi, M. M.; Abel, M. L.; Watts, J. F.; Digby, R. P., Surface chemical and thermodynamic properties of gamma-glycidoxy-propyltrimethoxysilane-treated alumina: an XPS and IGC study. *Journal of Materials Chemistry* **2001,** 11, (2), 533-543.

40. Ma, P. C.; Kim, J. K.; Tang, B. Z., Effects of silane functionalization on the properties of carbon nanotube/epoxy nanocomposites. *Composites Science and Technology* **2007,** 67, (14), 2965-2972.

41. Paquet, O.; Salon, M. C. B.; Zeno, E.; Belgacem, M. N., Hydrolysis-condensation kinetics of 3-(2-amino-ethylamino)propyl-trimethoxysilane. *Materials Science & Engineering C-Materials for Biological Applications* **2012,** 32, (3), 487-493.

42. Shokoohi, S.; Arefazar, A.; Khosrokhavar, R., Silane coupling agents in polymer-based reinforced composites: A review. *Journal of Reinforced Plastics and Composites* **2008,** 27, (5), 473-485.

43. Arkles, B.; Steinmetz, J. R.; Zazyczny, J.; Mehta, P., Factors Contributing to the Stability of Alkoxysilanes in Aqueous-Solution. *Journal of Adhesion Science and Technology* **1992,** 6, (1), 193-206.

44. Vandenberg, E. T.; Bertilsson, L.; Liedberg, B.; Uvdal, K.; Erlandsson, R.; Elwing, H.; Lundstrom, I., Structure of 3-Aminopropyl Triethoxy Silane on Silicon-Oxide. *Journal of Colloid and Interface Science* **1991,** 147, (1), 103-118.

45. Beari, F.; Brand, M.; Jenkner, P.; Lehnert, R.; Metternich, H. J.; Monkiewicz, J.; Siesler, H. W., Organofunctional alkoxysilanes in dilute aqueous solution: new accounts on the dynamic structural mutability. *Journal of Organometallic Chemistry* **2001,** 625, (2), 208-216.

46. Jiang, H. M.; Zheng, Z.; Xiong, J. W.; Wang, X. L., Studies on dialkoxysilane hydrolysis kinetics under alkaline conditions. *Journal of Non-Crystalline Solids* **2007,** 353, (44-46), 4178-4185.

47. Palencia, C.; Rubio, F.; Merino, C.; Rubio, J.; Oteo, J. L., Study of the Silanization Process in CNFs: Time, Temperature, Silane Type and Concentration Influence. *Journal of Nano Research* **2008,** 4, 33-43.

48. Luo, X.; Mather, P. T., Conductive shape memory nanocomposites for high speed electrical actuation. *Soft Matter* **2010,** 6, (10), 2146-2149.

49. Goertzen, S. L.; Theriault, K. D.; Oickle, A. M.; Tarasuk, A. C.; Andreas, H. A., Standardization of the Boehm titration. Part I. CO2 expulsion and endpoint determination. *Carbon* **2010,** 48, (4), 1252-1261.

50. Oickle, A. M.; Goertzen, S. L.; Hopper, K. R.; Abdalla, Y. O.; Andreas, H. A., Standardization of the Boehm titration: Part II. Method of agitation, effect of filtering and dilute titrant. *Carbon* **2010,** 48, (12), 3313-3322.

51. Zhao, X. S.; Lu, G. Q.; Whittaker, A. K.; Millar, G. J.; Zhu, H. Y., Comprehensive study of surface chemistry of MCM-41 using Si-29 CP/MAS NMR, FTIR, pyridine-TPD, and TGA. *Journal of Physical Chemistry B* **1997,** 101, (33), 6525-6531.

52. Nistal, A.; Palencia, C.; Mazo, M. A.; Rubio, F.; Rubio, J.; Oteo, J. L., Analysis of the interaction of vinyl and carbonyl silanes with carbon nanofiber surfaces. *Carbon* **2011,** 49, (5), 1635-1645.

53. Otake, Y.; Jenkins, R. G., Characterization of Oxygen-Containing Surface Complexes Created on a Microporous Carbon by Air and Nitric-Acid Treatment. *Carbon* **1993,** 31, (1), 109-121.

54. Zhou, J. H.; Sui, Z. J.; Zhu, J.; Li, P.; De, C.; Dai, Y. C.; Yuan, W. K., Characterization of surface oxygen complexes on carbon nanofibers by TPD, XPS and FT-IR. *Carbon* **2007,** 45, (4), 785-796.

55. Yue, Z. R.; Jiang, W.; Wang, L.; Gardner, S. D.; Pittman, C. U., Surface characterization of electrochemically oxidized carbon fibers. *Carbon* **1999,** 37, (11), 1785-1796.

56. Pamula, E.; Rouxhet, P. G., Bulk and surface chemical functionalities of type IIIPAN-based carbon fibres. *Carbon* **2003,** 41, (10), 1905-1915.

57. Pittman, C. U.; He, G. R.; Wu, B.; Gardner, S. D., Chemical modification of carbon fiber surfaces by nitric acid oxidation followed by reaction with tetraethylenepentamine. *Carbon* **1997,** 35, (3), 317-331.

58. Alexander, M. R.; Jones, F. R., Effect of Electrolytic Oxidation on the Surface-Chemistry of Type-a Carbon-Fibers .1. X-Ray Photoelectron-Spectroscopy. *Carbon* **1994,** 32, (5), 785-794.

59. Gardner, S. D.; Singamsetty, C. S. K.; Booth, G. L.; He, G. R.; Pittman, C. U., Surface Characterization of Carbon-Fibers Using Angle-Resolved Xps and Iss. *Carbon* **1995,** 33, (5), 587-595.

60. Xie, Y. M.; Sherwood, P. M. A., X-Ray Photoelectron Spectroscopic Studies of Carbon-Fiber Surfaces .11. Differences in the Surface-Chemistry and Bulk Structure of Different Carbon-Fibers Based on Poly(Acrylonitrile) and Pitch and Comparison with Various Graphite Samples. *Chemistry of Materials* **1990,** 2, (3), 293-299.

61. Boudou, J. P.; Parent, P.; Suarez-Garcia, F.; Villar-Rodil, S.; Martinez-Alonso, A.; Tascon, J. M. D., Nitrogen in aramid-based activated carbon fibers by TPD, XPS and XANES. *Carbon* **2006,** 44, (12), 2452-2462.

62. Garcia, P.; Espinal, J. F.; de Lecea, C. S. M.; Mondragon, F., Experimental characterization and molecular simulation of nitrogen complexes formed upon NO-char reaction at 270 degrees C in the presence of H2O and O-2. *Carbon* **2004,** 42, (8-9), 1507-1515.

63. Papirer, E.; Li, S.; Donnet, J. B., Contribution to the Study of Basic Surface Groups on Carbons. *Carbon* **1987,** 25, (2), 243-247.

64. Contescu, A.; Contescu, C.; Putyera, K.; Schwarz, J. A., Surface acidity of carbons characterized by their continuous pK distribution and Boehm titration. *Carbon* **1997,** 35, (1), 83-94.

65. Donnet, J. B., Chemical Reactivity of Carbons. *Carbon* **1968,** 6, (2), 161-&.

66. Pereira, L.; Pereira, R.; Pereira, M. F. R.; van der Zee, F. P.; Cervantes, F. J.; Alves, M. M., Thermal modification of activated carbon surface chemistry improves its capacity as redox mediator for azo dye reduction. *Journal of Hazardous Materials* **2010,** 183, (1-3), 931-939.

67. Papirer, E.; Dentzer, J.; Li, S.; Donnet, J. B., Surface Groups on Nitric-Acid Oxidized Carbon-Black Samples Determined by Chemical and Thermodesorption Analyses. *Carbon* **1991,** 29, (1), 69-72.

68. Gonzalez, M. T.; Sepulvedaescribano, A.; Molinasabio, M.; Rodriguezreinoso, F., Correlation between Surface-Areas and Micropore Volumes of Activated Carbons Obtained from Physical Adsorption and Immersion Calorimetry. *Langmuir* **1995,** 11, (6), 2151-2155.

69. Martin-Gullon, I.; Vera, J.; Conesa, J. A.; Gonzalez, J. L.; Merino, C., Differences between carbon nanofibers produced using Fe and Ni catalysts in a floating catalyst reactor. *Carbon* **2006,** 44, (8), 1572-1580.

70. Wu, M. Y.; Wang, Q. Y.; Li, K. N.; Wu, Y. Q.; Liu, H. Q., Optimization of stabilization conditions for electrospun polyacrylonitrile nanofibers. *Polymer Degradation and Stability* **2012,** 97, (8), 1511-1519.

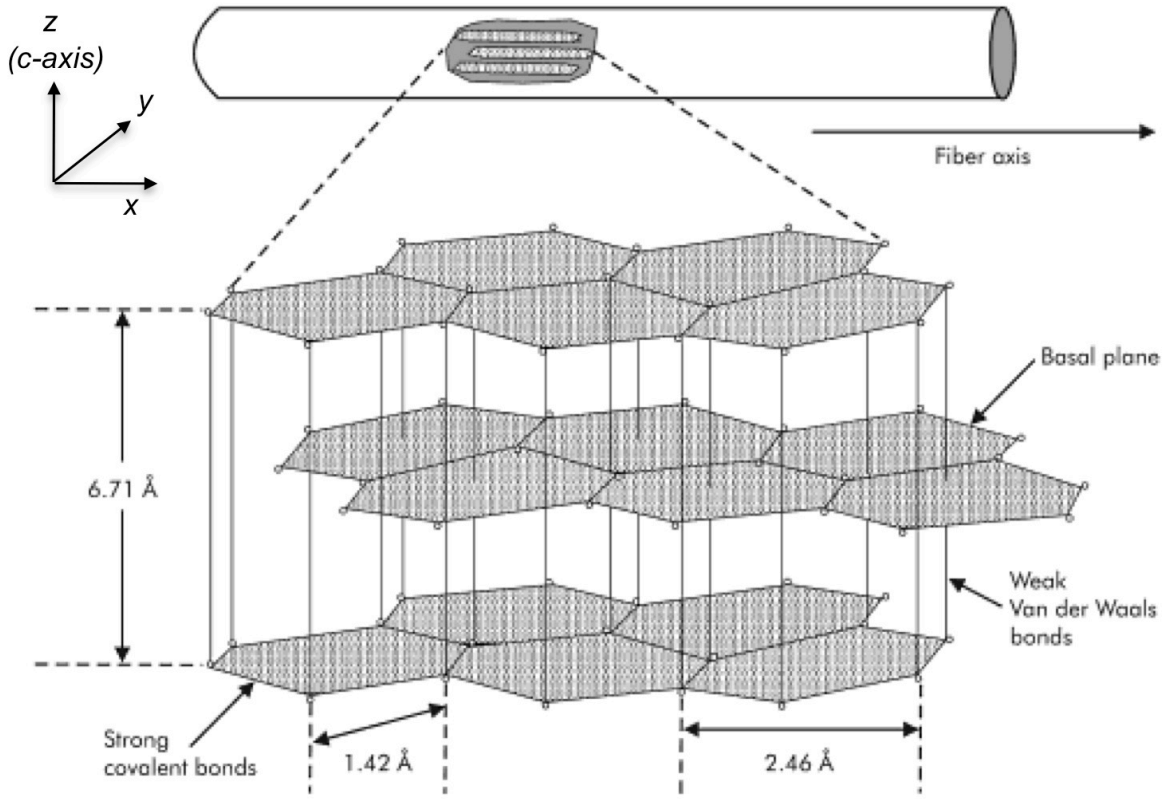

Figure 3-1. Basal plane dimensions and orientation within a hexagonal close-packed (ABAB) graphitic carbon fiber. [Screenshot from Fundamentals Of Composites Manufacturing: Materials, Methods and Applications, A. Brent Strong, (Pg 213)]

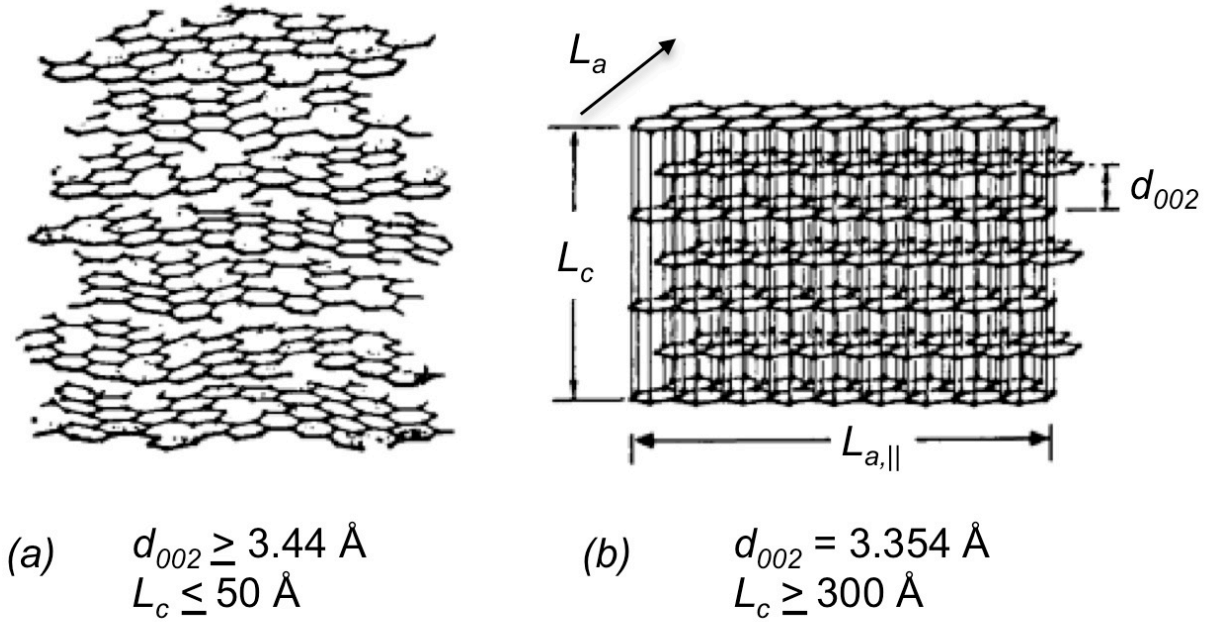

Figure 3-2. High temperature treatment of PAN results in (a) turbostratic basal planes compared to (b) highly ordered graphite. Turbostratic planes are near-parallel, but result in larger inter-plane spacing and reduced VDW interaction. The basal plane dimensions are also smaller in turbostratic carbon. [Screenshot of an image from Bokros JC, "Deposition, Structure, and Properties of Pyrolytic Carbon" (1969), arrived at through *Carbon Fibers and Their Composites* by P. Morgan.[17]]

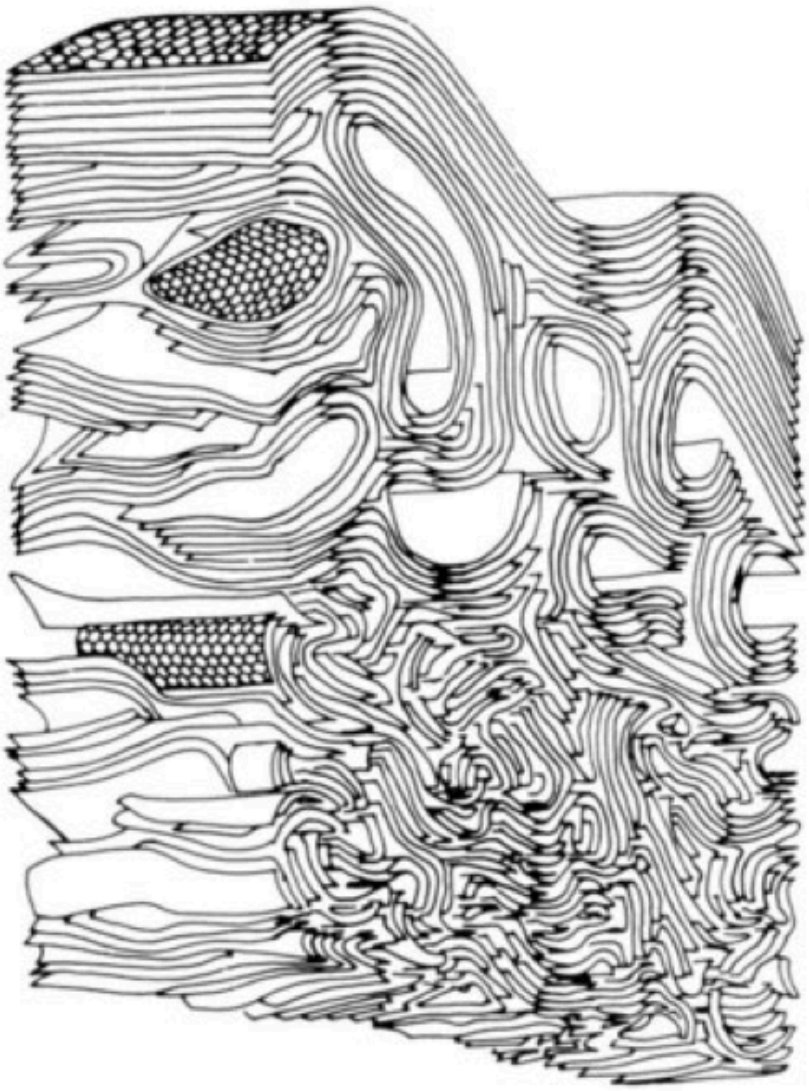

Figure 3-3. Schematic of high-modulus carbon fiber microstructure as proposed by Johnson. Lower treatment temperatures would result in a more disordered structure with respect to the skin. [Screenshot from "Structure-property relationships in carbon fibres," J. Phys. D: Appl. Phys. 20 286 1987]

Table 3-1. Refinement of turbostratic carbon structure in polyacrylonitrile based carbon fibers as measured by x-ray diffraction. Electrical conductivity was measured with fiber bundles in parallel and perpendicular orientation ($\sigma_{\parallel} / \sigma_{\perp}$). Ultimate tensile strength (σ_{UTS}) and Young's Modulus (E) were measured with traditional tensile testing, at crosshead speeds of 8.3×10^{-6} m/s and 3.3×10^{-3} m/s for Zhou[5] and Liu[11], respectively.

	Zhou et al.[5]				Liu et al.[11]		
Temperature (°C)	**L_c (nm)**	**d_{002} (Å)**	**$\sigma_{\parallel} / \sigma_{\perp}$ (S/cm)**	**σ_{UTS} (MPa) / E (GPa)**	**L_c (nm)**	**d_{002} (Å)**	**σ_{UTS} (MPa) / E (GPa)**
1000	0.88	3.62	200 / 10	325 / 40	-	-	-
1400	1.17	3.52	500 / 35	475 / 47	-	-	-
1800	4.25	3.46	700 / 40	500 / 55	2.5	3.51	3900 / 250
2200	4.94	3.44	820 / 60	550 / 58	3.6	3.49	3400 / 290
2400	-	-	-	-	4	3.46	3200 / 305
2800	-	-	-	-	6	3.43	2400 / 340

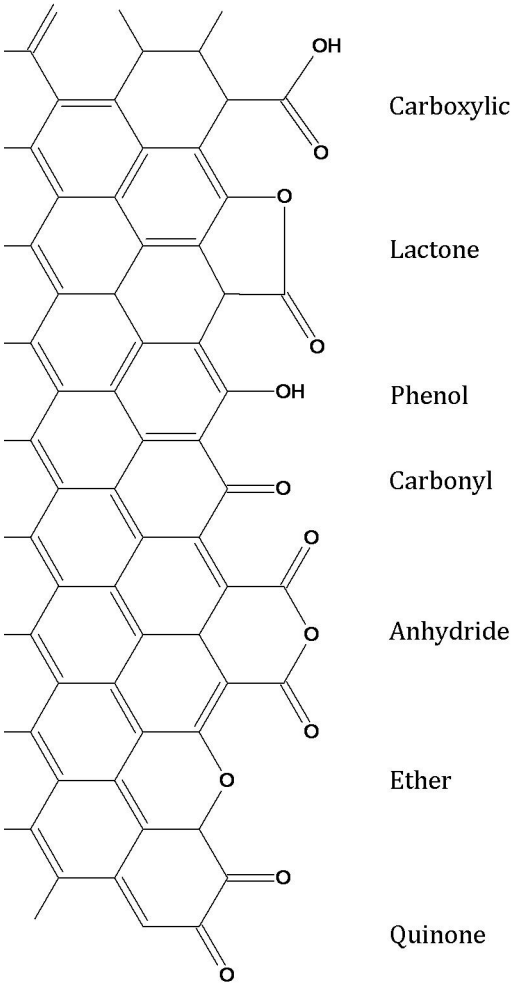

Scheme 3-1. Common oxygen groups introduced on carbon surfaces during oxidation and activation, adopted from Figueiredo et al.[29] Nitrogen functionalities were excluded, but are present on the fiber surface.

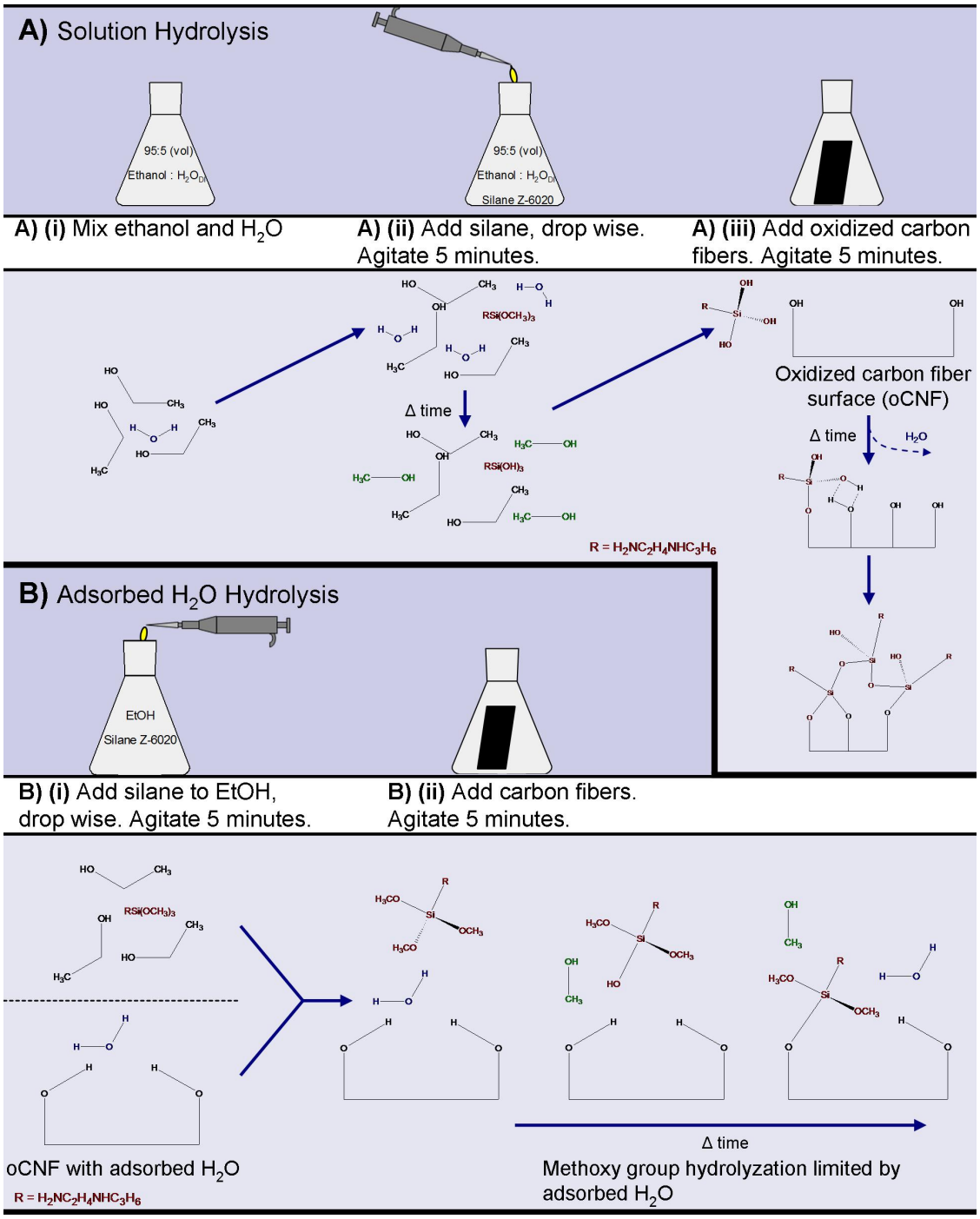

Scheme 3-2. Theoretical silanization mechanisms used to design experiment. Solution hydrolysis (A) functionalizes the coupling agent in solution, enabling accelerated reaction with the oxidized carbon nanofiber (oCNF) as well as silane-silane condensation in solution. Adsorbed H_2O hydrolysis (B) relies on moisture uptake by oxidized carbon fiber to locally hydrolize the methoxy groups on silane, reducing silane-silane condensation and promoting monolayer formation on the oxidized carbon fiber surface.

Table 3-2. Equipment parameters used during XPS acquisition. Survey scans are used for higher counts and more precise composition measurements, while element site scans provide resolution necessary to determine chemical binding states.

XPS Equipment Constants:			
Source, Al (K_α) (eV)		1486.6	
Spot Size (um) / Power (W)		800 / 200	
Dwell Time (s)		0.25	
Source / Detector Angle (°)		75 / 55	
	Variables:	**Survey Scans**	**Site Scans**
Pass Energy Filter (eV)		150	50
Resolution (eV)		4	2
eV/step		1	0.065
Width (eV)		-	22
Scans (#)	**Survey (Composition)**	4-5	-
	Carbon (1s, 285 eV)	-	6
	Nitrogen (1s, 400 eV)	-	6
	Oxygen (1s, 533 eV)	-	10
	Silicon (2p, 102 eV)	-	20

Table 3-3. Fitting parameters and group designations used for analysis of XPS spectra using OriginPro 8.6. Shirley-spline backgrounds were subtracted, and the FWHM of each peak was limited to parenthetical values. Fitting iterations were performed until convergence to a Chi-squared tolerance of 10^{-9} or less. Functional group binding energies were selected based on previous XPS analysis of carbons and silanized materials.[18, 26, 38, 47, 55, 56, 60, 70]

Peak Fitting Constants:			
Background	**Shirley-Spline**		
Gaussian:Lorentzian Ratio	**70:30 (*m* = 0.3)**		
Variables:			
Element (FWHM Bounds, eV)	**Peak**	**Center (eV)**	**Group Assignment**
Carbon 1s	I	284.8	-C=C- (sp^2/sp^3), C-H
(1.6 – 2)	II	286.5	C-OH, C-O-C, C-N (Phenol, alcohol, ether)
	III	288.8	C=O, C=N (Carbonyl, quinone, carboxyl, ester)
	IV	289.2	COOH, COOR (Carboxyl, Carbonate)
	V	291	C-C Shakeup/Satellite
Nitrogen 1s	I	398.5	Pyridine, Ar-N-Ar
(1.8 – 2.2)	II	400	-NH, -O-C=N (Pyrrole, pyridine, lactam, imide, amide, amine)
	III	401	N-quaternary
	IV	403	Pyridine-N-Oxide
	V	405	NOx, N-O-C
Oxygen 1s	I	530.5	O=C (Carbonyl, carbonate)
(1.5 – 1.9)	II	531.3	O=C (Quinone, carbonyl, carboxyl)
	III	532.5	C=O-H, C=O-C (Amide, ester, hydroxyl, anhydride)
	IV	533	C-O-C (Carboxyl, phenol, ester, anhydride)
	V	534.5	Chemisorbed oxygen
Silicon 2p	I	102.3	Si-O_2 (Si-C), Si-N
(1.5 – 1.9)	II	103.5	Si-O_2 (Silica)

Table 3-4. Surface composition changes continually during oxidation with nitric acid (70%) at 90 °C. The first 10 minutes were responsible for a large part of oxidation at superficial defect sites and saturated edges.

		Nitric Acid (70%) Oxidized, 90 °C Time (min)				
Element	**Pristine**	**10**	**20**	**40**	**60**	**90**
C	91.7	80.5	79.0	81.5	76.6	76.3
N	5.0	5.7	5.0	4.7	3.3	2.3
O	3.3	13.8	16.0	13.9	20.1	21.3

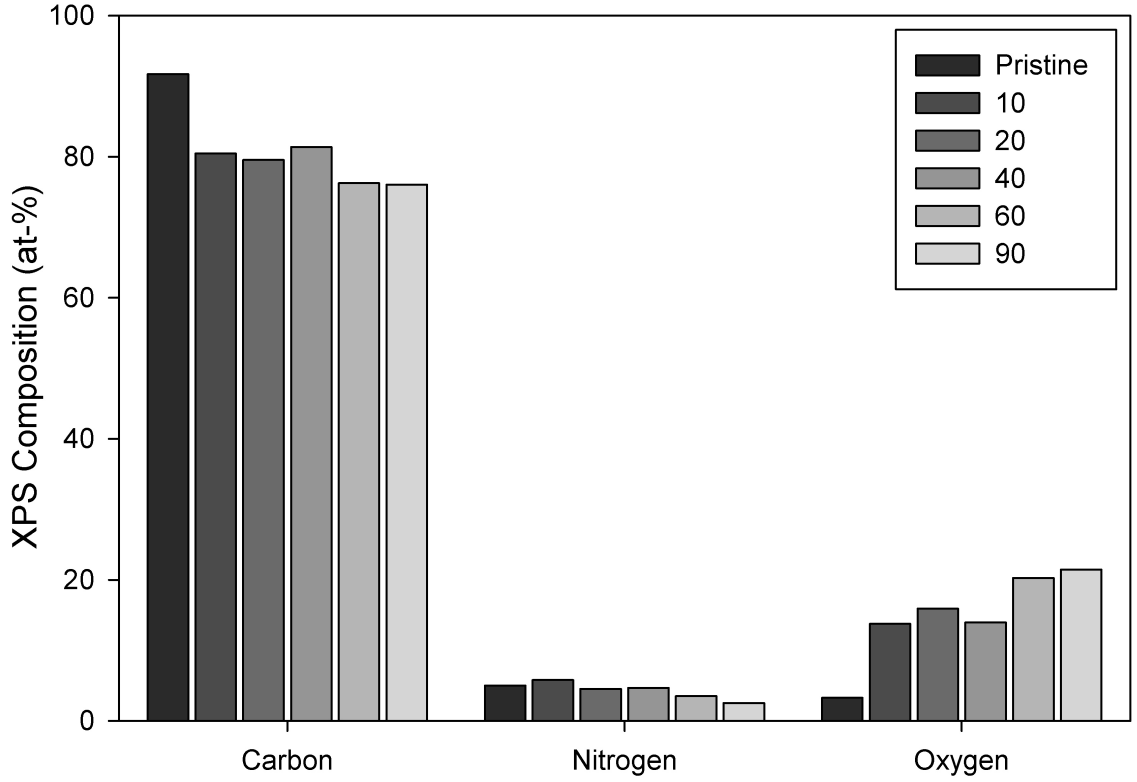

Figure 3-4. Surface composition measured by XPS changed steadily during oxidation with nitric acid (70%) at 90 °C. The initial 10 minutes were responsible for a large part of oxidation. Grey-scale decreases with oxidation time (min).

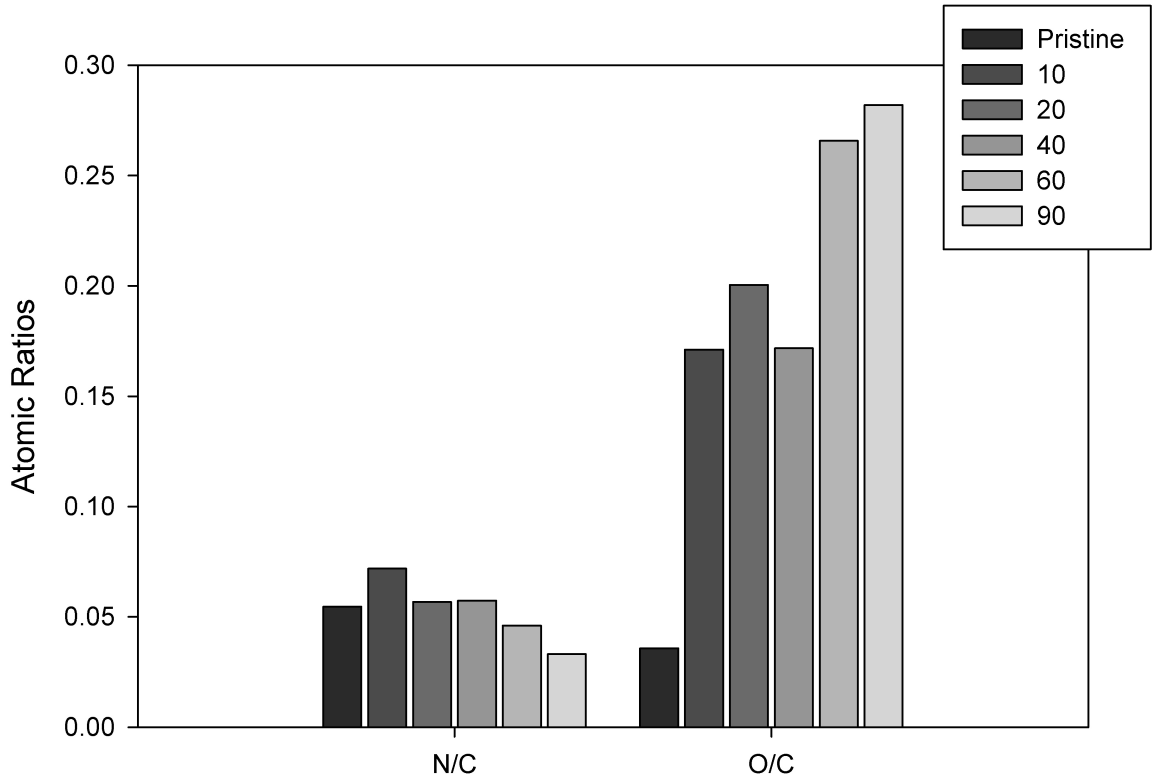

Figure 3-5. Atomic ratios measured by XPS during oxidation revealed N/C remained relatively steady during early oxidation, but declined at long time points, while O/C initially increased dramatically followed by a decreasing rate of oxygen uptake with extended oxidation. Initial increases in nitrogen were attributed to adsorbed HNO_3, which reduced to oxygen groups after producing NO_x. Oxygen content almost reached an steady state after 90 minutes, but continued to react at a much reduced rate.

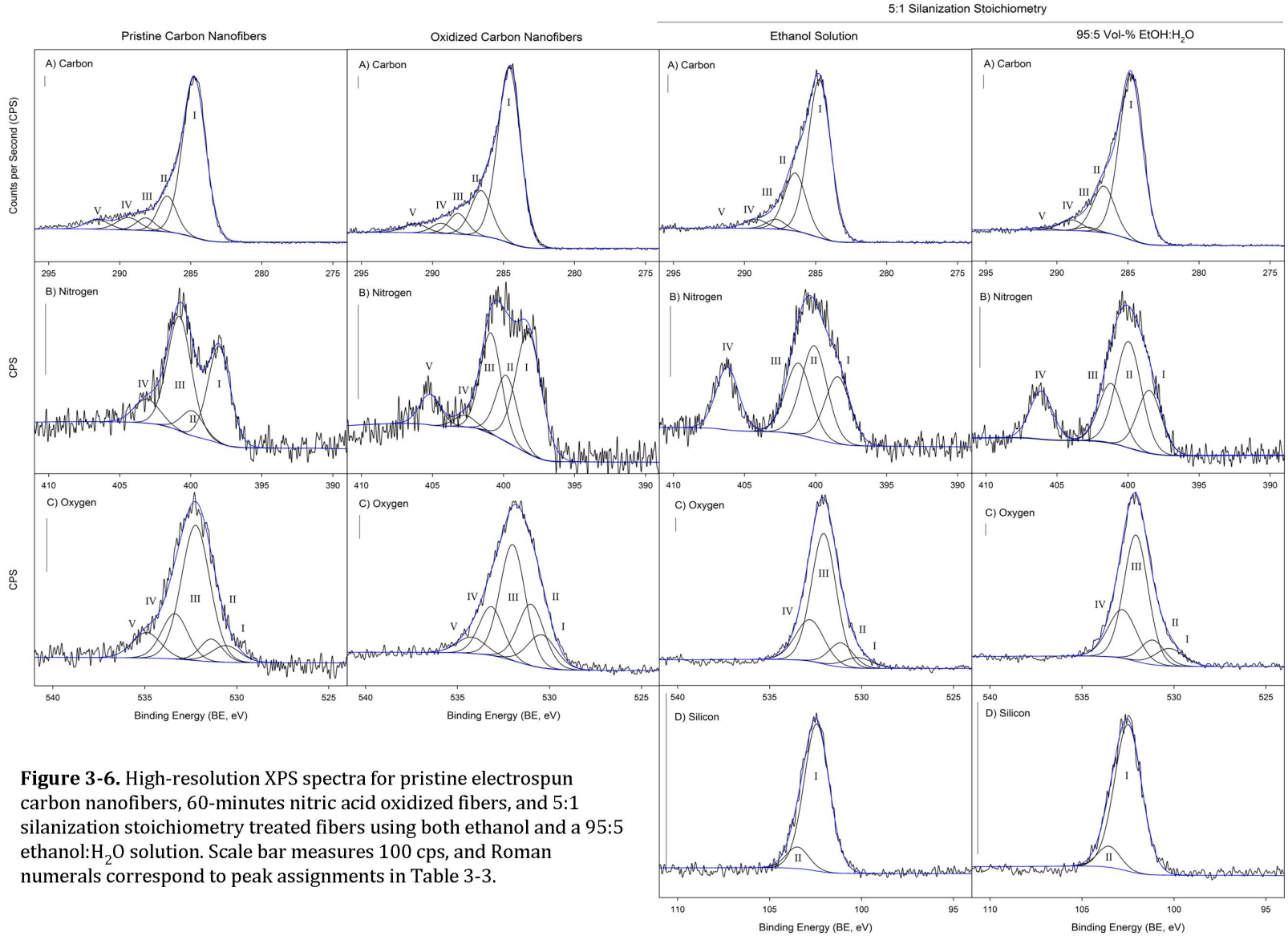

Figure 3-6. High-resolution XPS spectra for pristine electrospun carbon nanofibers, 60-minutes nitric acid oxidized fibers, and 5:1 silanization stoichiometry treated fibers using both ethanol and a 95:5 ethanol:H_2O solution. Scale bar measures 100 cps, and Roman numerals correspond to peak assignments in Table 3-3.

Table 3-5. Element weighted functional group analysis based on high resolution XPS data acquired at various time points during nitric acid oxidation provides insight into the subtle shifts in functionality within an element during oxidation.

				Nitric Acid (70%) Oxidized, 90 °C Time (min)			
Element	**BE (eV)**	**Peak**	**Pristine**	**10**	**20**	**40**	**60**
C	284.8	I	74.3	70.1	69.2	67.9	67.5
	286.5	II	13.3	15.1	14.5	15.5	14.5
	288.8	III	4.3	8.5	11.3	9.5	12.2
	289.2	IV	4.9	3.8	2.5	3.8	3.6
	291	V	3.2	2.6	2.5	3.3	2.1
N	398.5	I	32.9	39.2	33.0	26.8	22.1
	400	II	-	41.1	32.8	33.1	42.2
	401	III	56.3	8.1	21.7	24.1	16.6
	403	IV	10.8	-	-	-	-
	405	V	-	11.6	12.4	16.0	19.1
O	530.5	I	27.1	20.8	18.8	16.6	19.1
	531.3	II	20.5	33.6	34.8	36.0	32.3
	532.5	III	32.4	30.6	32.6	26.4	28.1
	533	IV	20.0	11.6	12.2	15.1	17.6
	534.5	V	-	3.4	1.5	5.9	2.8

Table 3-6. Bulk composition weighted functional group analysis based on XPS data provides more insight into actual surface concentrations of functional groups of interest, critical to understanding wetting by a composite matrix and the related interphase reactions.

				Nitric Acid (70%) Oxidized, 90 °C Time (min)			
Element	**BE (eV)**	**Peak**	**Pristine**	**10**	**20**	**40**	**60**
C	284.8	I	68.1	56.4	54.6	55.3	51.7
	286.5	II	12.2	12.2	11.4	12.6	11.1
	288.8	III	4.0	6.8	8.9	7.8	9.4
	289.2	IV	4.5	3.1	2.0	3.1	2.8
	291	V	2.9	2.1	2.0	2.7	1.6
N	398.5	I	1.7	2.2	1.6	1.2	0.72
	400	II	-	2.4	1.6	1.6	1.4
	401	III	2.8	0.46	1.1	1.1	0.54
	403	IV	0.54	-	-	-	-
	405	V	-	0.66	0.62	0.75	0.62
O	530.5	I	0.88	2.9	3.0	2.3	3.8
	531.3	II	0.67	4.6	5.6	5.0	6.5
	532.5	III	1.1	4.2	5.2	3.7	5.7
	533	IV	0.65	1.6	2.0	2.1	3.6
	534.5	V	-	0.47	0.24	0.81	0.57

Table 3-7. Functional group determination via Boehm titrations for nitric acid treated carbons, where parenthetical values highlight the percentage of each type of functionality. [§] 95:5 indicates an ethanol:H_2O solution was used for silanization, and 1:4 and 1:1 are stoichiometric ratios of silane-to-carbon fiber functionality. [†]Surface area and micropore volume were determined using BET theory for N_2 adsorption, except where krypton was used.[56]

Sample		Total (µmol/g)	Phenol (µmol/g)	Lactone (µmol/g)	Carboxylic (µmol/g)	Specific Surface Area (m^2/g)[†]	Micropore Volume (cm^3/g)[†]
Pristine (n=1)		310		-		4.53	0.00207
Oxidized (n=2)		970		-		6.00	0.00295
1:4 95:5[§] (n=1)		800		-		-	-
1:1 95:5[§] (n=1)		860		-		15.6	0.00488
PAN CF[56]	Pristine	9.9		-		1.06	-
	90 min, reflux (15 M)	936		-		0.35	-
Cellulose CF[64]	1 hour, 60 ºC (5 M)	2790	1430 (51%)	230 (8%)	1130 (41%)	1180	0.61
	2 hours, 60 ºC (15 M)	6520	1480 (23%)	350 (5%)	4690 (72%)		
MPC,[67] Boiling Nitric (7 M)	Pristine	287	56 (20%)	188 (65%)	43 (15%)	110	-
	1 hour	1333	336 (25%)	432 (33%)	565 (42%)		
	2 hours	1769	365 (21%)	687 (39%)	717 (40%)		

Table 3-8. Surface characterization using N_2 adsorption.

Sample	Specific Surface Area (m^2/g)	Average Pore Diameter (nm)	BJH Method Mode (nm)	DR Method Width (nm)	Micropore Volume (cm^3/g)
Pristine	4.53	15.0	3.43	4.87	0.00207
Oxidized	6.00	8.97	4.33	4.07	0.00295
1:1 95:5	15.6	6.75	0.653	2.80	0.00488

Table 3-9. Surface composition of pristine, 60 minute (80°C) oxidized, and silanized carbon nanofibers (CNFs) using XPS.

Element	Pristine CNF	Oxidized CNF	EtOH Stoichiometric Ratio			95:5 Vol-% (EtOH:H_2O) Stoichiometric Ratio		
			10:1	5:1	1:1	10:1	5:1	1:1
Carbon	85	76	62.6	59.3	63.4	58.9	63.4	71.2
Nitrogen	9.0	8.7	11.8	13.4	12.1	12.1	10.6	10.7
Oxygen	5.8	14.5	20.9	22.8	20.7	22.7	21.1	15.4
Silicon	<1	<1	4.7	4.5	3.8	6.3	4.9	2.8

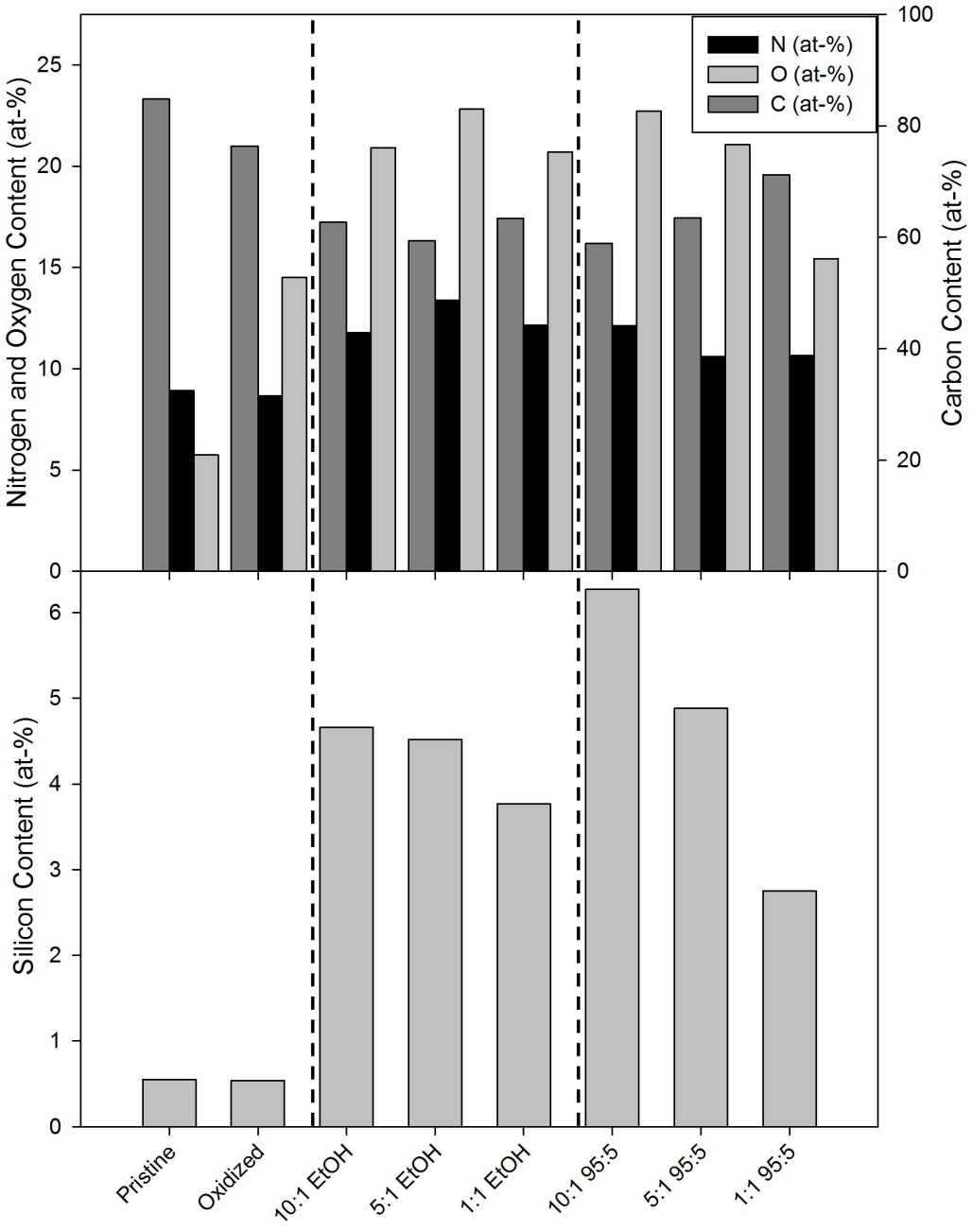

Figure 3-7. Composition of pristine, oxidized, and silanized fibers using a stock ethanol (EtOH) solution and a 95:5 vol-% mix of EtOH:H_2O. Trace amounts of silicon on pristine and oxidized fibers may be due to oil residue from electrospinning substrate (Aluminum foil); detection limits for XPS are ~0.1-1 at-%, and the trace amount was too low for high-resolution analysis.

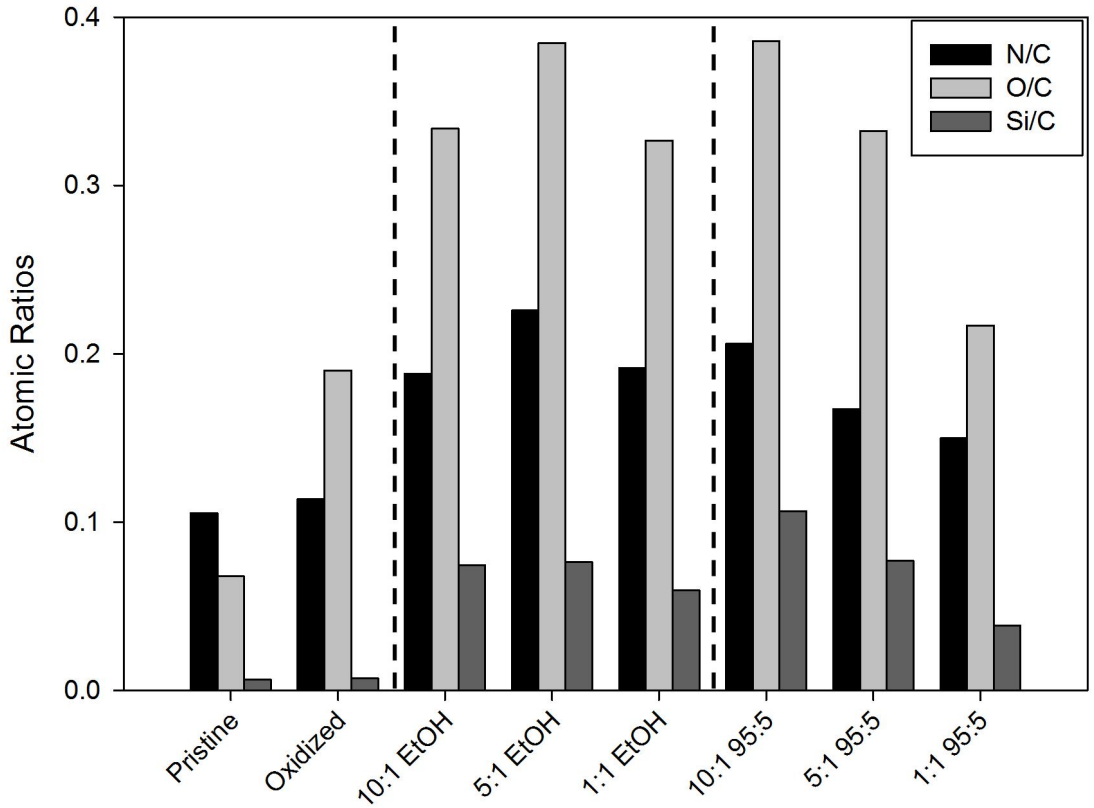

Figure 3-8. Atomic ratios of silanized fibers using XPS. With oxidation, nitrogen and carbon changed similarly and provided a steady N/C ratio, while oxygen content greatly increased. With silanization, the 95:5 vol-% EtOH:H_2O solutions showed clear trends of decreasing N/C, O/C, and Si/C towards values of the oxidized fiber due to decreasing silanization stoichiometry. The EtOH solution did not provide as clear a trend, where carbon content stayed relatively even at between 59 at-% and 63 at-% for the three stoichiometric silane ratios.

Table 3-10. Element weighted functional group analysis ased on high resolution XPS data acquired under various treatment regimes provides insight into the subtle shifts in functionality within an element during surface treatment.

					EtOH Stoichiometric Ratio			95:5 Vol-% (EtOH:H_2O) Stoichiometric Ratio		
Element	**BE (eV)**	**Peak**	**Pristine**	**Oxidized**	**10:1**	**5:1**	**1:1**	**10:1**	**5:1**	**1:1**
C	284.8	I	71	69	68	68	69	70	73	73
	286.5	II	13	17	24	24	19	20	20	14
	288	III	5	7	4	4	9	8	1	5
	289.2	IV	6	3	5	4	1	2	5	6
	291	V	6	4	-	-	2	-	1	2
N	398.5	I	36	41	22	23	27	23	22	24
	400	II	9	19	36	33	26	37	40	37
	401	III	45	28	25	25	27	22	21	20
	403	IV	10	3	-	-	-	-	-	7
	406	V	-	9	17	19	20	18	16	12
O	530.2	I	7	13	6	6	4	6	9	9
	531	II	8	23	9	11	19	6	11	15
	532	III	57	41	64	61	59	68	55	60
	533	IV	17	16	20	22	18	20	25	16
	534.5	V	11	7	-	-	-	-	-	-
Si	102.3	I	-	-	95	88	81	75	89	93
	103.5	II	-	-	5	12	19	25	11	7

Table 3-11. Bulk composition weighted functional group analysis based on XPS data provides insight into actual surface concentrations of functional groups of interest, critical to understanding wetting by a composite matrix and the related interphase reactions.

					EtOH Stoichiometric Ratio			95:5 Vol-% (EtOH:H_2O) Stoichiometric Ratio		
Element	**BE (eV)**	**Peak**	**Pristine**	**Oxidized**	**10:1**	**5:1**	**1:1**	**10:1**	**5:1**	**1:1**
C	284.8	I	60.3	53.3	42.5	40.5	43.8	41.4	46.5	52.3
	286.5	II	11.0	12.8	14.9	14.3	11.9	11.8	12.5	10.0
	288	III	3.9	5.2	2.4	2.1	5.7	4.8	0.9	3.2
	289.2	IV	4.8	2.6	2.8	2.4	0.7	0.9	3.0	4.0
	291	V	5.3	2.9	-	-	1.3	-	0.6	1.7
N	398.5	I	3.2	3.6	2.6	3.1	3.3	2.7	2.4	2.6
	400	II	0.8	1.6	4.3	4.4	3.1	4.5	4.3	3.9
	401	III	4.0	2.4	2.9	3.4	3.3	2.7	2.2	2.1
	403	IV	0.9	0.3	-	-	-	-	-	0.8
	406	V	-	0.7	2.0	2.6	2.4	2.1	1.7	1.3
O	530.2	I	0.4	1.9	1.3	1.3	0.8	1.4	1.9	1.4
	531	II	0.4	3.3	2.0	2.5	4.0	1.3	2.3	2.3
	532	III	3.3	6.0	13.5	13.9	12.2	15.4	11.6	9.2
	533	IV	1.0	2.4	4.2	5.1	3.7	4.6	5.3	2.5
	534.5	V	0.6	0.9	-	-	-	-	-	-
Si	102.3	I	-	-	4.4	4.0	3.1	4.7	4.4	2.6
	103.5	II	-	-	0.2	0.5	0.7	1.6	0.5	0.2

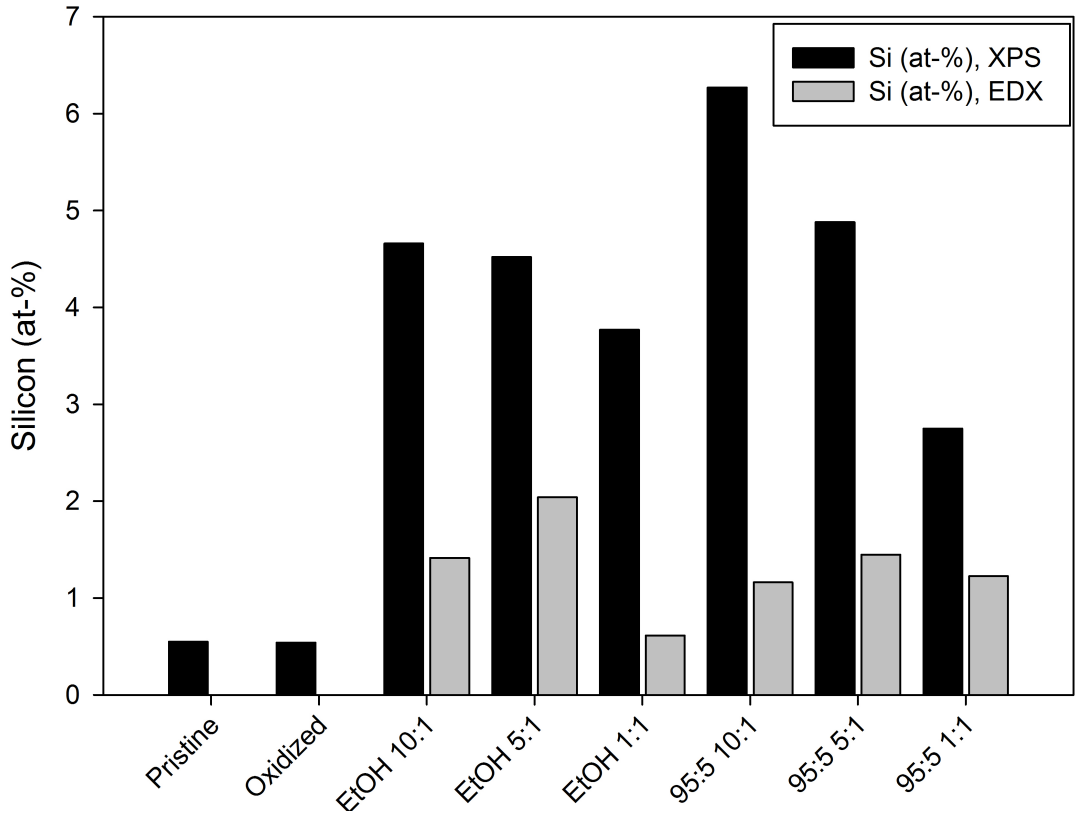

Figure 3-9. Comparison of XPS and EDX composition measurements using silicon content as the primary indicator for silanization. Samples used for both techniques came from common silanization batches. Small levels of silicon on pristine and oxidized fibers are considered contamination and were below the threshold for high-resolution analysis; this contamination is possibly due to oils present on standard aluminum foil used during electrospinning.

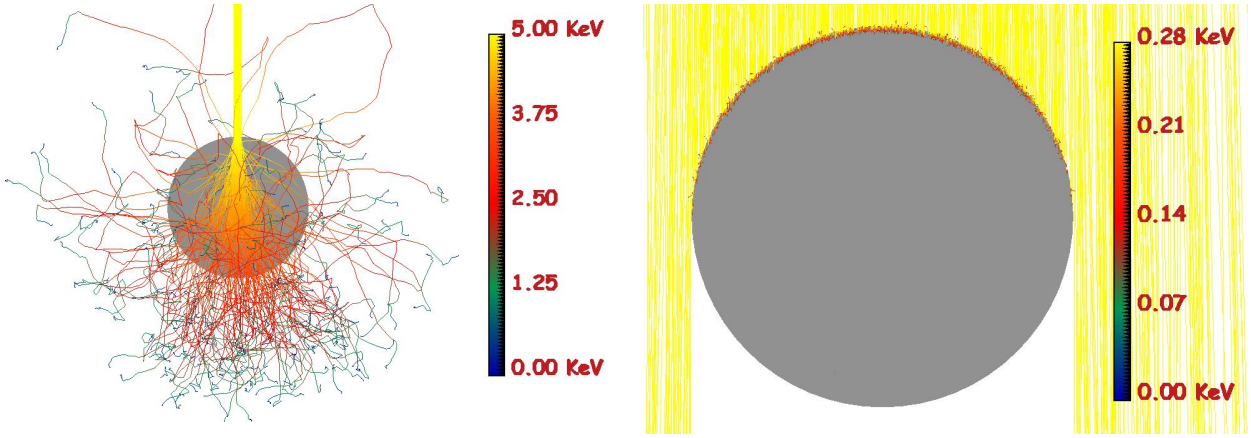

(A) (B)

Figure 3-10. Electron trajectory simulations using CASINO with a 200 nm carbon fiber, including (A) the large interaction volume for high-energy electrons used in EDX, and (B) the small escape depth (indicated in red) for C1s photoelectrons excited during XPS. In (A) yellow lines indicate incident electrons, and trajectories from orange to blue indicate varying levels of energy due to scattering

Chapter 4. Summary of Findings and Future Work

4.1. Summary of Findings

In the current study, a broad overview of carbon fiber development and modification was provided, as well as a thorough analysis, divided into two sections: 1) precursor fiber fabrication and stabilization, and 2) fiber carbonization and surface modification. In both sections, consideration was taken to provide information pertaining to common industrial practices where they differ from those followed in the current study. These were included in order to provide the groundwork for future development outside the scope of the current methods. The following is a summary of conclusions from research performed in each section.

4.1.1. Polyacrylonitrile (PAN) Precursor Fiber Fabrication and Stabilization

(1) Drying electrospun polyacrylonitrile nanofiber mats under vacuum at 70 °C is insufficient to remove residual DMF, shown by FTIR and gravimetric weight loss when heating to the solvent boiling point (153 °C). As of yet, no attention has been paid to molecular orientation, but residual solvent would facilitate molecular relaxation and reduce axial alignment in the duration between electrospinning and stabilization. Solvent could be better removed by reducing residual solvent using humidity controlled electrospinning, or increasing drying temperature, though fibers are typically not stored above 80 °C due to the glass transition. Alternatively, residual solvent could be used to facilitate axial molecular orientation by applying tension during stabilization. An additional finding included the suspected surface contamination by silicon due to electrospinning onto aluminum foil, likely from

residual oil used in manufacturing. This contamination was almost completely removed with pyrolization, but could be prevented using aluminum foil intended for use under ultrahigh vacuum, or by thoroughly cleaning before electrospinning.

(2) Between 200 and 250 °C, cyclization and crosslinking processes initiate, as well as oxygen integration predominantly in the form of ketones. Fiber diameter initially reduced (through 150 °C) due to solvent removal, but increased slightly through 250 °C; stress-free shrinkage using DMA also showed slight entropic relaxation through 215 °C, attributed to elevation above T_g (~85°C) and theoretical T_m (~215 °C), after which the sample contracted to its original dimension by 250 °C. The contraction between 215 and 250 °C signaled the initiating of cyclization and crosslinking.

(3) The majority of the stabilization processes occurred between 250 and 280 °C, where the fiber mat lost 10% of its mass, fiber diameter reduced by 30 nm, and the mat shrinkage reached 10%. Stress-free stabilization conditions allowed polyacrylonitrile molecules to lose orientation as they reacted with adjacent molecules during cyclization and chemical crosslinking, resulting in mat shrinkage. 60 minutes of isothermal treatment caused the mat to exhibit ~26% shrinkage, and fibers reached a diameter plateau by this time point. Continued treatment at 280 °C resulted in small increases in shrinkage, indicating only small levels of continued cyclization during the 2 hours of treatment. These results were supported by FTIR, where the dominant peak at 1595 cm^{-1} for cyclization became relatively stable between 60 and 180 minutes. On a shorter timescale, the nitrile peak shifted almost completely to its conjugated wavenumber after only 30 minutes isothermal. The dominant effect of the

last 2 hours of isothermal treatment included ~4% weight loss and additional oxygen uptake, but no significant chemical stabilization processes occurred.

(4) Given the above results, it was determined that the current precursor fiber would benefit from having stabilization time reduced to 60 minutes isothermal at 280 °C. As soon as the isothermal step is reached, the rate of stabilization processes (cyclization, crosslinking, etc) as observed by FTIR, DMA, and fiber dimension starts to decrease. Stabilization beyond 60 minutes reduces the fiber mat yield and oxidizes the surface more than that expected to be beneficial; surface oxygen reaches 17 at-% after 1 hour isothermal, and nearly 20 at-% measured by XPS after 3 hours, though oxygen is recommended to be ~5-15 at-%.

4.1.2. Polyacrylonitrile (PAN) Carbon Fiber Fabrication and Modification

The funding grant for this research highlighted the expected importance of the interphase between fiber and matrix on shape memory properties. Before we could evaluate the influence of the interphase, it was deemed necessary to analyze the surface of the selected carbon fibers; in this way, and through chemical modification, the effect of the fiber surface on resulting shape memory performance could be determined. Due to the scope of this goal, the current project was limited to understanding the surface of carbon fibers treated with nitric acid oxidation and silanization.

(1) Pristine carbon fibers developed using the current procedure of heating the stabilized electrospun precursor to 1000 °C in nitrogen resulted in low strength fibers. Pyrolized fibers contained roughly 92, 5, and 3 at-% carbon, nitrogen, and oxygen, respectively. Oxygen functionalities varied, including hydroxyl groups and O=C groups. The small

percentage of oxygen and nitrogen resulted in a surface that did not readily wet with epoxy during composite fabrication.

(2) Chemical oxidation using nitric acid (70%) resulted in rapid oxygen integration, understood to be at the defect sites and saturated basal plane edges. The first 10 minutes of oxidation resulted in a nearly 10 at-% increase in oxygen paired with an equivalent decrease is carbon. Continued oxidation resulted in increased oxygen content at the expense of carbon; nitrogen content also decreased with prolonged treatment. Oxygen was again found in various forms, though there was a shift to carbonyl/carboxyl/quinone type groups with extended oxidation. The increasing oxygen content resulted in a much more polar surface character, increasing the surface to wetting during composite fabrication. This is essential to creating a favorable interphase for properties like off-axis tensile strength. Additionally, creating a more functional carbon surface is believed to affect the shape memory properties of the resulting composite.

(3) An equation was developed based on an acid neutralization to provide qualitative stoichiometric ratios of silane coupling agent to functional sites on carbon nanofibers oxidized for 60 minutes at 80 °C. This equation was used to systematically study the effect of silane content and type of solution on silanization efficiency.

(4) Silanization of oxidized fibers was performed using two solutions, ethanol and a 95:5 vol-% solution of ethanol:H_2O, and three stoichiometric ratios of silane to fiber functionality, 10:1, 5:1, and 1:1. The two solutions were formulated with unique theoretical reaction mechanisms in mind; the ethanol:H_2O solution was expected to hydrolyze silane in solution, promoting fiber silanization and silane condensation

reactions, while the ethanol solution was used to promote monolayer formation using hydrolysis from oxygen adsorbed to the oxidized surface. The 95:5 vol-% solution of ethanol:H_2O produced surface concentrations of silicon (used to determine the presence of silane) that scaled directly with stoichiometry, while the ethanol solution resulted in silicon concentrations that did not scale with stoichiometry. As such, it is expected that surface hydrolysis failed to adequately functionalize the silane, and they adsorbed or reacted to the carbon fibers using a different mechanism. Even though the ethanol solution produced higher levels of bulk silanization, the 95:5 vol-% solution of ethanol:H_2O was considered the more favorable solution due to the high stoichiometric dependence of silicon which would allow better control of the amount of surface treatment compared to the ethanol solution.

(5) In addition to types of solution affecting silanization, the relative concentration of silane to carbon fiber and solution was determined to have an effect on silanization efficiency in the bulk of the fiber mat using EDX. It was proposed that three situations occurred: (I) the 1:1 stoichiometry, which used 0.1 vol-% silane in solution, resulted in a 'silane-limited' solution, where there was insufficient silane to adequately coat the fibers. (II) The 5:1 stoichiometry, which used 0.25 vol-% silane in solution, resulted in a more appropriate ratio of fiber:solution:silane and the highest bulk silicon concentration. (III) The 10:1 stoichiometry, which also used a 0.25 vol-% silane in solution, resulted in a 'dilution-limited' solution due to too little fiber mass relative to the amount of solution, preventing diffusion of silane into the fiber mat. With the given ratios, the 5:1 stoichiometry proved most efficient at silanizing the bulk fiber mat while also achieving relatively high concentrations on outermost fiber

mat surface. If higher stoichiometries are desired, it is suggested that a ratio of fiber mass (mg):silane (μl) of ~1:1 be used, keeping solution volume enough to only cover the fibers.

4.2. Future Work

Further development of the fibers studied in this thesis could take several avenues depending on the area of interest. Key areas include: fiber development, surface modification, and evaluation of shape memory composite performance.

More generally, the study of these carbon fibers would benefit from careful environmental control to enhance reproducibility. In typical industrial processes, humidity and temperature are monitored and controlled, but this is not possible in the current setup; humidity in the lab ranged from 23% to 68% (record courtesy of Derek Weed) and temperature ranged from 70 to >80 °F over the course of research. Variations in electrospinning humidity and temperature are less noticeable for as-spun fiber mats, but introduce confounding changes to carbonized products, which makes resulting changes in properties difficult.

4.2.1. Fiber Development

Higher integrity fibers could be developed in various ways, and doing so could promote a number of favorable properties for the fibers (i.e., tensile strength, modulus, electrical conductivity). In order of processing step: (I) using a copolymer precursor would accelerate stabilization and could improve carbon yield and tensile properties; (II) electrospinning uniaxially aligned fibers and stabilizing under tension would prevent loss of molecular orientation that is critical to high strength fibers; and (III) carbonizing at a higher temperature

would result in a more ordered carbon structure, improving strength and modulus. Increasing the molecular orientation and basal plane order in steps (II) and (III) is considered advantageous for fiber integrity, and also increases carbon fiber conductivity. Electrical conductivity is of particular interest to the application of electrically activated shape memory composites, which was the original platform of this research.

4.2.2. Surface Modification

Surface modification and evaluation methods were assessed in the current thesis, but these may need to be tailored based on further experimental need. Nitric acid oxidation was performed and the time point chosen based on creating a highly functionalized surface, though increased levels of oxidation can have the undesirable effect of reducing fiber integrity and electrical conductivity. Additionally, silanization was performed in relatively small amounts in an effort to produce near monolayer coverage, which has been reported to produce the optimal composite performance, but higher levels of silanization could increase the size of the interphase and make analysis of the effect of surface treatment on shape memory easier to detect; furthermore, the interphase could be greatly increased by selecting a higher molecular weight coupling agent. The highly functionalized surface of oxidized carbon fibers, including a large proportion of carboxylic groups, could allow investigation of a number of more complex coupling agents.

Without regard to composite performance, and using the methods in the current thesis, both oxidation and silanization could systematically be studied to determine their relative effects on electrical conductivity.

4.2.3. Shape Memory Polymer Composite: Interphase and Performance Evaluation

The primary goal of the current research grant was to study the effect of the interphase on shape memory composite performance. In further pursuit of this goal, the current surface treatment methods could be used to determine their effect on shape memory. Research is currently being conducted to determine properties of pristine carbon fiber composites, and the effects of fiber modification could build upon this foundation. One area of interest could include examination of shape recovery force. Shape memory polymers could be favorable to shape memory alloys for many applications due to the high levels of strain and fatigue life, but their actuating force is greatly reduced compared to alloys. Through improvement of the carbon fibers, or through enhancement of the interphase, actuation strength could increase and produce electrically activated shape memory actuators. Other areas that could highlight the effect of the interphase include shear strength and studies of tension perpendicular to uniaxial aligned fibers, an area where fiber composites typically perform weakly. These tests would provide an indirect measure of the composite interphase.

Parallel to studying shape memory performance, evaluation of the carbon fiber interphase in the composite form could contribute provide an additional metric to gauge the strength of the interphase. The composite interphase could be directly studied in various ways, including: (I) AFM phase modulus mapping, where the thickness of the interphase could be assessed by observing the change from high modulus fiber to low modulus epoxy, and (II) fiber pullout under tension, including quantifying the amount of pullout (e.g., fiber length as a measure of adhesion strength, density of pullout holes, etc). Some representative SEM images are included below for fiber pullout in epoxy composites at 80 °C.

Pristine Carbon Fiber	Oxidized Fiber	EtOH Solution (Stoichiometry) 1:1	EtOH Solution (Stoichiometry) 10:1
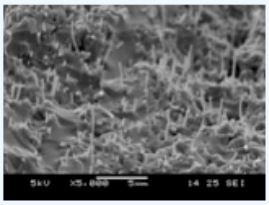	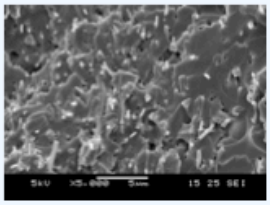	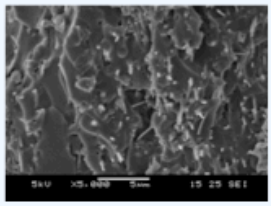	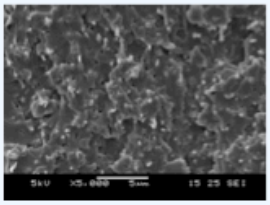
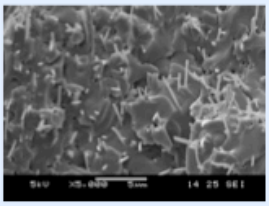			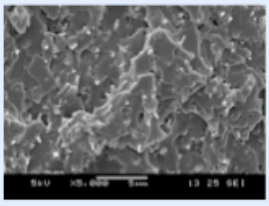

Christian B. Iversen

313 Schaffer Ave. Apt. E09, Syracuse, NY 13206 • (812) 870-4081 • civersen@gmail.com

Education

Syracuse University, L.C. Smith College of Engineering, Syracuse, NY — *Expected December 2012*
MS, Bioengineering *(Concentration: Polymer Science) (GPA: 3.9/4.0)*
Adviser: Prof. Patrick T. Mather (PhD)

Rose-Hulman Institute of Technology, Terre Haute, IN — *May 2010*
BS, Engineering Physics *(Concentration: Biomedical Engineering), Cum Laude*

Research and Development Experience

Syracuse Biomaterials Institute, Graduate Research Assistant — *Sept. 2010-Current*
Adviser: Prof. Patrick T. Mather (PhD), Syracuse University, Syracuse, NY

- Assessed development of in-house electrospun polyacrylonitrile (PAN) based carbon fibers with FTIR, DMA, EDX, and XPS to provide recommendations for improved fabrication methods
- Compared effects of surface modification – via acid oxidation and silane coupling agent – on fiber surface groups (acid-base titration, FTIR, XPS), morphology (SEM, AFM, N_2 adsorption), and electrical conductivity
- Assisted in analysis of surface modification on epoxy composite properties through fracture behavior, fiber-matrix adhesion, and electrical conductivity

Rose-Hulman, Senior BME Project (High Intensity Focused Ultrasound Device) — *Aug. 2009-May 2010*

- Designed a high intensity focused ultrasound (HIFU) device for acoustocautery with a multidisciplinary team of electrical and biomedical engineering students
- Conducted market assessment, cost analysis, and review of relevant FDA regulations in order guide device design, construction, and testing
- Personally responsible for transducer design, 3D modeling (SolidEdge) and rapid prototyping of the device, and assisting in test design and performance analysis

Material Characterization Experience [* technician performed experiment, I analyzed results]

Spectroscopy/Microscopy:

- Optical, crossed-polar
- FTIR (transmission, ATR*)
- Atomic force microscopy (AFM-tapping)
- Scanning electron (SEM), energy dispersive (EDX)
- X-ray photoelectron (XPS*)

Other:

- Thermogravimentric analysis (TGA)
- Differential scanning calorimetry (DSC)
- Dynamic mechanical analysis (DMA)
- Wide- and small-angle x-ray diffraction (XRD)
- Tensile testing

Skills

- Strong computer skills (acted as computer administrator for research lab)
- Strong written and oral communication skills
- Experience in cross-discipline teams and collaborative research environments

Memberships, Affiliations and Activities

Syracuse Biomaterials Institute, *Mentor* — *Jan. 2011-May 2012*

- Mentor to junior/senior chemical engineering student on research methods and lab techniques towards the development and characterization of polymer composites

Society for Biomaterials, *Member* — *2010-Present*

National Association of Science Writers, *Member* — *2011-Present*

Sigma Pi Sigma (Physics Honors Society), *Member* — *0209*

Publication

RR Letfullin, **CB Iversen**, TF George. "Modeling nanophotothermal therapy: kinetics of thermal ablation of healthy and cancerous cell organelles and gold nanoparticles." *Nanomedicine: NBM*. 7; 137-145 (2011).